Williams, George Clay

STEEL CONNECTION DESIGNS BASED ON INELASTIC FINITE ELEMENT ANALYSES

The University of Arizona PH.D. 1986

PLEASE NOTE:

In all cases this material has been filmed in the best possible way from the available copy. Problems encountered with this document have been identified here with a check mark __√__.

1. Glossy photographs or pages _____
2. Colored illustrations, paper or print _____
3. Photographs with dark background _____
4. Illustrations are poor copy _____
5. Pages with black marks, not original copy _____
6. Print shows through as there is text on both sides of page _____
7. Indistinct, broken or small print on several pages ✓
8. Print exceeds margin requirements _____
9. Tightly bound copy with print lost in spine _____
10. Computer printout pages with indistinct print _____
11. Page(s) _____ lacking when material received, and not available from school or author.
12. Page(s) _____ seem to be missing in numbering only as text follows.
13. Two pages numbered _____. Text follows.
14. Curling and wrinkled pages _____
15. Dissertation contains pages with print at a slant, filmed as received _____
16. Other _____

_____

_____

University
Microfilms
International

STEEL CONNECTION DESIGNS BASED ON INELASTIC FINITE ELEMENT ANALYSES

by

George Clay Williams

A Dissertation Submitted to the Faculty of the

DEPARTMENT OF CIVIL ENGINEERING AND ENGINEERING MECHANICS

In Partial Fulfillment of the Requirements
For the Degree of

DOCTOR OF PHILOSOPHY
WITH A MAJOR IN ENGINEERING MECHANICS

In the Graduate College

THE UNIVERSITY OF ARIZONA

1 9 8 6

THE UNIVERSITY OF ARIZONA
GRADUATE COLLEGE

As members of the Final Examination Committee, we certify that we have read the dissertation prepared by George Clay Williams

entitled STEEL CONNECTION DESIGNS BASED ON INELASTIC FINITE ELEMENT ANALYSES

and recommend that it be accepted as fulfilling the dissertation requirement for the Degree of Doctor of Philosophy.

Ralph M. Richard	7 Jan 86 Date
D. A. DaDeppo	7 Jan 86 Date
Tribikram Kundu	7th Jan. '86 Date
	Date
	Date

Final approval and acceptance of this dissertation is contingent upon the candidate's submission of the final copy of the dissertation to the Graduate College.

I hereby certify that I have read this dissertation prepared under my direction and recommend that it be accepted as fulfilling the dissertation requirement.

Ralph M. Richard	7 Jan 86
Dissertation Director	Date

STATEMENT BY AUTHOR

This dissertation has been submitted in partial fulfillment of requirements for an advanced degree at The University of Arizona and is deposited in the University Library to be made available to borrowers under rules of the Library.

Brief quotations from this dissertation are allowable without special permission, provided that accurate acknowledgment of source is made. Requests for permission for extended quotation from or reproduction of this manuscript in whole or in part may be granted by the head of the major department or the Dean of the Graduate College when in his or her judgment the proposed use of the material is in the interests of scholarship. In all other instances, however, permission must be obtained from the author.

SIGNED: George C. Williams

ACKNOWLEDGEMENTS

Appreciation is gratefully acknowledged to the many people who made contributions to this study.

The American Institute of Steel Construction (AISC) provided the grant for this research. Their financial support was greatly appreciated.

Much thanks goes to Dr. Ralph Richard who, as major advisor, spent many hours in guidance and discussion.

Additional thanks are also given to Dr. Donald DaDeppo and Dr. Tribikram Kundu for their careful review of this work and for serving as members of the graduate committee.

For her meticulous care in typing this document and the revisions, appreciation is expressed to Jan Andersen.

Finally, Staci Walker and my parents deserve a special thanks for their support and encouragement.

TABLE OF CONTENTS

TABLE OF CONTENTS -- Continued

LIST OF ILLUSTRATIONS

LIST OF ILLUSTRATIONS -- Continued

LIST OF ILLUSTRATIONS -- Continued

LIST OF ILLUSTRATIONS -- Continued

LIST OF ILLUSTRATIONS -- Continued

LIST OF ILLUSTRATIONS -- Continued

LIST OF TABLES

ABSTRACT

Analytical and experimental studies were made to develop design procedures for steel gusset plate connections in diagonally braced frames. Stiffness and strength models of structural fasteners based on physical tests were incorporated into inelastic finite element analyses. The modeling techniques were verified by comparing analytical and experimental results for full scale connection tests.

Finite element models of bracing connections were generated to determine gusset plate force, stress, strain, and displacement distributions for a variety of connection designs including K-bracing and X-bracing. Based on these results current design procedures were scrutinized and new design procedures were proposed for predicting the tensile strength, buckling strength, and force distributions for bracing connections. Additionally, it was found that gusseted beam-to-column connections are rigid (AISC Type I) and the centroidal axes of the brace, beam, and column members do not necessarily need to intersect at a common working point.

Chapter 1

INTRODUCTION

Steel connections are used to join beams, columns, and bracing members of framed buildings. Providing adequate strength and stiffness at minimal cost for all elements in a steel connection is a challenging problem for the structural engineer. As shown in Figure 1, diagonal bracing members are often connected to the major framing to resist lateral loads, such as wind forces and earthquakes. Gusset plates, bolts, double angles, welds, plates, and structural tees are elements used to create diagonal bracing connections. Presented herein are the procedures for designing diagonal bracing connections, and the analysis techniques and results utilized to derive and verify these procedures.

Early gusset plate research was directed towards determining the stress distributions in truss connections. Rust (33, 34), Perna (23), Sandel (35), and Vasarhelyi (39) performed photoelastic stress analyses on model gusset plates. Whitmore (41, 42) developed a criterion, based on an experimental test, to estimate the maximum normal stress in a gusset plate. Additional experimental work was conducted on truss gussets by Irvan (19), Hardin (18), Chesson and Munse (7, 8), Birkemoe, Eubanks, and Munse (2), and Vasarhelyi (39). Bjorhovde and Chakrabarti published results of full scale diagonal

bracing connection tests (4) that comprised a stub beam and a stub column.

Early gusset plate design procedures were based on beam theory (40, 14). Whitmore's work (41, 42) is currently employed to design gusset plates (13, 37). Recently, Richard (32) proposed applying the block shear concept to gusset plate design. Hardash and Bjorhovde (17) tested small plates in tension to study the block shear method of design.

Previous to this study, gusset plate analyses did not include the nonlinear behavior of the fasteners; furthermore, the frame to which the gusset is attached was excluded from the model. Davis (11) simulated Whitmore's test using an elastic finite element model. Additional elastic analyses were made by Desai (12) and Vasarhelyi (39). Struik (36) made a nonlinear finite element analysis of Whitmore's gusset model which verified the location of the maximum gusset plate normal stresses. Detailed analyses have not been made to determine the fastener force distributions in diagonal bracing connections, and the buckling strength of gusset plates.

Nonlinear analysis techniques were developed in this study to determine the force, stress, strain, and displacement distributions in steel connections subjected to static loads. Plate and framing members were analyzed using plane stress and bar elements. Welds, bolts, and double framing angles were modeled using a simple two-dimensional

connector element based on experimental tests. Analytical force-deformation curves derived from physical tests of the fasteners were inputted into the nonlinear finite element program INELAS (28). The analysis methods were verified by modeling full scale connection tests (4, 24, 32). This procedure has been employed to predict the moment-rotation curves for beam-to-column double angle framing connections (16). Furthermore, current design procedures for single plate framing connections (31) were developed utilizing this method.

A variety of bracing connections were analyzed to determine the tensile and compressive strength of gusset plates and the fastener force distributions. Various bracing configurations, including K-bracing and X-bracing, were considered. Eccentric connections were studied in which the brace axis does not intersect with the beam-column working point. Existing design procedures were compared to finite element results. New design procedures were developed and verified using the analytical and experimental results.

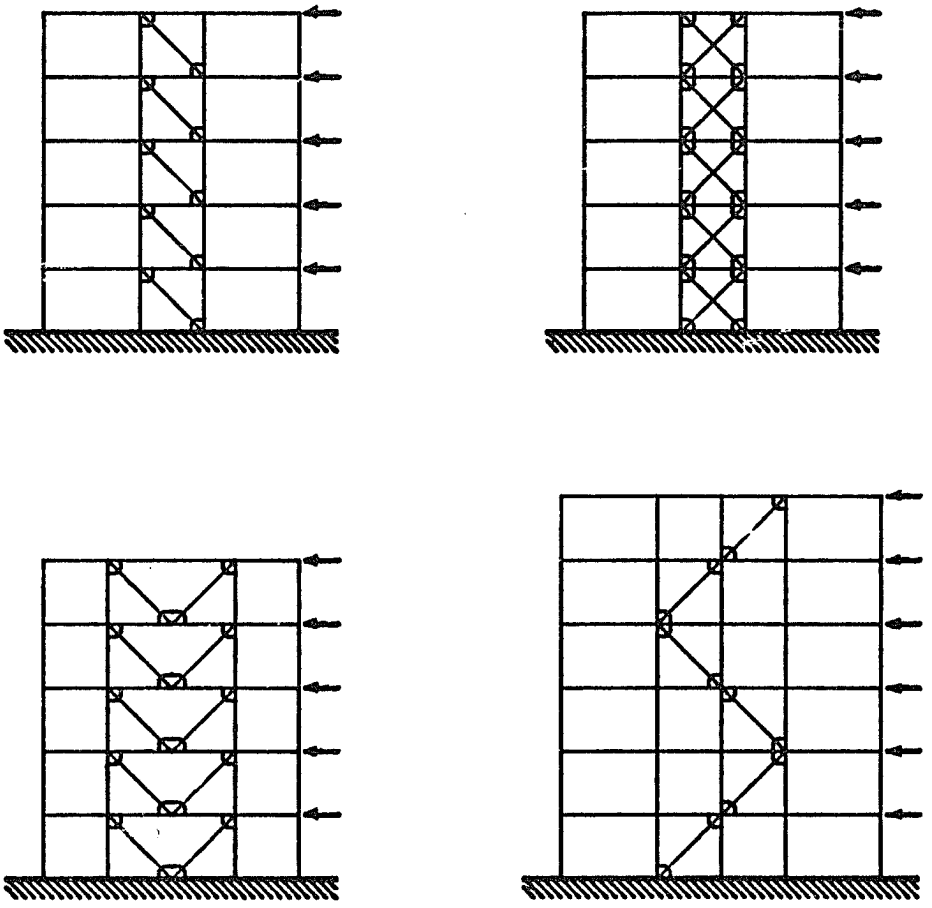

Figure 1. Braced Frames.

Chapter 2

MODELING TECHNIQUES

To analyze structural systems such as diagonal bracing connections, the behavior of the following components must be modeled accurately:

- beams
- columns
- bracing members
- connection plates
- structural tees
- double framing angles
- bolts (in tension, single shear, and double shear)
- welds

The finite element method was used to analyze the connections considered in this study. Each component of the connection was divided into a mesh of elements. A finer mesh was generated in regions of large stress gradients and requiring high accuracy. The material behavior was accounted for by using stress-strain relationships for plate and bar elements and force-deformation relationships for fastener elements. The behavior at the model boundaries was prescribed using support conditions, applied loads, and rigid bars. All analyses conducted were nonlinear so that as load was applied, the

redistribution of gusset plate stresses and fastener forces could be monitored as a function of the applied loads.

Since plane stress assumptions adequately describe the structural behavior of the webs of the beam, column, and bracing members, as well as the gusset and splice plates, these components can be accurately modeled using two-dimensional triangular, rectangular and quadralateral membrane elements (9). The flanges of the beam, column, and bracing members carry primarily axial forces, and therefore can be modeled using one-dimensional bar elements. To describe the nonlinear material behavior of steel, the theory of plasticity is utilized (22). The von Mises yield criteria and the associated Prandtl Reuss flow rule for ductile metals is used to predict the inelastic behavior of the gusset plate. The framing members (beams, columns, and braces) were not allowed to yield in order to insure that only the nonlinear behavior of the gusset and fasteners was considered in this study.

While plate and framing members can be analyzed using two-dimensional plane stress assumptions, fastener systems in general can not. For example, to accurately model the structural action of bolted double framing angles loaded in tension, as illustrated in Figure 2, the analysis method must include the following material and mechanical behaviors:

- material nonlinearities
- geometric nonlinearities
- coupling of bending and membrane plate forces
- contact stresses and forces
- sliding surfaces with friction
- bolt-plate bearing action
- plate tearing

An accurate three-dimensional finite element analysis of this fastener system would be extremely expensive. Instead, the complex behavior of the fasteners can be accounted for by developing fastener stiffness and strength models based on experimental tests.

A simple two-dimensional fastener element for each type of connector (welds, bolts, double framing angles, etc.) can be developed using experimental tests by following these steps (refer to Figure 3):

1. Isolate connector from real structure.
2. Design experimental tests to duplicate forces and deformations that would occur in a real structure.
3. Perform experimental tests and record force vs. deformation data for the connector.
4. Fit an analytical force-deformation curve (e.g., the Richard equation) to the experimental data obtained in Step (3). Determine curve parameters that characterize the stiffness and strength of the connector.

5. Input curve parameters calculated in Step (4) for spring (fastener) element in a nonlinear finite element program (e.g., INELAS). The analytical model will follow the force-deformation path found experimentally.

If results from the experimental tests are already available, they can be used to replace Steps (1) through (3).

The Richard equation (29) was employed to analytically describe the stress-strain relationship of steel and the force-deformation path of fasteners. Four curve parameters, K, K_p, R_o, and n, combine to create the Richard equation:

$$R(\Delta) = \frac{(K - K_p)\Delta}{\left[1 + \left|\frac{(K - K_p)\Delta}{R_o}\right|^n\right]^{1/n}} + K_p\Delta$$

where

R = force (or stress)

Δ = deformation (or strain)

K = elastic (initial) stiffness (or Young's modulus)

K_p = plastic (final) stiffness (or plastic modulus)

R_o = reference load (or reference stress)

n = curve sharpness parameter

All curve parameters have physical significance as shown in Figures 4 and 5. Curves generated by this equation were used to describe the structural behavior of welds, double framing angles, and bolts in single and double shear.

Force-deformation data for welds subjected to tension and shear were published by Butler and Kulak (6). Shown in Figure 6 are the experimental data and corresponding analytical curves for a one-inch tributary length of 1/4" E60 weld loaded in shear. The strength and stiffness parameters for other electrode strengths, weld sizes, and tributary lengths may be computed by direct ratios as given in Appendix A.

Experimentally determined force-deformation data and Richard curve parameters for high strength bolts in single shear were published by Richard, et al (31). Shown in Figure 7 are typical data and the analytical curve for two 3/8" A36 plates connected together with a 3/4" A325 bolt. Curves similar to this one were used to analyze and develop design criteria for single plate (or shear tab) framing connections. Appendix A contains a summary of the force-deformation curve parameters presented in Reference 31. Crawford and Kulak (10) published data for bolts loaded in double shear which were used in this research.

Beaufoy and Moharram (1), and Lewitt, Chesson, and Munse (20) published force-deformation data for double framing angles loaded in tension and compression, as shown in Figure 8. These data were used to

predict moment-rotation curves for flexible beam-to-column framing connections. Blewitt and Richard (5) published experimental data and analytical curve parameters for bolted double framing angles subjected to tension, compression, and shear. The compressive and shear deformations of double framing angles resulted primarily from bolt hole deformations. In contrast, the tensile deformations of the angles resulted predominantly from angle leg deformations as illustrated in Figure 2. This variation causes the fastener to act anisotropically. Richard (32) developed the yield surface shown in Figure 9 to model the anisotropic strength of double angles. Formulation of the double framing angle element is summarized in Figure 10. Summarized in Appendix A are the force-deformation curve parameters for bolted double framing angles.

To demonstrate the validity of this concept, two flexible beam-to-column connections tested at the University of Illinois were modeled using the double framing angle element. Moment-rotation curves were calculated from finite element analyses independently from the experimentally measured curves. Experimental and analytical results are compared for a four-bolt connection in Figure 11, and a ten-bolt connection in Figure 12. The finite element analyses and the experimental results show excellent agreement.

Shown in Figure 13 are the results of a finite element analysis in which fastener elements were used to model the bolted double framing

angles along one edge of a gusset plate. Fastener forces and displacements are shown simultaneously to illustrate the anisotropic behavior of the double angle element.

The finite element computer program INELAS, developed by Richard et al. (26, 15, 30) was utilized to predict connection force, stress, strain, and displacement distributions. Program INELAS, written in FORTRAN, generates and solves the nonlinear first order differential equations that simulate the structural model by fourth order Runge Kutta quadrature with Simpson Rule coefficients.

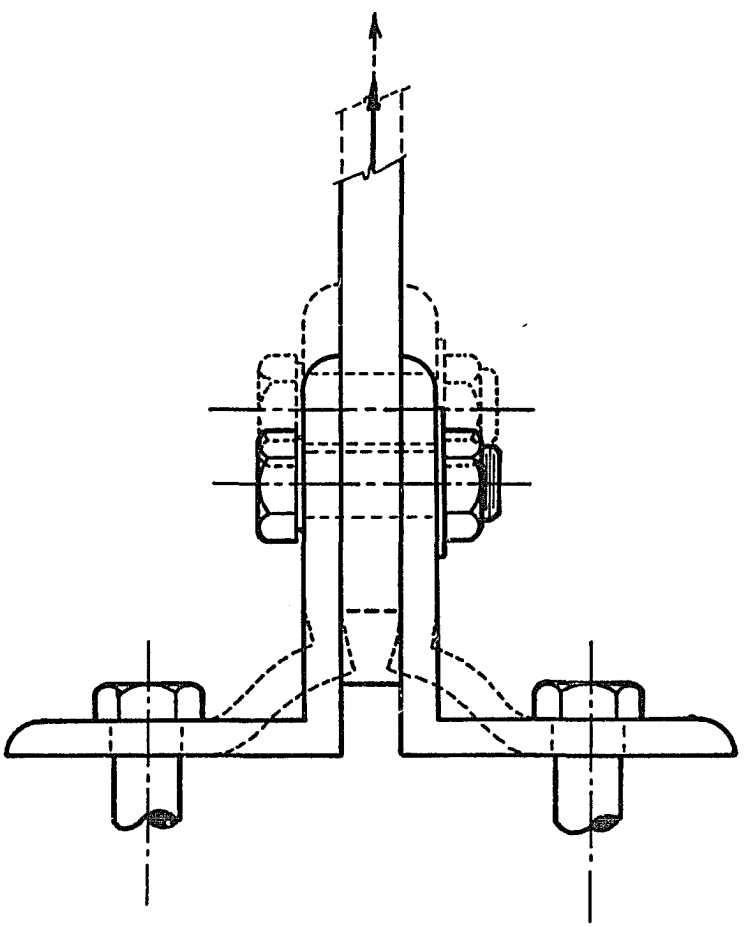

Figure 2. Behavior of Double Framing Angles Loaded in Tension.

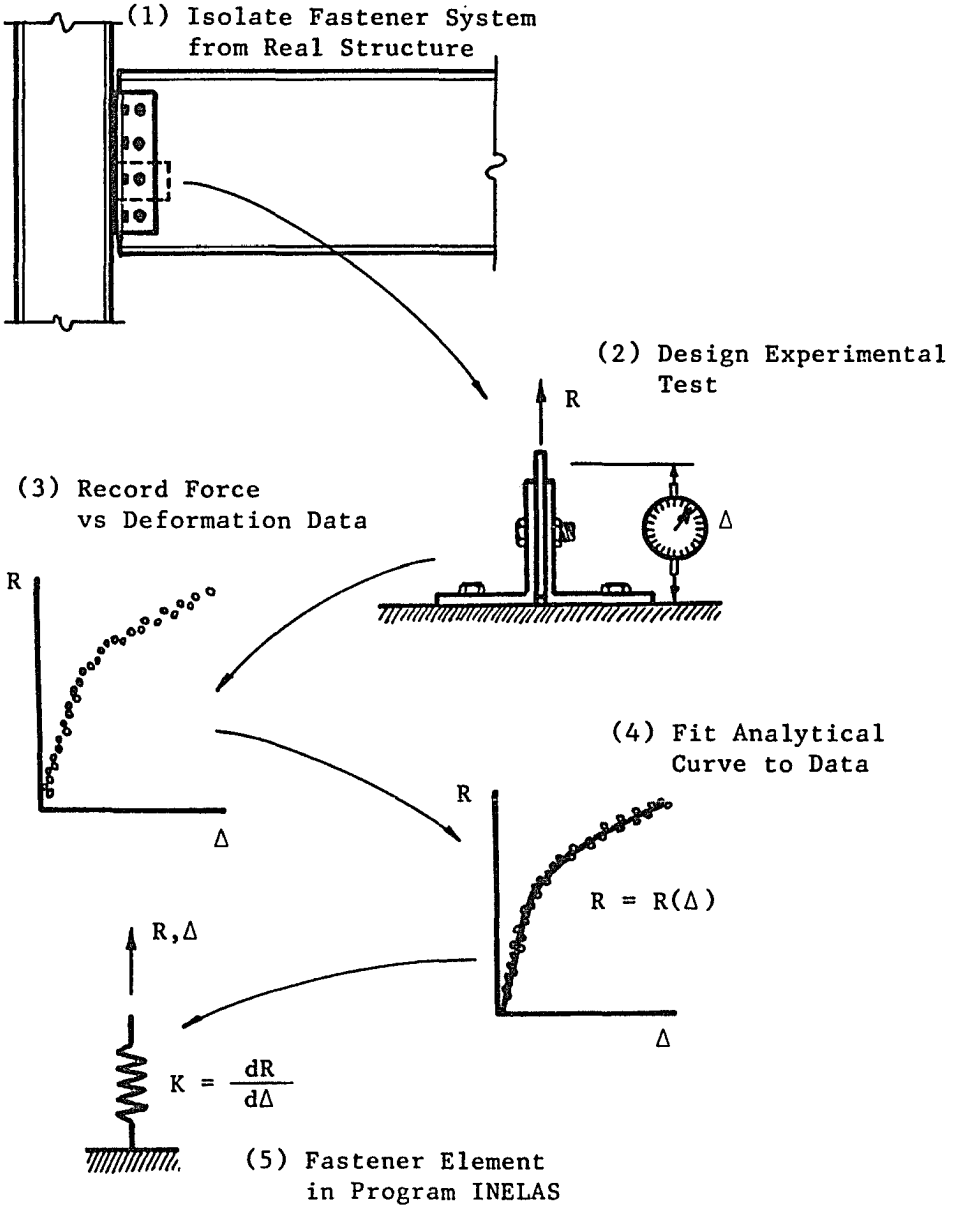

Figure 3. Development of Fastener Element from Experimental Tests.

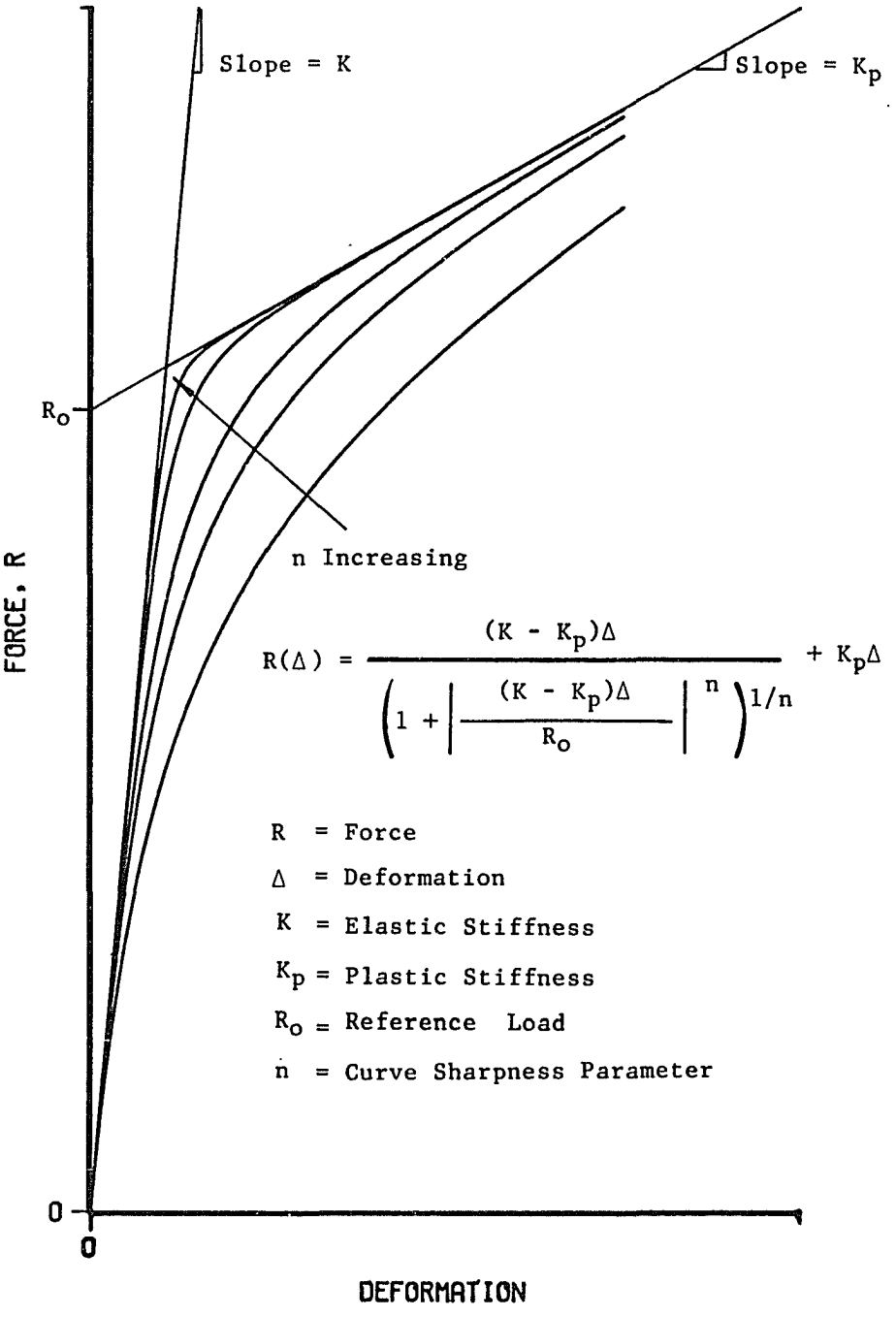

Figure 4. The Richard Equation.

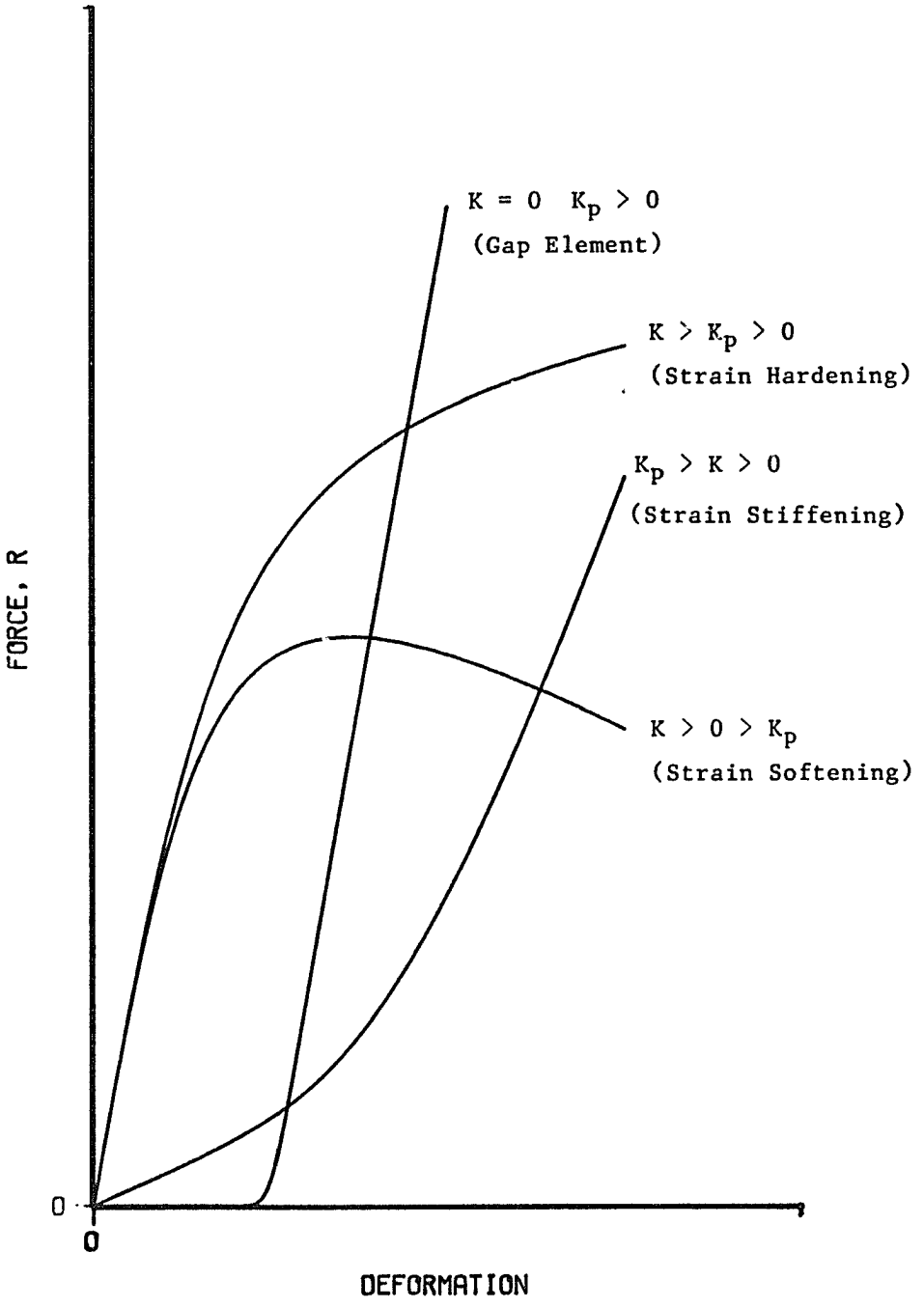

Figure 5. Richard Curve Shapes.

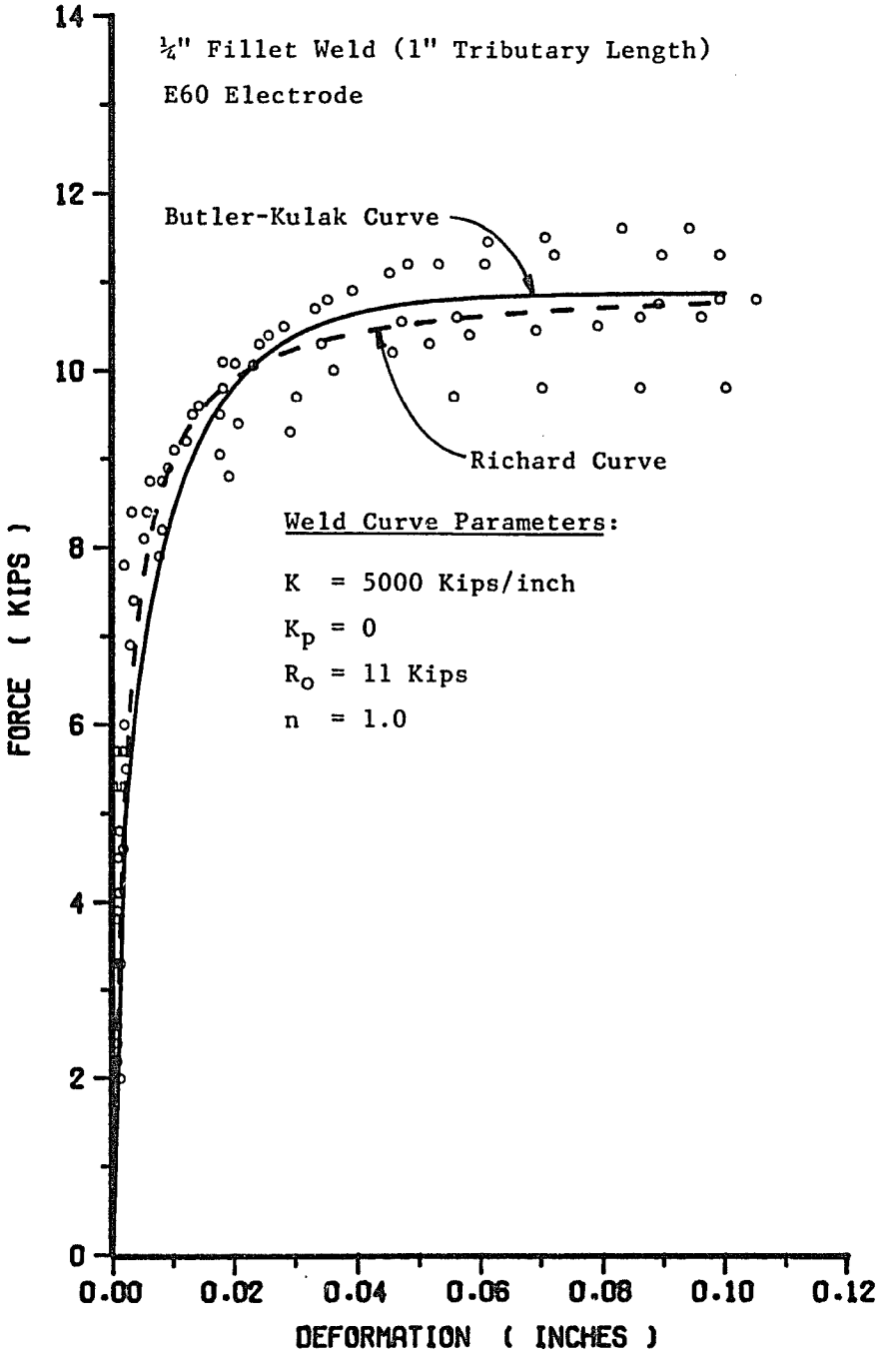

Figure 6. Weld Force-Deformation Behavior.

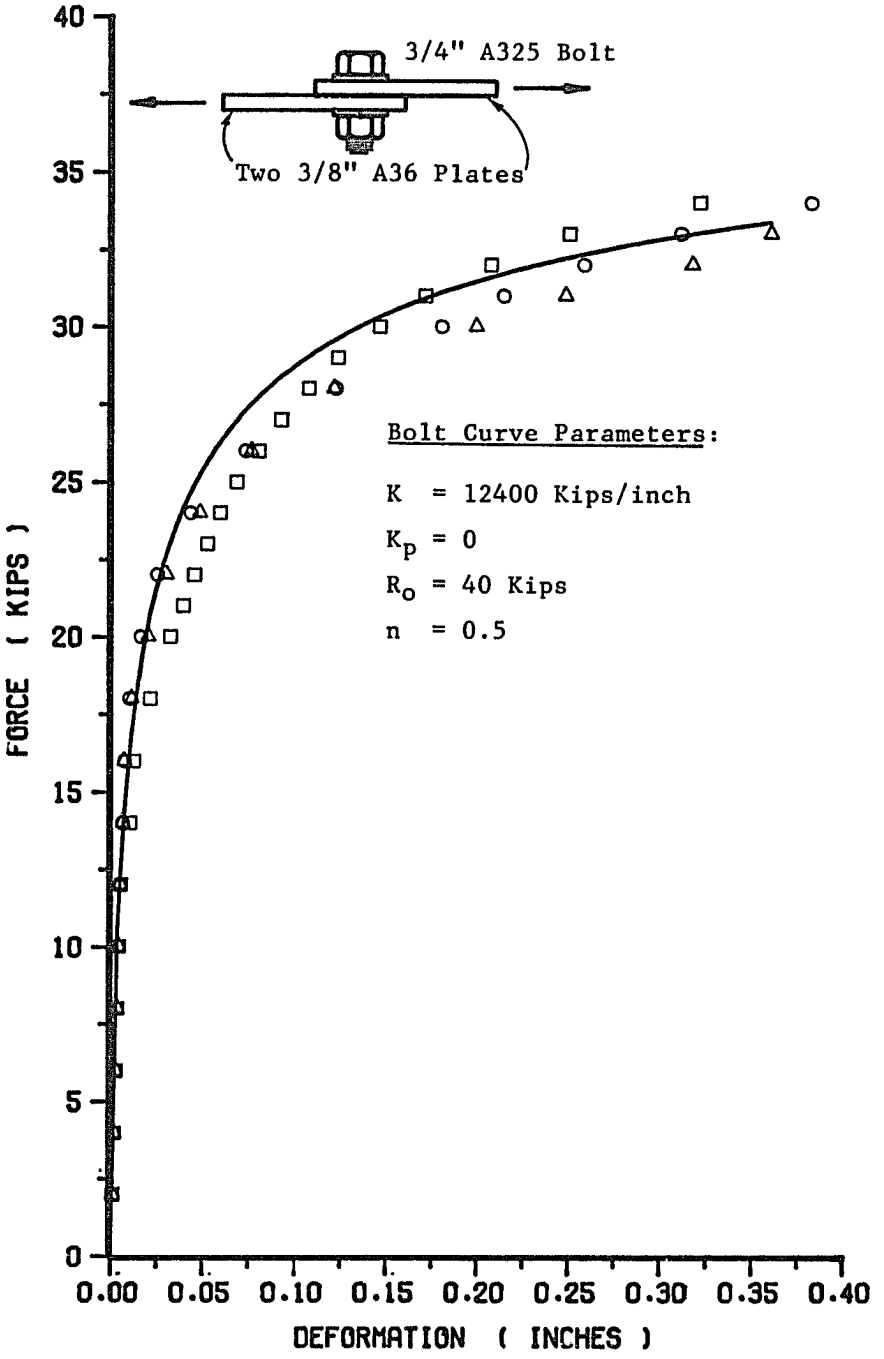

Figure 7. Single Shear Bolt Force-Deformation Behavior.

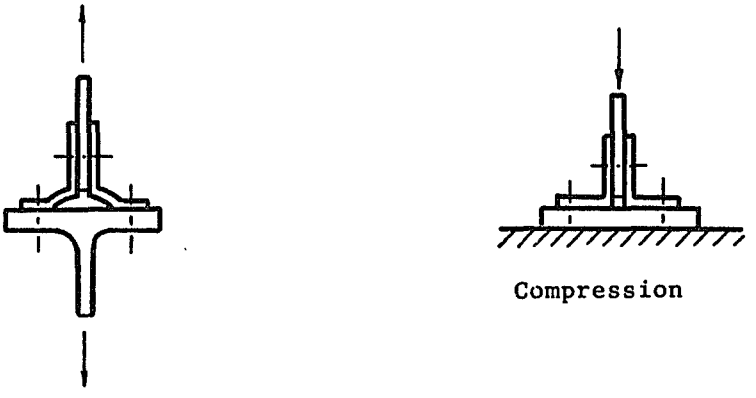

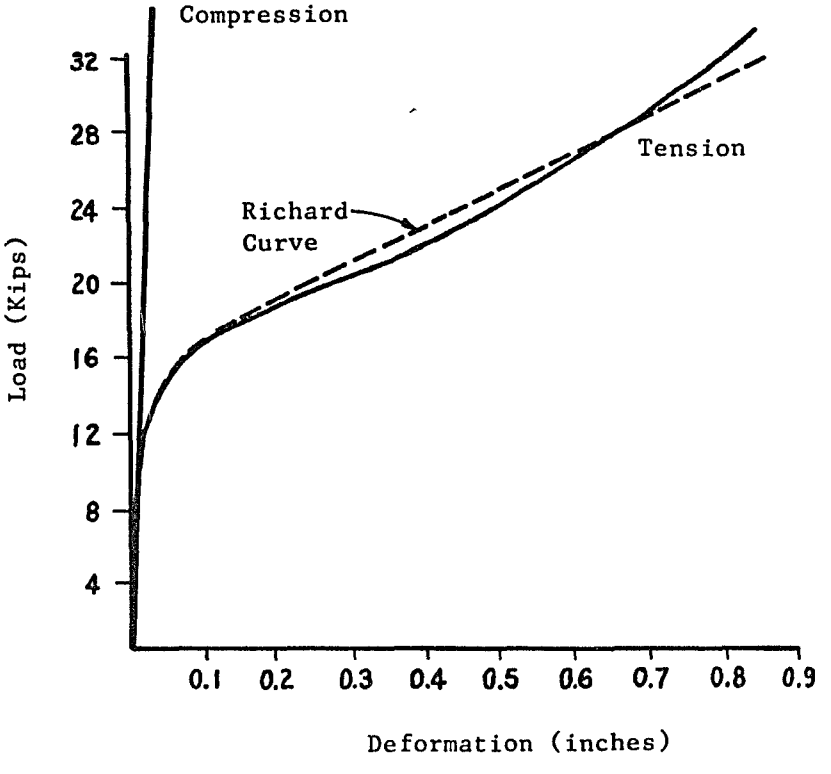

Figure 8. Force-Deformation Behavior of Bolted Double Angles.

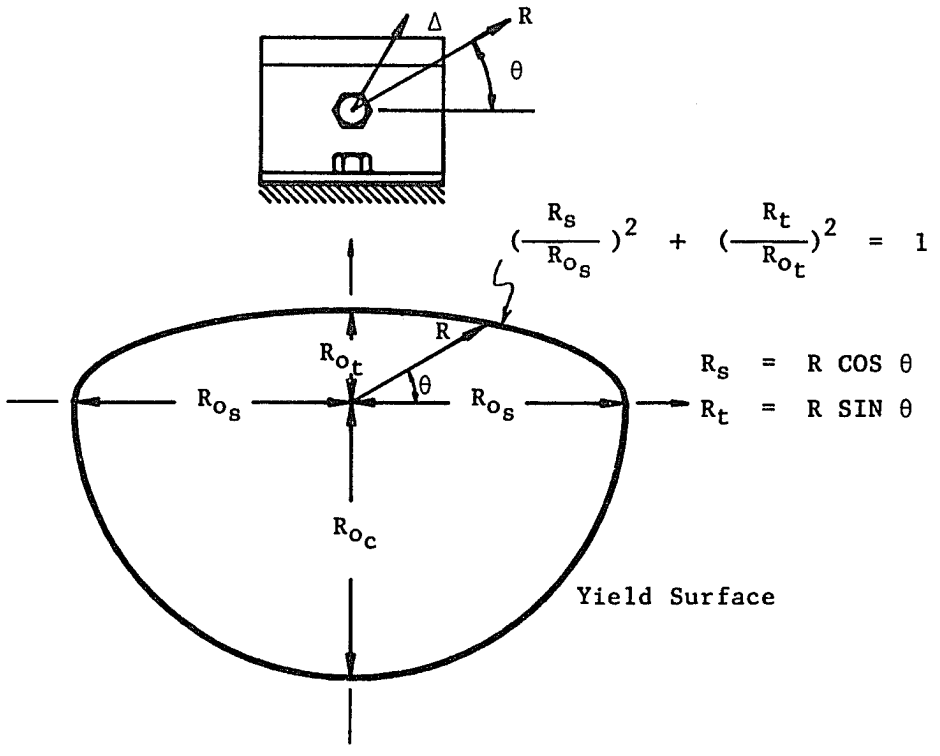

R_{o_t} = Tensile Strength

R_{o_c} = Compressive Strength

R_{o_s} = Shear Strength

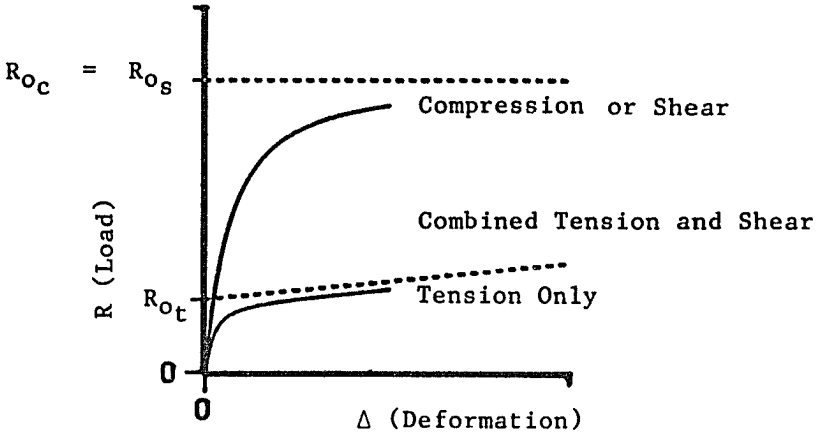

Figure 9. Anisotropic Yield Surface for Double Framing Angle Element.

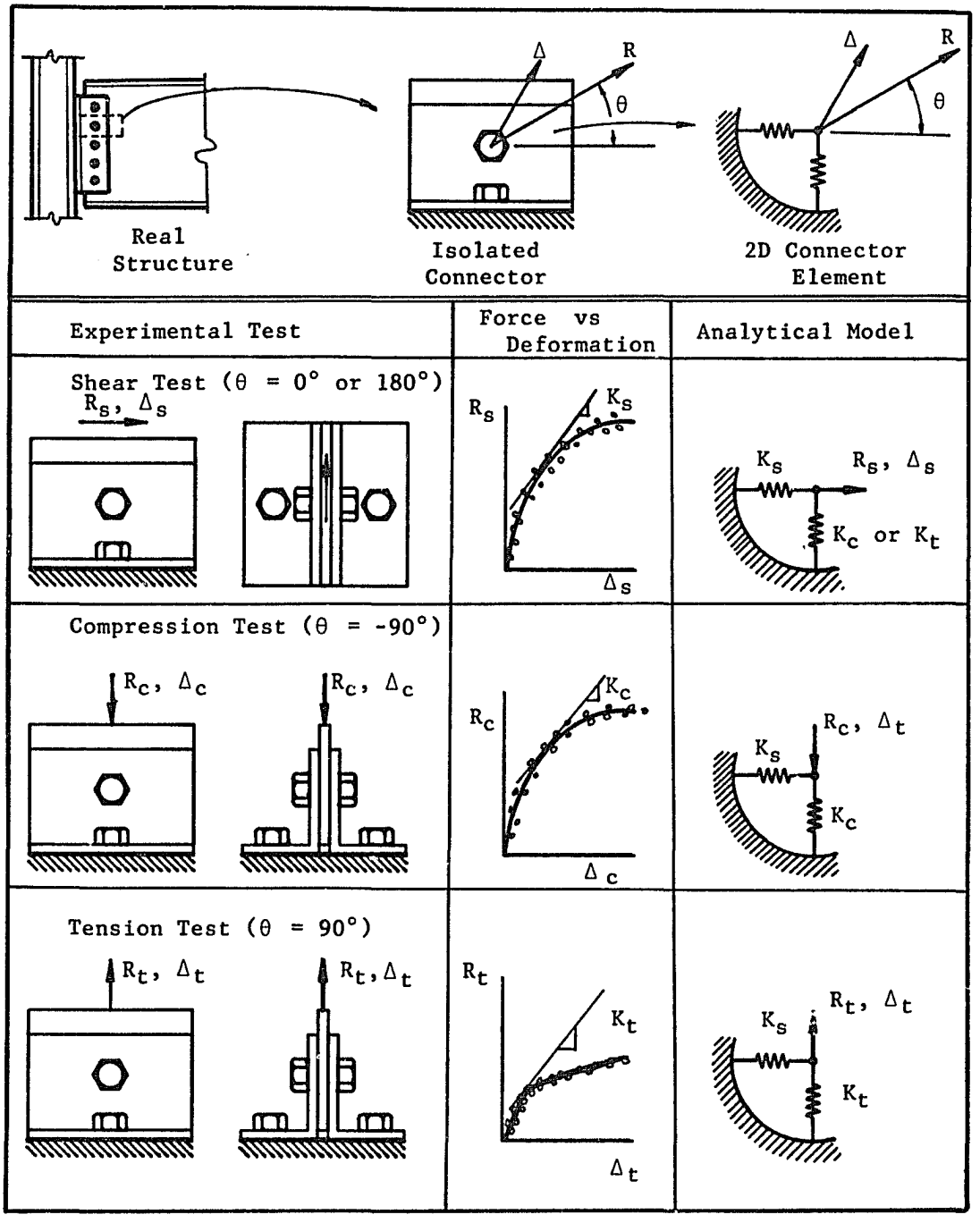

Figure 10. Formulation of Double Framing Angle Element.

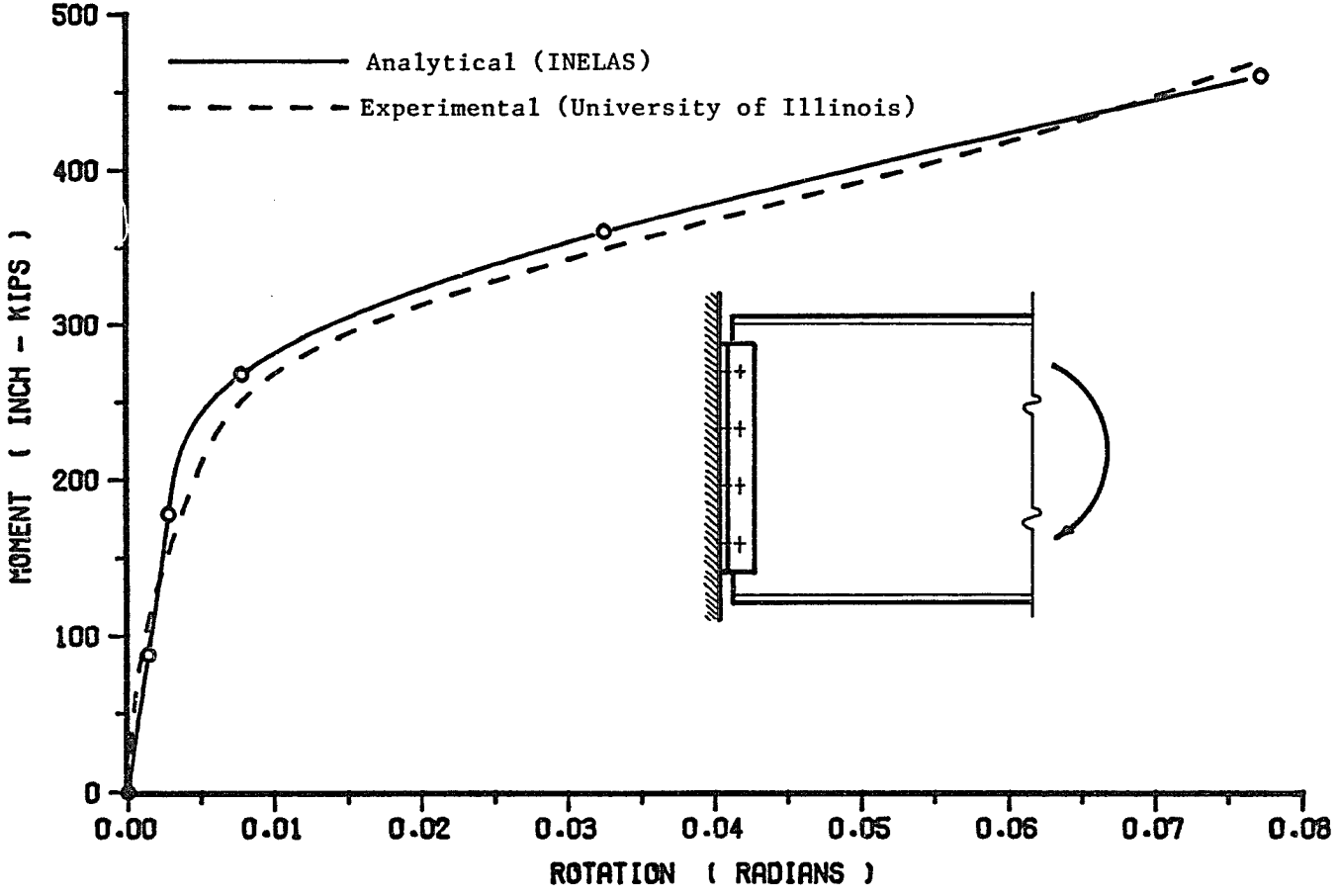

Figure 11. Comparison of Analytical and Experimental Results for a Four-Bolt Framing Connection

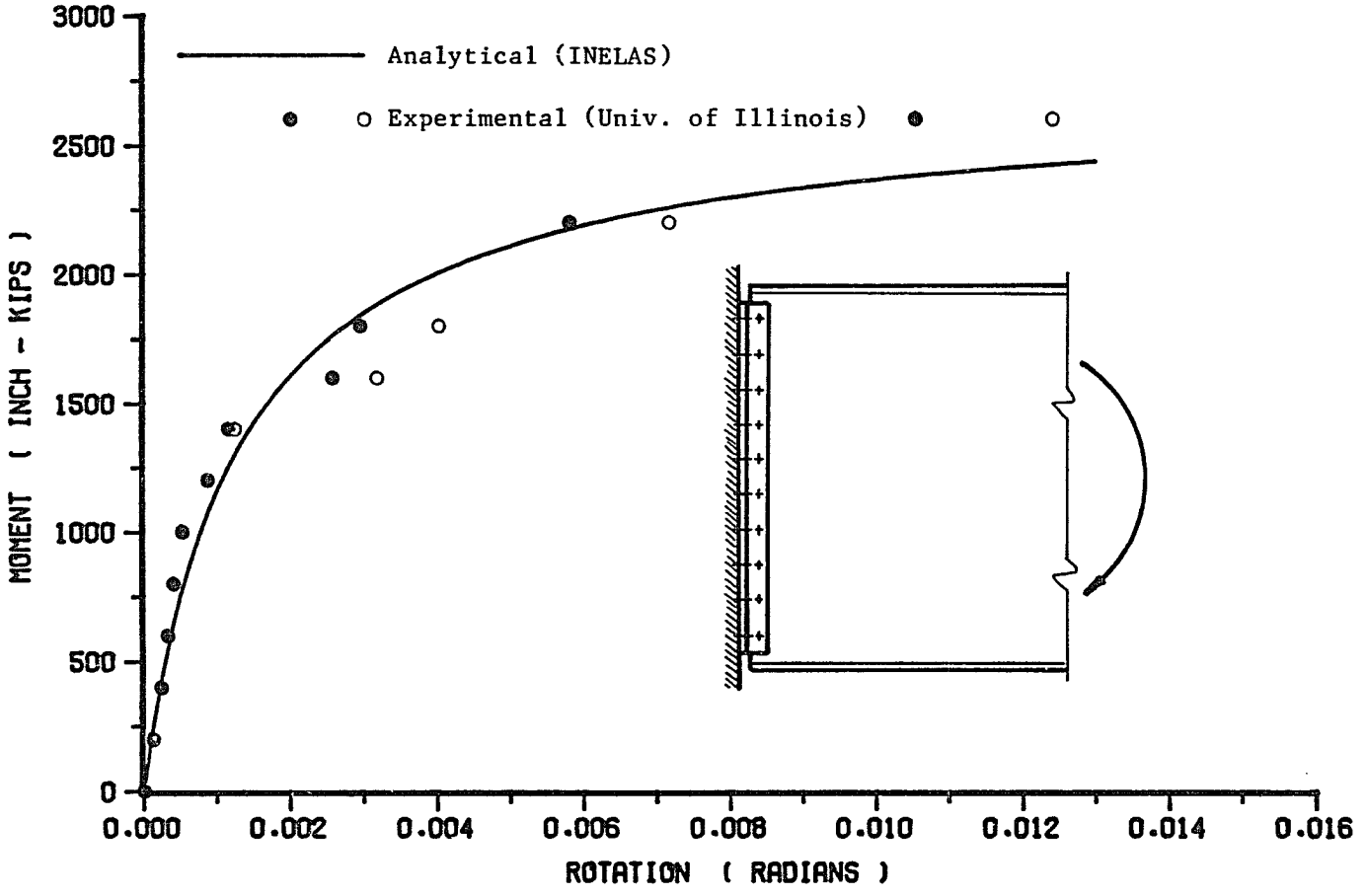

Figure 12. Comparison of Analytical and Experimental Results for a Ten-Bolt Framing Connection.

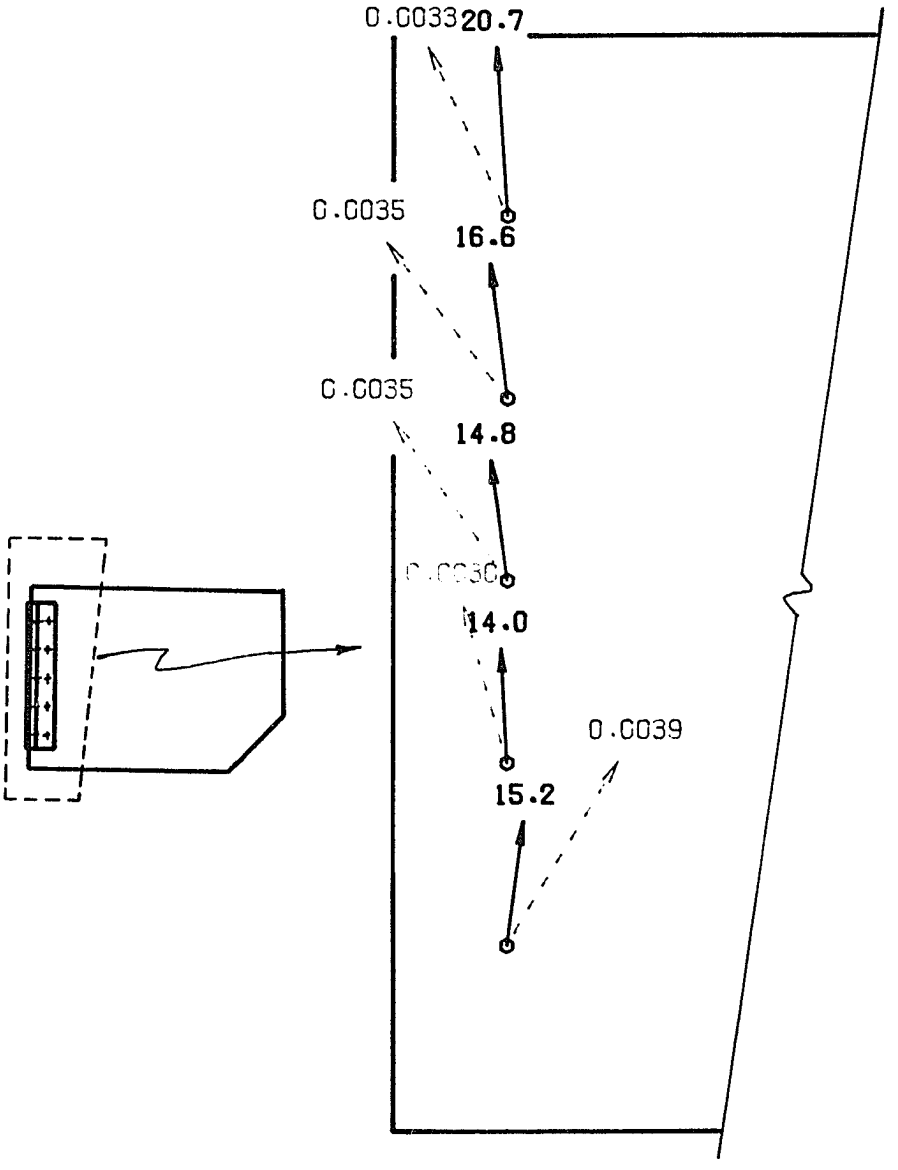

Figure 13. Anisotropic Behavior of Bolted Double Framing Angle Elements.

Chapter 3

PRELIMINARY STUDIES

Effect of Gusset Plates on Beam-to-Column Connections

In the diagonal bracing connection shown in Figure 14 the gusset plate is welded to the beam, and the beam-gusset combination is bolted to the column with double framing angles. To analyze this connection, the finite element model illustrated in Figure 15 was developed using the modeling techniques described in Chapter 2. The beam flanges were not connected to the column; therefore, the beam-to-column connection would normally be considered flexible. However, the finite element results demonstrated that the additional stiffness provided by the gusset plate causes the beam to develop end moments approximately equal to moments that would occur in an equivalent haunched fixed-end beam. Summarized in Table 1 are the actual (finite element), fixed-end uniform, and fixed-end haunched beam end moments at three different uniform load intensities which include nonlinear effects. It is noted that the gusset and its connectors may be subjected to the effects of the gravity loads acting on the beam in addition to the brace forces generated by lateral loads; however, these effects are not included herein.

Analytical vs. Experimental Studies

Results of six full-scale bracing connection tests conducted at the University of Alberta were published by Bjorhovde and Chakrabarti (4). Gusset plate geometries for 30°, 45°, and 60° bracing angles are shown in Figure 16. The gusset plate, beam, column, and bracing test setup for the 45° specimen is shown in Figure 17. Each specimen was tested with both 1/8" and 3/8" gusset plates; however, only the 1/8" plates were tested to failure because of load limitations on the test fixture. Summarized in Table 2 are the test schedules.

The finite element analysis techniques presented in Chapter 2 were used to model the University of Alberta tests (32). Two models were generated for each test conducted. Both models contained the gusset plate and its connectors, one with and one without the beam stub and its beam-to-column connection. Because the column stub was supported along its outer flange on the structural laboratory floor and the beam stub was free of load, these tests did not model the connections as they would occur in a real structure. However, by modeling these structures as tested, the modeling techniques could be verified. The deflected shapes, yield patterns, failure locations, strain magnitudes, and response of framing angles, welds, and bolts compared favorably between analytical and physical tests.

Table 3 describes the twelve models generated, each corresponding to a physical test. Example finite element meshes are

shown in Figures 18 and 19. These models were loaded to the maximum test load in increments of 50%, 35%, and 15%. Stress and strain distributions and bolt force and displacement vectors were plotted at each increment of load.

Strain gages located on both sides of the University of Alberta test plates were monitored at all increments of load. Slight eccentricities caused the strains in opposing gages to be unequal, indicating bending in the plates. For the experimental and analytical comparisons, these gage readings were averaged to eliminate out-of-plane bending effects. Compared in Figures 20 through 22 are the finite element and experimental strain values at critical gusset plate locations. In areas of low strain gradients, values agree quite well; however, in areas of high gradients the results differ significantly as may be expected. Strain values change by an order of magnitude at locations 1/2" apart in many of these high gradient zones. A finer element mesh in these areas would have provided better results.

Brace splice-to-gusset plate bolt force magnitudes and directions are shown in Figure 23. As predicted by previously reported tests and analyses of bolted splice joints (13) the force distribution is parabolic, and the outer bolts have approximately twice the load of the inner bolts.

Effective (von Mises) stress distributions are plotted in Figures 24 and 25 for the 45° 1/8" gusset model at 50% and 100% of the

total load. As the load increases from 50% to 100%, the stress gradients decrease significantly, indicating a redistribution of stresses as the steel yields. The contour pattern at the end of the splice plates matches the tear pattern at failure in the actual physical tests. All other models produced similar stress patterns indicating that the von Mises stress distributions around the brace-to-gusset connection depend only on the connection geometry, gusset plate thickness, and brace load. These conclusions support the block shear failure criterion presented in Chapter 4.

Table 1. Beam End Moments in Bracing Connection with Uniform Loading

MOMENTS	LOAD		
	WORKING	YIELD	2.25 X YIELD
Actual (Finite Element)	2757 k"	4063 k"	5855 k"
Fixed-End Uniform Beam	2520 k"	3780 k"	5670 k"
Fixed-End Haunched Beam	2814 k"	4221 k"	6331 k"
$\frac{\text{Actual}}{\text{Uniform}}$	1.09	1.07	1.03
$\frac{\text{Actual}}{\text{Haunched}}$	0.98	0.96	0.92

Table 2. University of Alberta Test Summary.

Test	Max Load (Kips)	Failure Location in Gusset
1/8" 30°	158	At last two bolt holes in splice plate bolt pattern
3/8" 30°	399	Did not fail
1/8" 45°	150	At last two bolt holes in splice plate bolt pattern
3/8" 45°	324	Did not fail
1/8" 60°	143	At holes connecting to column framing angles
3/8" 60°	320	Did not fail

Table 3. Finite Element Models Generated to Simulate the University of Alberta Tests.

Bracing Angle	Gusset or Beam-Gusset Model	Gusset Plate Thickness	Maximum Brace Load
30°	Gusset	1/8"	140 kips
	Beam-Gusset	1/8"	140 kips
	Gusset	3/8"	320 kips
	Beam-Gusset	3/8"	320 kips
45°	Gusset	1/8"	150 kips
	Beam-Gusset	1/8"	150 kips
	Gusset	3/8"	300 kips
	Beam-Gusset	3/8"	300 kips
60°	Gusset	1/8"	158 kips
	Beam-Gusset	1/8"	158 kips
	Gusset	3/8"	320 kips
	Beam-Gusset	3/8"	320 kips

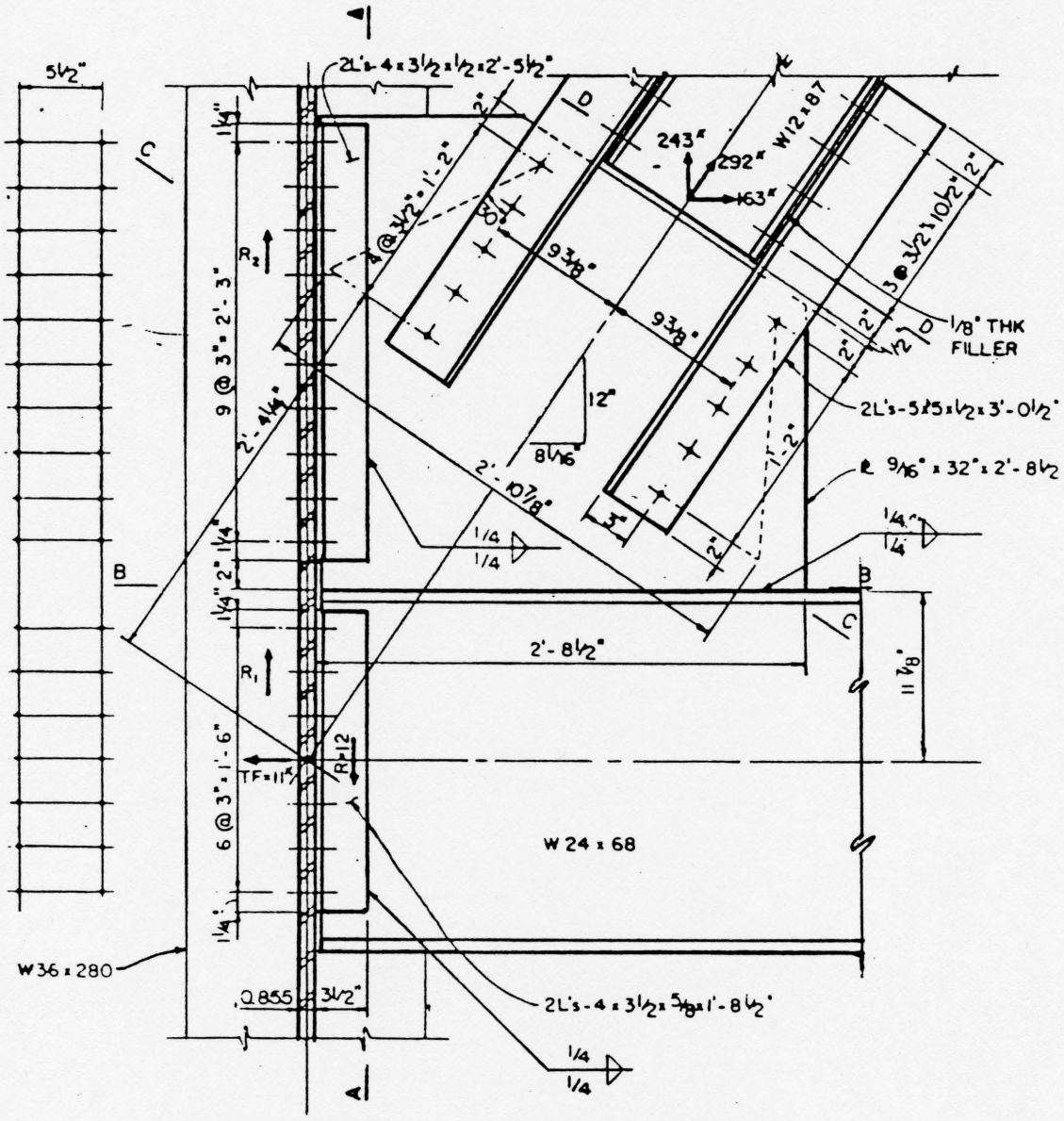

Figure 14. Diagonal Bracing Connection

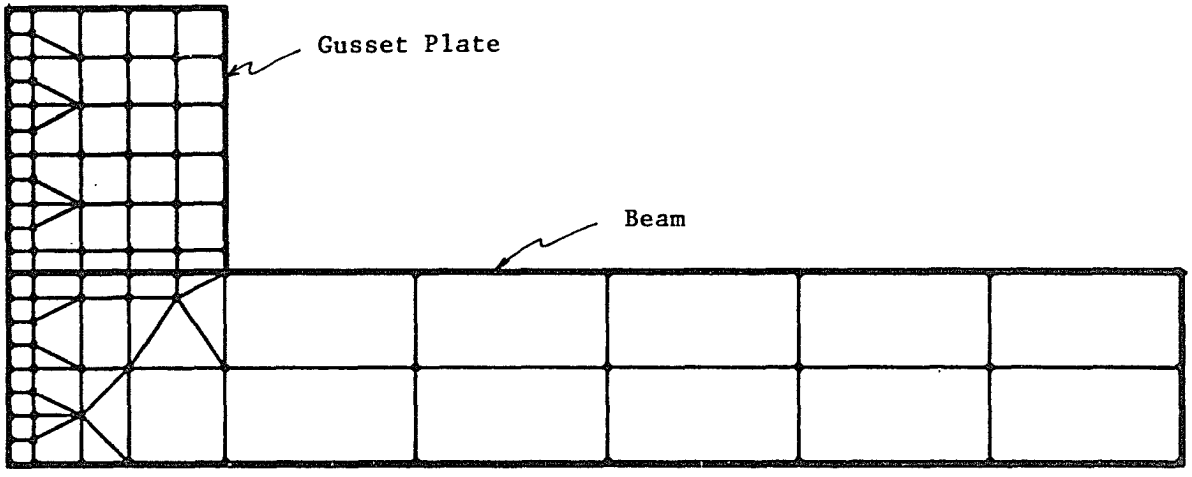

Figure 15. Finite Element Model of Diagonal Bracing Connection.

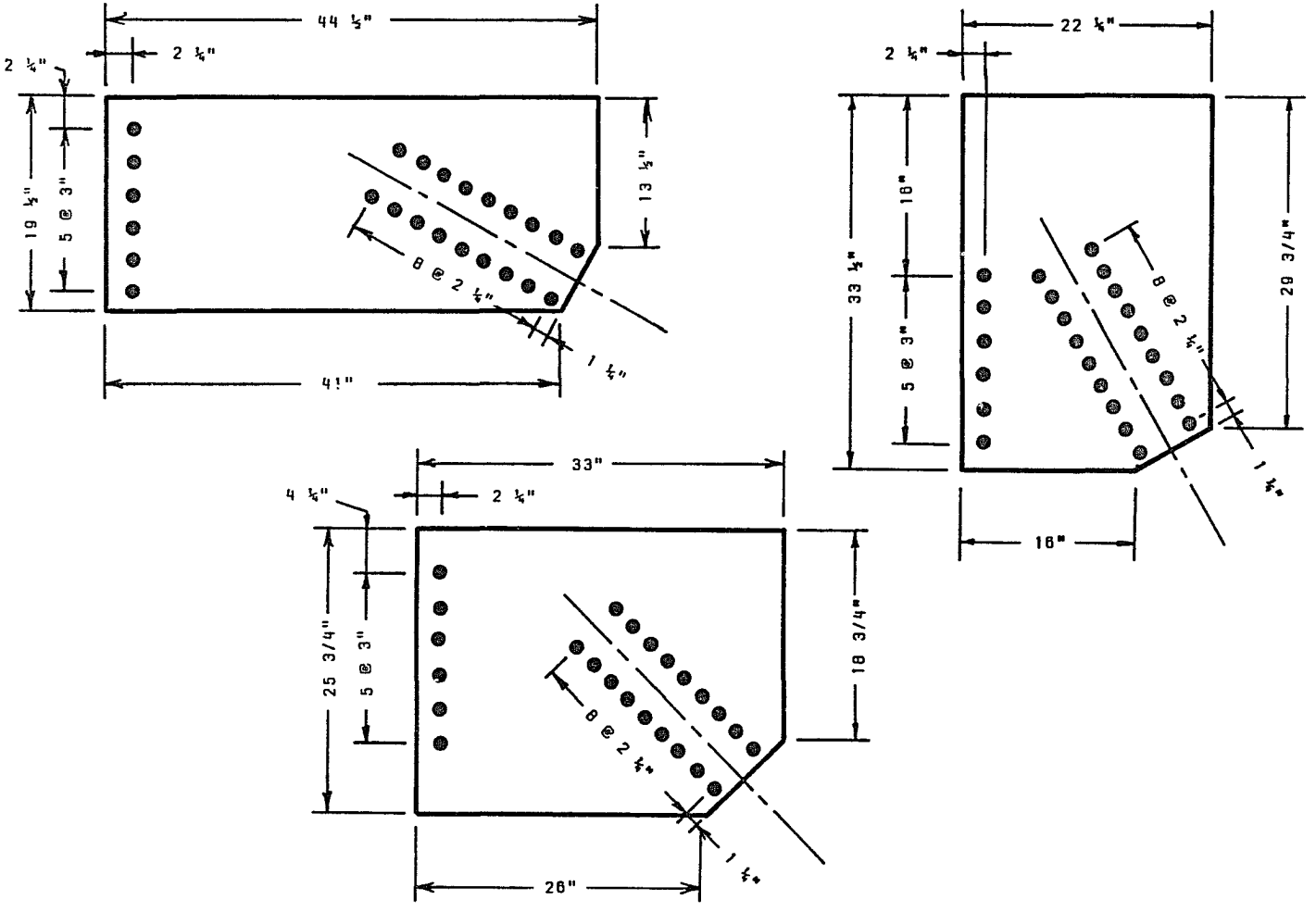

Figure 16. University of Alberta Gusset Plate Geometries.

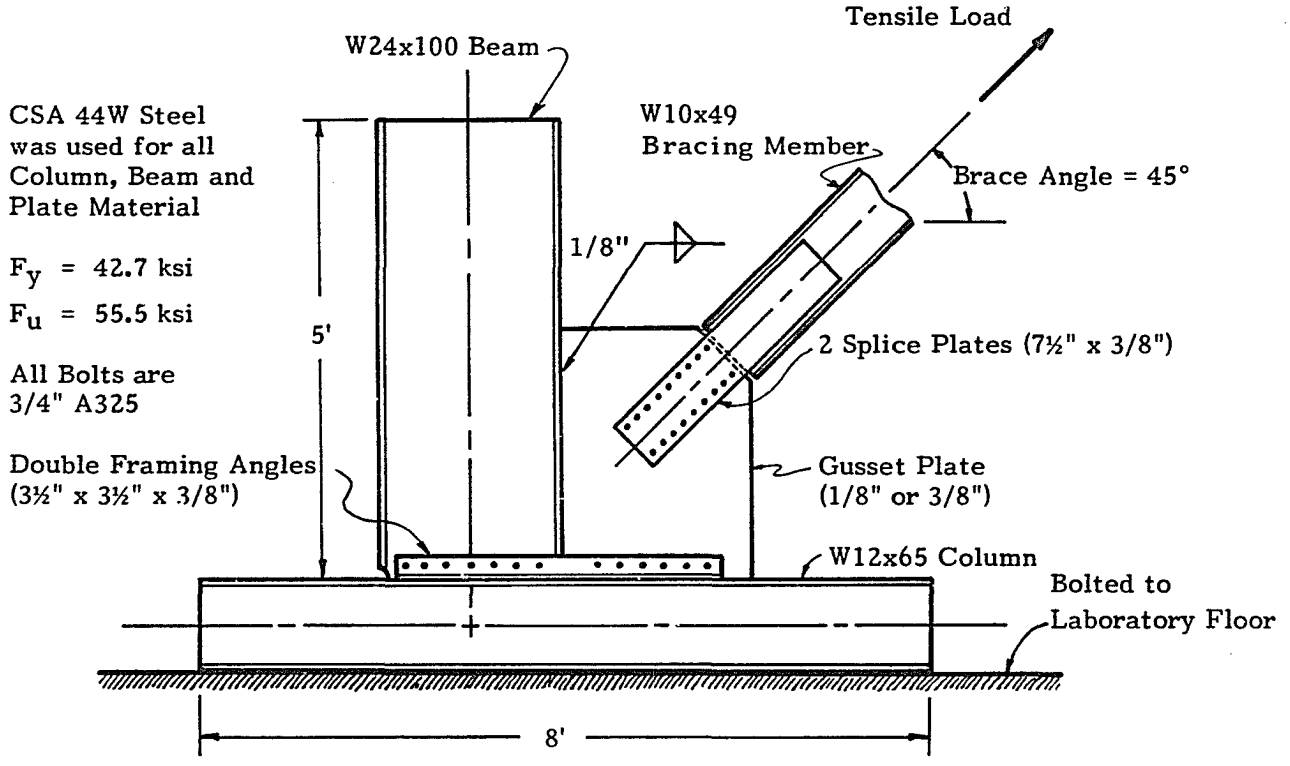

Figure 17. University of Alberta 45° Test Specimen.

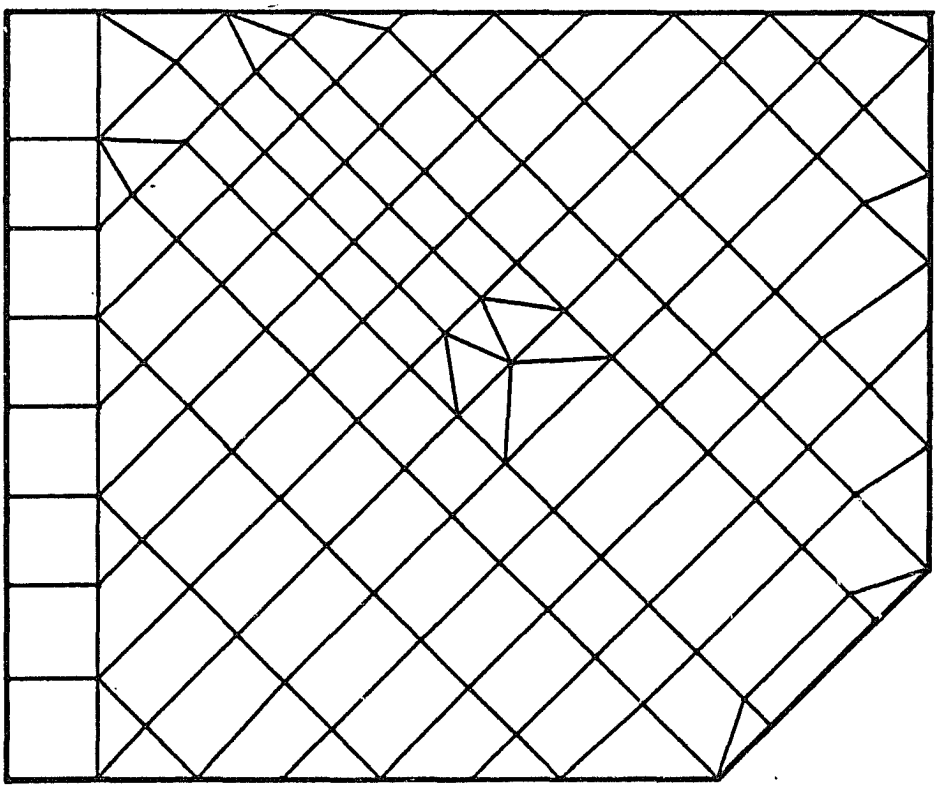

Figure 18. 45° Alberta Gusset Mesh.

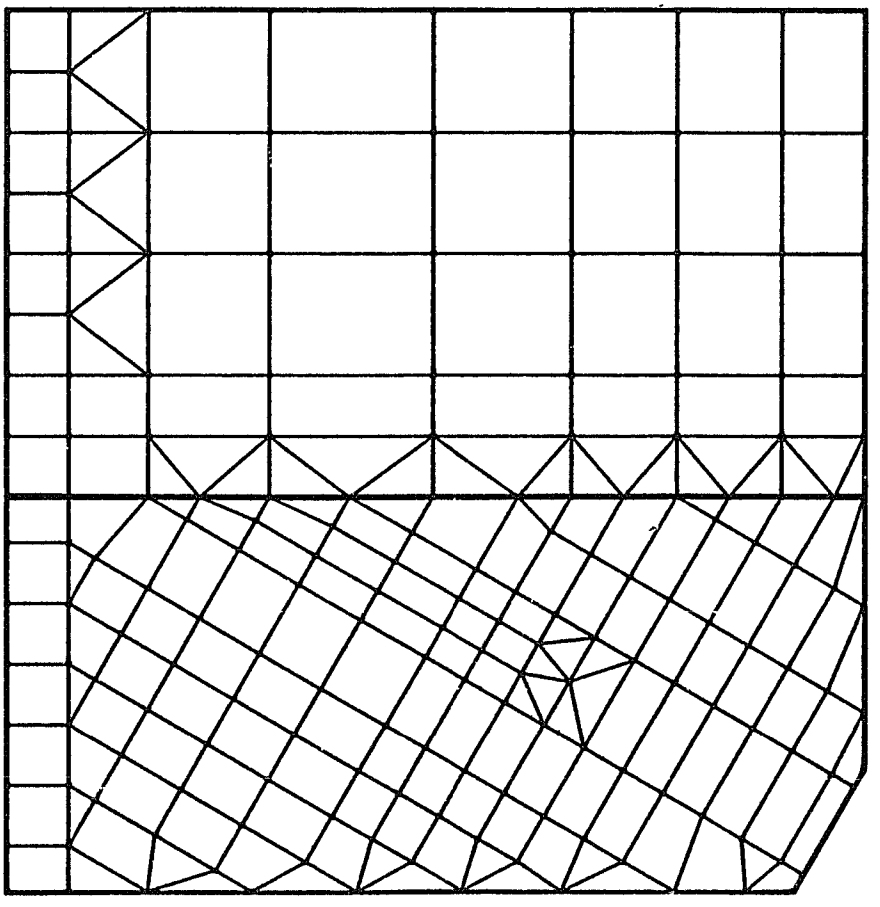

Figure 19. 60° Alberta Beam-Gusset Mesh.

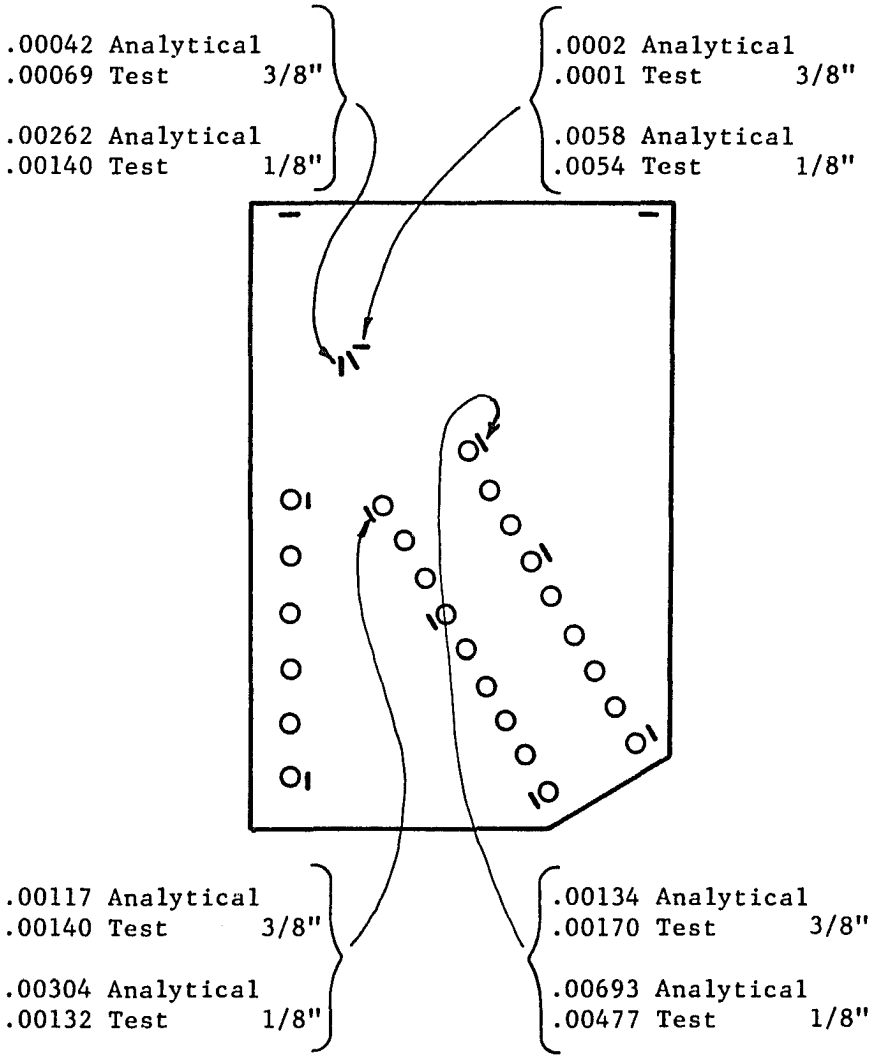

Figure 20. Comparison of Analytical vs. Test Strains for 30° Gusset.

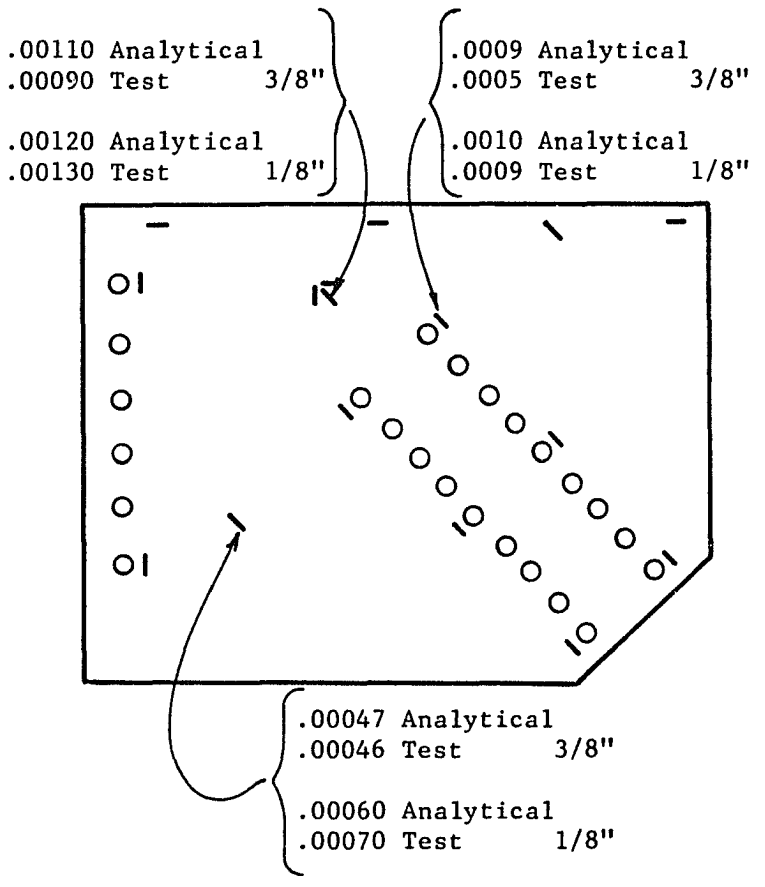

Figure 21. Comparison of Analytical vs. Test Strains for 45° Gusset.

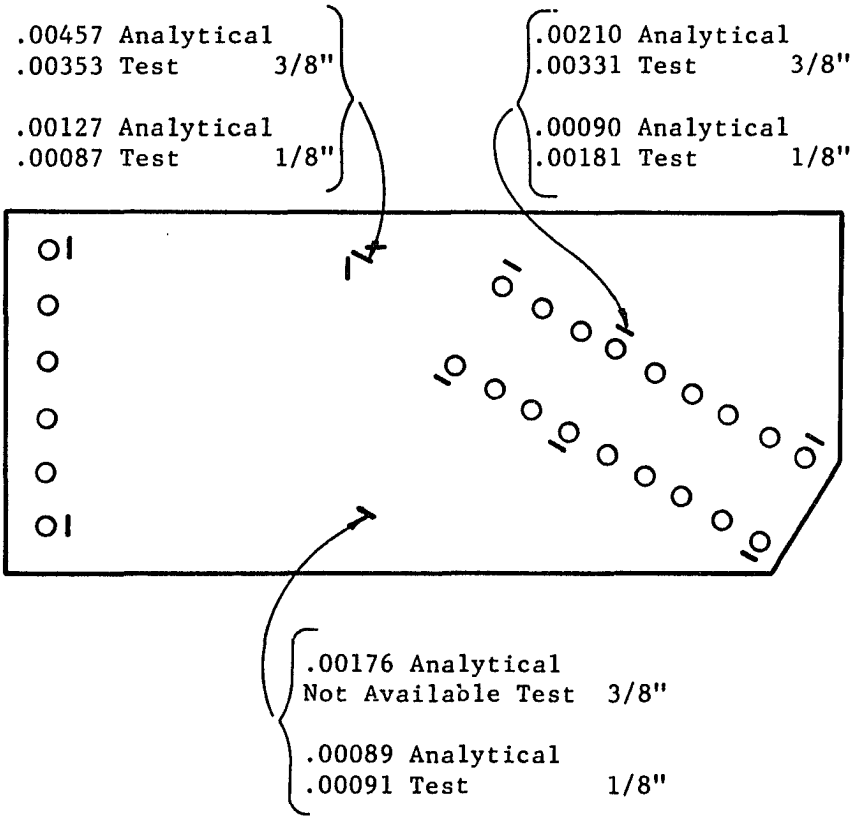

Figure 22. Comparison of Analytical vs. Test Strains for 60° Gusset.

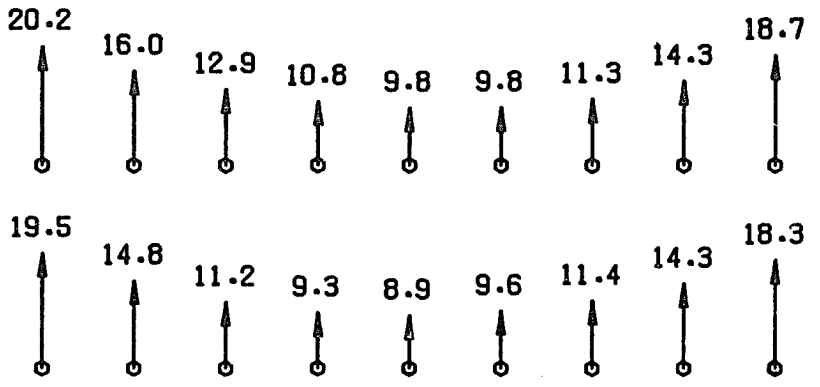

BOLT FORCE MAGNITUDES (KIPS)

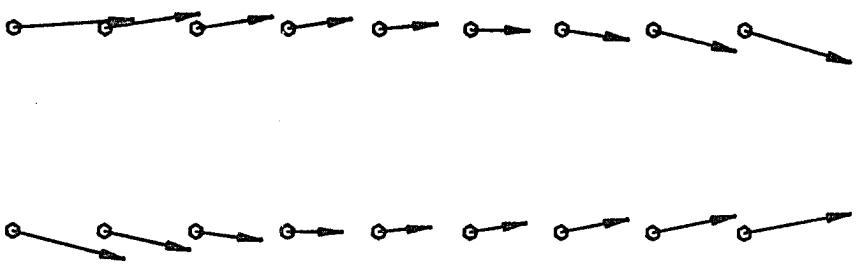

BOLT FORCE DIRECTIONS

Figure 23. Splice-to-Gusset Plate Bolt Force Distribution.

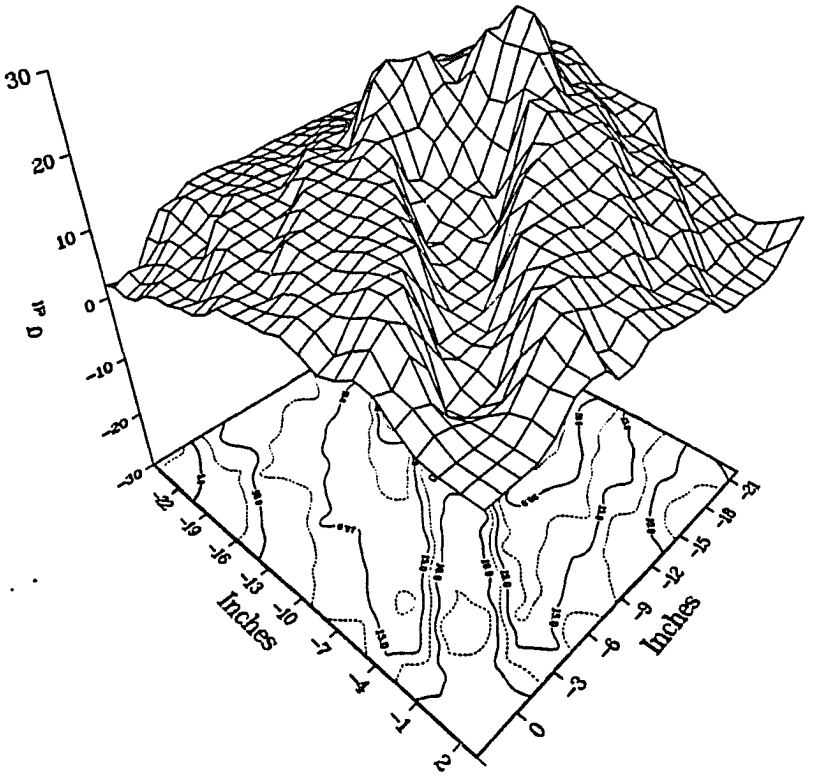

Figure 24. 45° 1/8" Gusset, Effective Stresses (ksi) at 50% of Total Load.

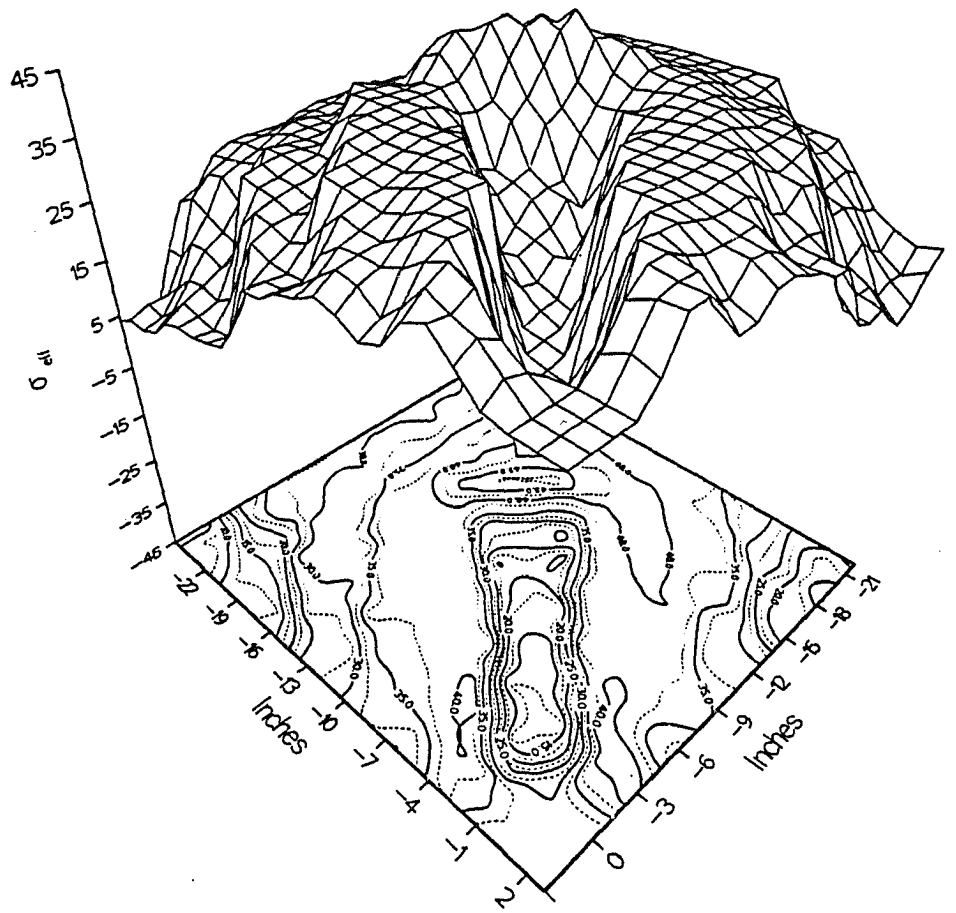

Figure 25. 45° 1/8" Gusset, Effective Stresses (ksi) at 100% of Total Load.

Chapter 4

TENSILE STRENGTH OF GUSSET PLATES

One major consideration to be made when designing a diagonal bracing connection is the determination of an adequate gusset plate thickness to resist the tensile brace loads. Early design methods relied on the application of elementary beam equations ($\sigma = P/A \pm Mc/I$ and $\tau = VQ/Ib$) to critical sections through the gusset (40). These critical sections were found by trial and error, and from the previous experience of the connection designer. As shown in Figure 26, the early methods based on beam assumptions are at best approximate (42), particularly at the plate edges.

Whitmore Criterion

In 1952, Whitmore (42) presented an alternative design criterion to the beam formulas. A scaled typical Warren truss bridge gusset plate, as illustrated in Figure 26, which was fabricated from aluminum and had extensive instrumentation, was tested at the University of Tennessee.

High strains were measured at the ends of the tension and compression diagonals. The "Whitmore criterion" was established from this test to predict the maximum normal stress in a gusset plate. This criterion assumes that the brace force is distributed uniformly over an

effective area which is computed by multiplying the gusset plate thickness by an effective length, which is determined by constructing 30° line segments from the beginning to the end of the bolt pattern, as shown in Figure 27. The finite element results obtained in this study support the validity of the Whitmore criterion. Note that the 30° Whitmore pattern is similar to the maximum effective stress pattern illustrated in Figure 25.

Block Shear Criterion

More recently, a gusset plate design method has been developed based on the block shear concept, as discussed in the 8th edition of the AISC commentary section 1.5.1.2. (21). The block shear concept was initially developed from experimental and analytic studies to determine the web strength of coped beams (3, 43, 25). Richard (32) developed a modified block shear criterion in which it is assumed that the plate will fail along the gross section of the bolt pattern in large diagonal bracing connections. The gross section is used because the interior bolts generally do not slip into bearing as illustrated in Figure 23. The strength of a gusset plate may be determined by combining the tensile stress resultant acting at the end of the bolt pattern along with the shear stress resultants acting along the sides of the bolt pattern.

Referring to Figure 28, the block shear ultimate, yield, and working loads of a gusset plate are calculated as follows:

$P_u = A_{vg} F_{vu} + A_{tg} F_{tu}$ = block shear ultimate load

$P_y = A_{vg} F_{vy} + A_{tg} F_{ty}$ = block shear yield load

$P_a = 0.6 P_y$ = block shear allowable (working) load

where,

$A_{vg} = (2)(L)(t)$ = gross shear area

$A_{tg} = (s)(t)$ = gross tensile area

L = bolt pattern length

s = bolt pattern width

t = gusset plate thickness

$F_{vu} = F_y / \sqrt{3}$ = shear ultimate stress

$F_{tu} = F_u$ = tensile ultimate stress

$F_{vy} = F_y / \sqrt{3}$ = shear yield stress

$F_{ty} = F_y$ = tensile yield stress

Thus, the minimum required gusset plate thickness for working stress design is

$$t_{reqd} = P (2 L / \sqrt{3} + s) / 0.6 F_y$$

where P is the brace load obtained from the braced frame analysis.

The block shear concept for gusset plate design evolved from the study of the effective stress contour plots similar to the plot shown in Figure 25. Although not presented here, the maximum shear stress contour plots support the block shear concept equally well. As shown in Figure 29, a typical load-deformation curve obtained from the finite element analysis validates the block shear concept and

shows that gusset plates have considerable reserve strength. As illustrated in Figure 30, the block shear criterion and the Whitmore criterion give identical gusset plate yield strengths. However, the block shear failure pattern does not extend outside of the plate boundaries like the Whitmore pattern may in some cases as shown in Figure 27. The block shear criterion also unifies concepts currently used in design practice.

The block shear ultimate load for the 1/8" gusset plates tested at the University of Alberta is:

$$P_u = [(2)\ (8)\ (2.25")\ (42.7\ ksi)\ /\sqrt{3}$$
$$+\ (5.0")\ (55.5\ ksi)]\ (0.125") = 146\ kips$$

which is in excellent agreement with the experimental ultimate loads of 140, 150, and 158 kips.

Hardash and Bjorhovde (17) developed a more complex block shear design formula based on ultimate strength tests of gusset plates at the Universities of Illinois (20), Alberta (4), and Arizona (17). However, for large bracing connections the two formulas give comparable results. When applied to smaller connections, the formula presented above is conservative by 10% to 30%. In the case of bracing connections containing less than six bolts per row, it may be appropriate to use the net shear area, as opposed to the gross shear area in the block shear formula.

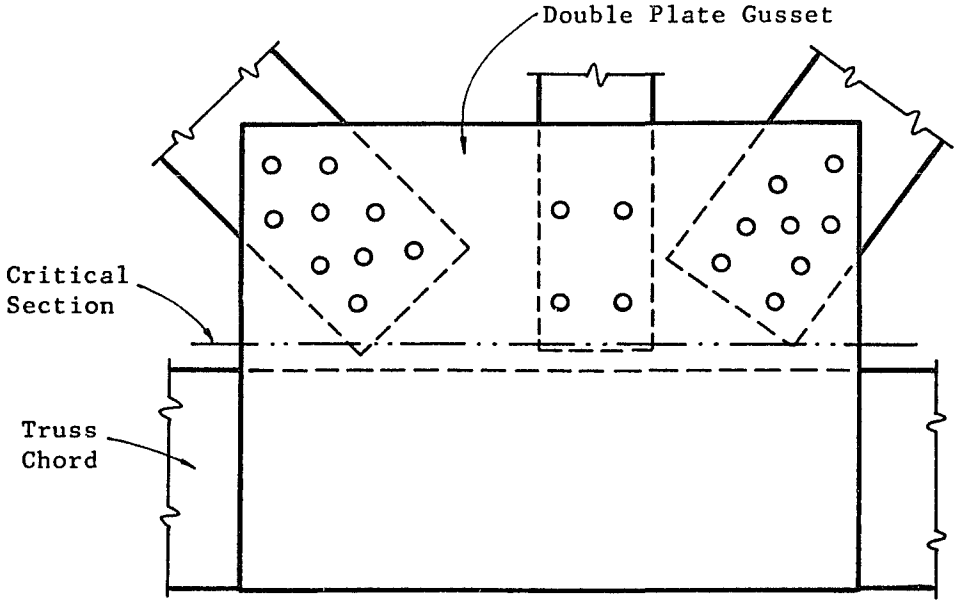

Warren Truss Connection

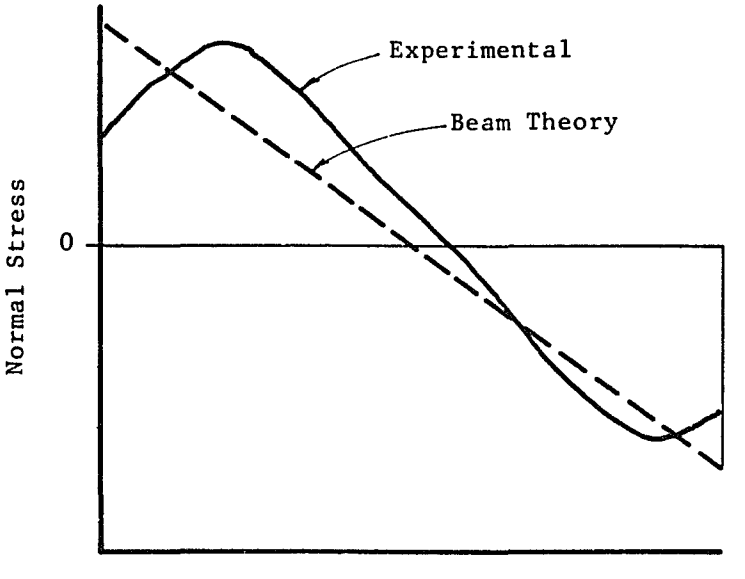

Distance Along Critical Section

Figure 26. Whitmore Gusset Plate and Stress Distributions.

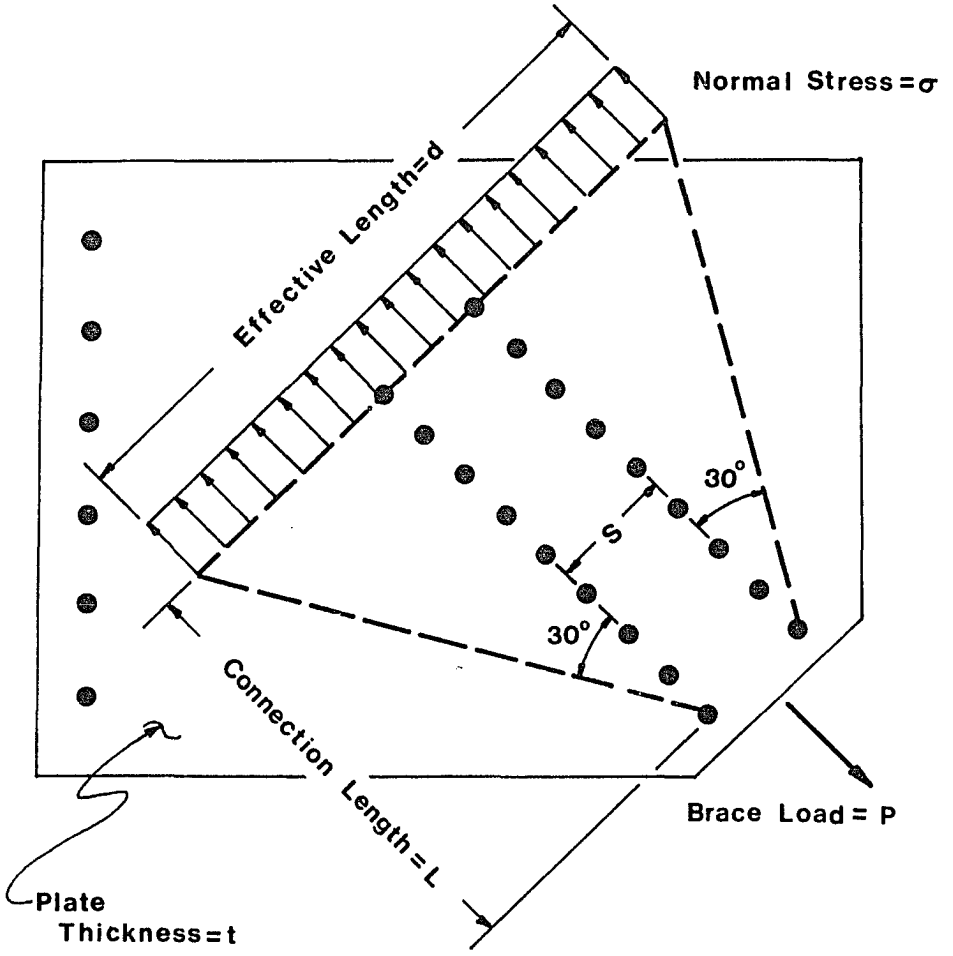

Effective Area = d t

P = Aσ

Figure 27. The Whitmore Criterion.

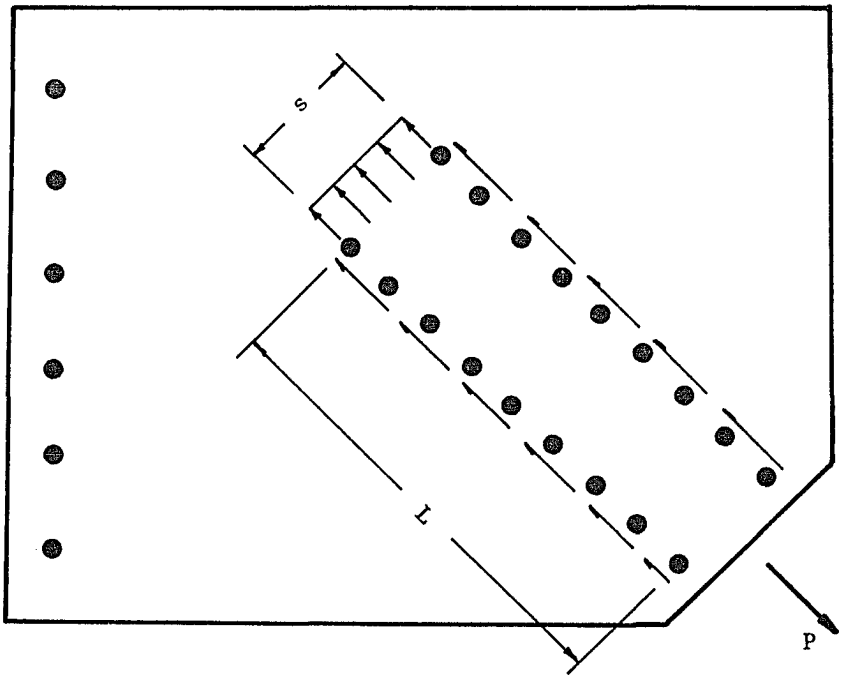

$P_y = (2L/\sqrt{3} + s)t\ F_y$ = Block Shear Yield Load

$P_u = (2L\ F_y/\sqrt{3} + sF_u)t$ = Block Shear Ultimate Load

where,

t = gusset plate thickness

L = connection length

s = connection width

F_y = tensile yield stress

F_u = tensile ultimate stress

Figure 28. The Block Shear Criterion.

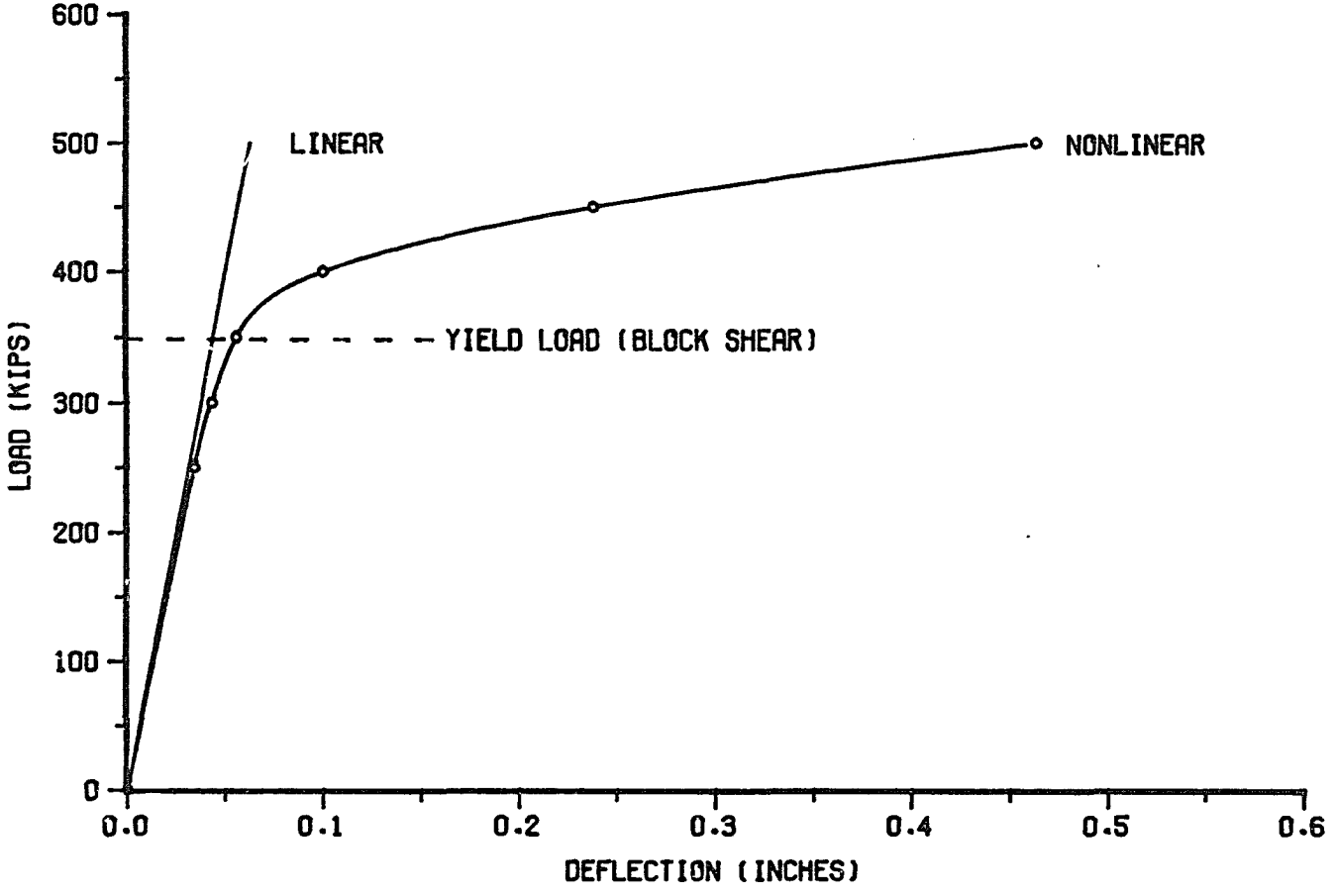

Figure 29. Gusset Plate Load vs. Deformation Response.

Whitmore Criterion

L = Bolt Pattern Length

S = Bolt Pattern Width

F_y = Yield Stress

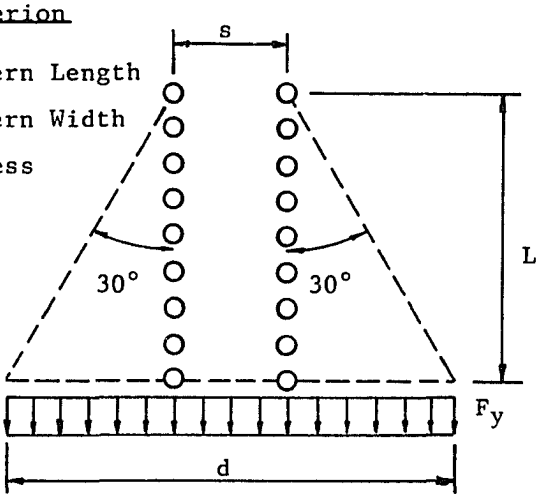

$$P_y = F_y t d = F_y t\ (s + 1.15L) \qquad d = s + 2L \tan 30^\circ$$

Block Shear Criterion

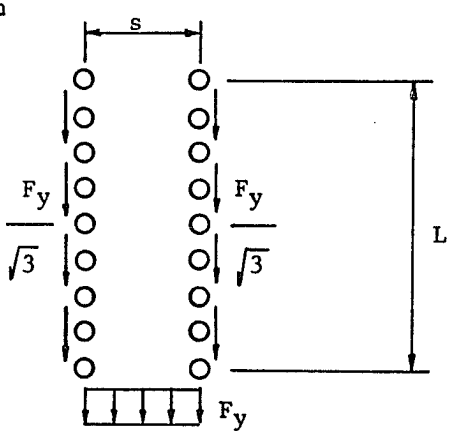

$$P_y = F_y ts + 2tL\ F_y/\sqrt{3} \quad = \quad F_y t\ (s + 1.15L)$$

Thus, Block Shear and Whitmore give the same result.

Figure 30. Comparison of Block Shear and Whitmore Criteria.

Chapter 5

FINITE ELEMENT MODELS

To determine the gusset-to-frame fastener force distributions, 51 different finite element models were generated and analyzed. To study the effect of various parameters, the following connection and frame properties were varied:

- bracing configurations: single, drag through, double, and the K-brace
- brace angles: 30°, 45°, and 60°
- brace loads: working, yield and ultimate
- column-to-beam stiffness ratios: from 0.03 to 1.73
- gusset-to-frame fastener modes: bolted double angles and welds
- plate dimensions: from 24" x 46" to 58" x 24"
- brace eccentricities: from -8" to +14"

All gussets utilized 3/8" thick A36 steel plates. Analysis of the gusset plates for the K-bracing configurations is discussed in Chapter 8.

Shown in Figures 31 through 33 are three of the bracing configurations considered in this study. Illustrated in Figure 31 is the single gusset configuration, where only one gusset exists at the beam-column-brace intersection. The arrangement shown in Figure 32, wherein alternate bays are braced, causes a drag through force;

therefore, it is called the drag through configuration. The double gusset configuration is depicted in Figure 33. Summarized in Table 4 are the models generated to determine the force distributions in diagonal bracing connections. A fourth arrangement, the K-brace configuration, will be discussed separately in Chapter 8 since the gusset does not connect to a column.

As shown in Figure 34, a subassembly can be isolated from the braced frame for analysis. As discussed in Chapter 3, the presence of the gusset plate results in rigid (AISC Type I) beam-to-column connections. Therefore, a portal frame analysis model is valid wherein inflection points occur at the mid-story height of the columns. Thus, pin supports can be used to provide the boundary conditions for the subassembly. Shown in Figures 35 through 38 are the typical finite element models of the subassemblies.

Bracing members were connected to the gusset plates with splice plates. These splice plates were bolted to the gusset with 18 A325 bolts as shown in Figure 39. The block shear yield load was calculated as described in Chapter 4:

$$P_y = [(2)(8)(2.25") / \sqrt{3} + 5."](0.375")(36\ ksi) = 348\ kips$$

To insure that the gusset plate would be subjected to brace loads in excess of the block shear yield load, a lateral load of 500 kips was applied to the rigid bar, as shown in Figure 34. This load represents

the lateral loads originating in the above stories of the frame, and was applied in six increments of 30%, 10%, 10%, 10%, 20%, and 20%.

The brace angle, as shown in Figure 34, is defined as the angle that the bracing member makes with the beam. To envelop most configurations found in practice, brace angles of 30°, 45° and 60° were considered.

Three column sections (a weak axis W12x65, a strong axis W12x65, and a strong axis W24x100) were used to study the effect of the column-to-beam bending stiffness ratios. The length (or story height) of all columns was kept constant at 16', resulting in beam lengths (or bay widths) of approximately 28', 16', and 9' for the 30°, 45°, and 60° brace angles respectively. A W24x100 was utilized for all beam sections. Thus, the column-to-beam stiffness ratio, as defined below, varied from 0.03 to 1.73.

$$\text{Stiffness Ratio} = (I_c/L_c) \;/\; (I_b/L_b)$$

where

I_c = column moment of inertia

L_c = column length

I_b = beam moment of inertia

L_b = beam length

A number of fastener modes are available to connect the gusset plate to the framing members. These include combinations of bolts, welds, double angles, single plates (shear tabs), and structural tees.

Of these possibilities, bolted double angles are the most flexible, while welds are the stiffest. Therefore, to envelop all possible combinations, a bolted-welded design was compared to a welded-bolted design, as depicted in Figure 40. This comparison was made using the single gusset configuration. The difference between the two fastening designs was not significant; therefore, a welded-welded design was used for all other bracing configurations including the eccentric connection models. To assure an even transfer of load, the gusset was connected along the entire length of the plate edges.

Listed in Table 5 are the gusset plate dimensions studied. These dimensions are required to provide sufficient space to attach the bracing member to each plate. In addition, if the brace, beam, and column axes are required to intersect at a common working point, the plate dimensions are increased significantly. However, if the working point requirement is eliminated, then the plate dimensions decrease and the connection becomes eccentric, as shown in Figure 41. The frame must be designed to accommodate the moment generated by this eccentricity, as discussed in Chapter 10. All but the nine eccentric models used the working point configuration. The gusset plate dimensions of nine models were minimized creating a compact, yet eccentric connection. In these analyses the eccentricity is positive if it causes a positive moment (right-hand rule) on the frame when the brace is subjected to tension.

Table 4. Finite Element Models Generated to Determine the Gusset-to-Frame Force Distributions

Bracing Configuration	Gusset-to-Column Fastener Type	Gusset-to-Beam Fastener Type	Number of Models*
Single	Bolted	Welded	9
Single	Welded	Bolted	9
Drag Through	Welded	Welded	9
Double	Welded	Welded	9
Single (Eccentric Brace)	Welded	Welded	9

*Each set of 9 models contains all combinations of 30°, 45°, and 60° brace angles matched with weak axis W12x65, strong axis W12x65, and strong axis W24x100 columns.

Table 5. Gusset Plate Dimensions and Eccentricities

Brace Angle	Column Sections*	Working Point Models (e=0) a	b	Eccentric Models a	b	e
30°	W12 x 65 (WA)	58"	24"	30"	24"	14"
30°	W12 x 65 (SA)	52"	24"	30"	24"	11"
30°	W24 x 100 (SA)	46"	24"	30"	24"	8"
45°	W12 x 65 (WA)	39"	27"	27"	27"	8"
45°	W12 x 65 (SA)	33"	27"	27"	27"	4"
45°	W24 x 100 (SA)	27"	27"	27"	27"	0"
60°	W12 x 65 (WA)	27"	30"	24"	30"	3"
60°	W12 x 65 (SA)	24"	35"	24"	30"	-3"
60°	W24 x 100 (SA)	24"	46"	24"	30"	-8"

*WA - Weak axis column
SA - Strong axis column

a = horizontal dimension of gusset plate
b = vertical dimension of gusset plate
e = connection eccentricity

Dimensions a, b, and e are depicted in Figure 41.

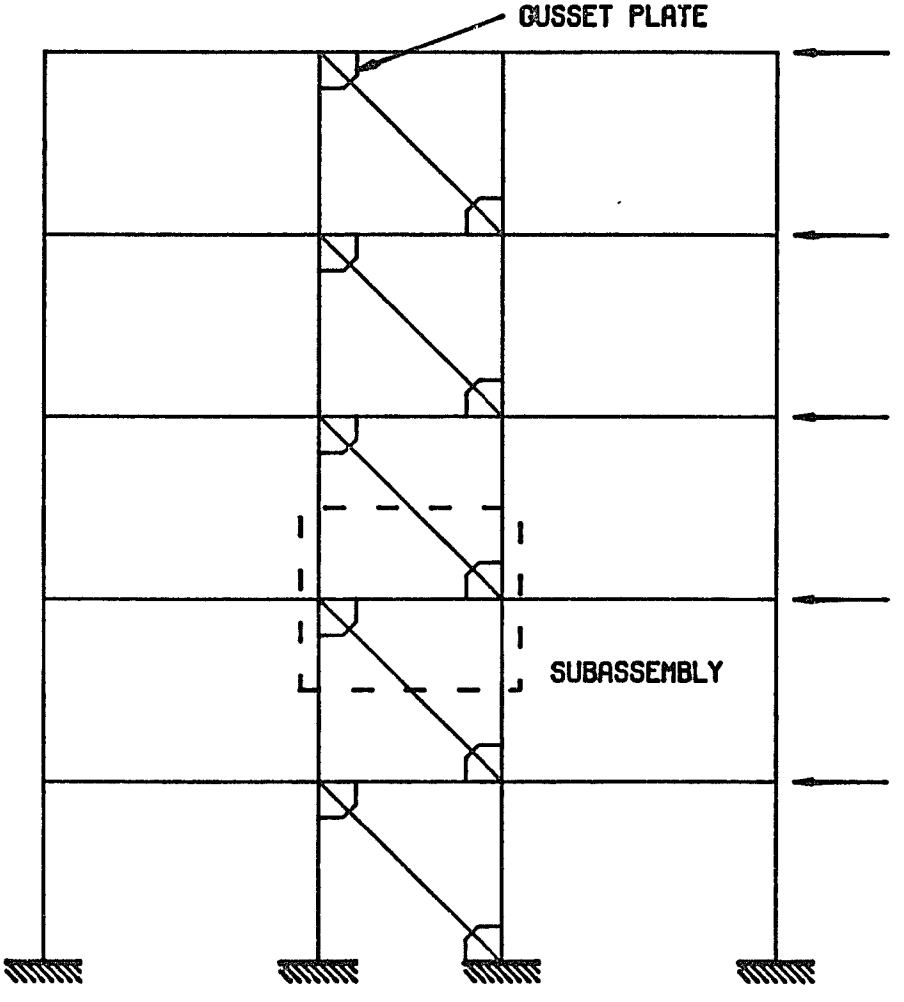

Figure 31. Single Bracing Configuration.

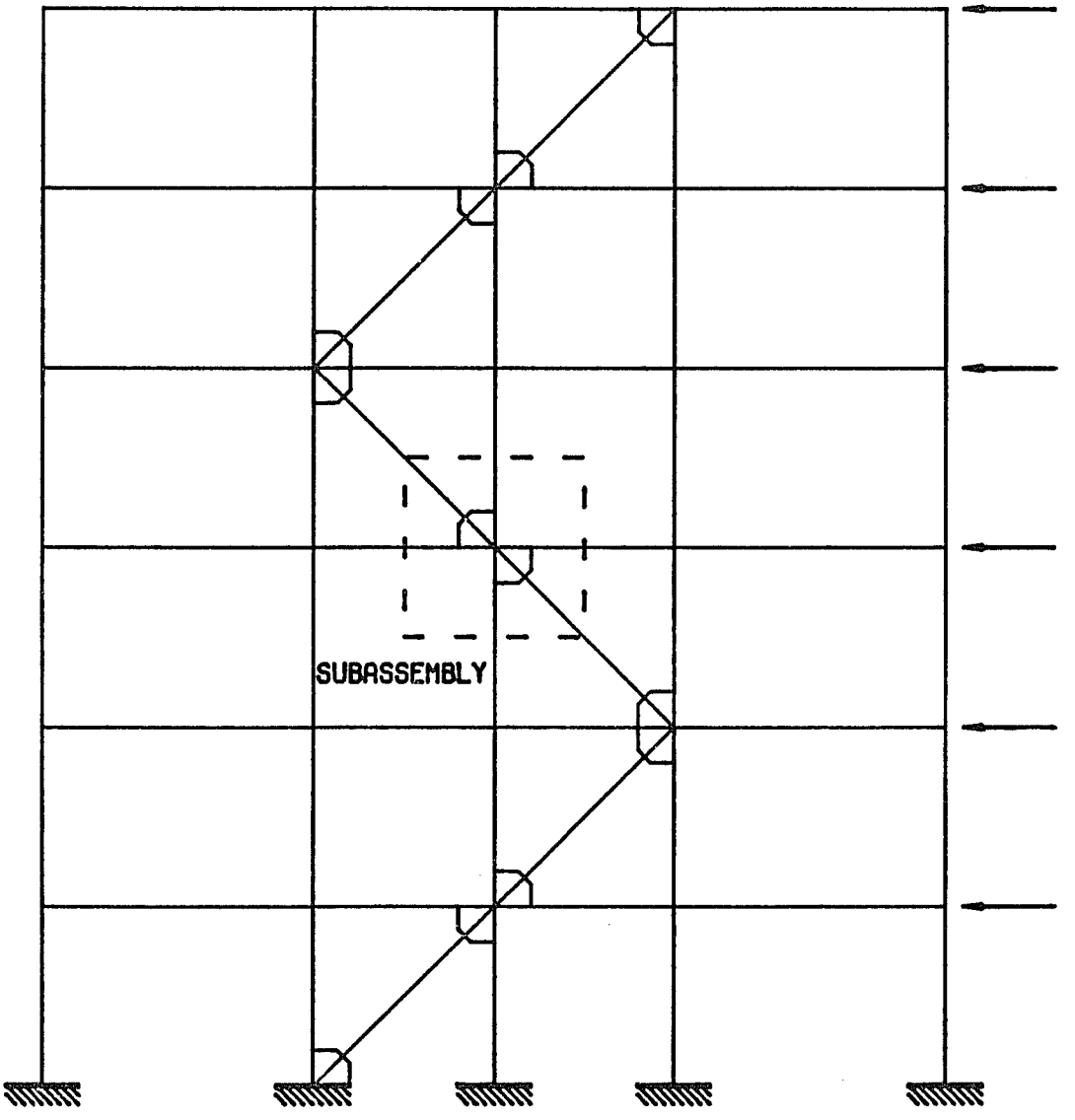

Figure 32. Drag Through Configuration.

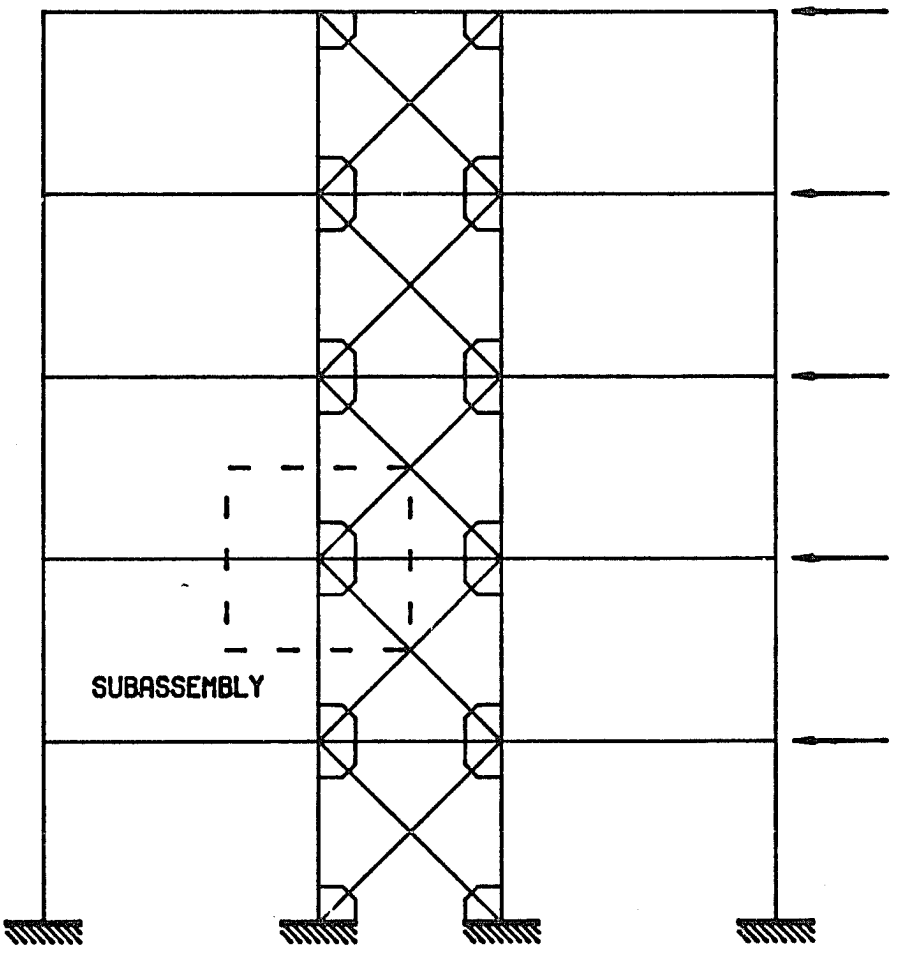

Figure 33. Double Gusset Configuration.

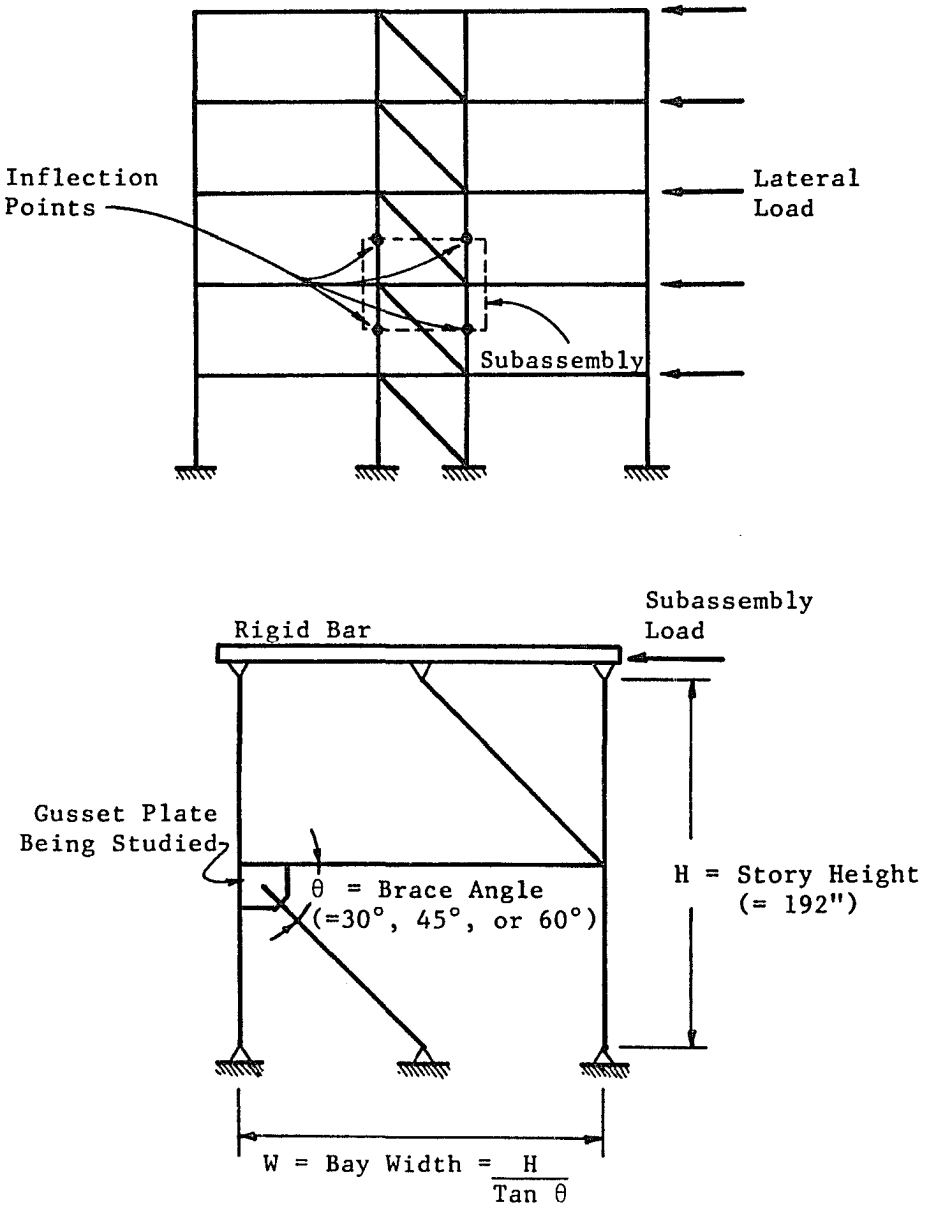

Figure 34. Isolation of Subassembly for Analysis.

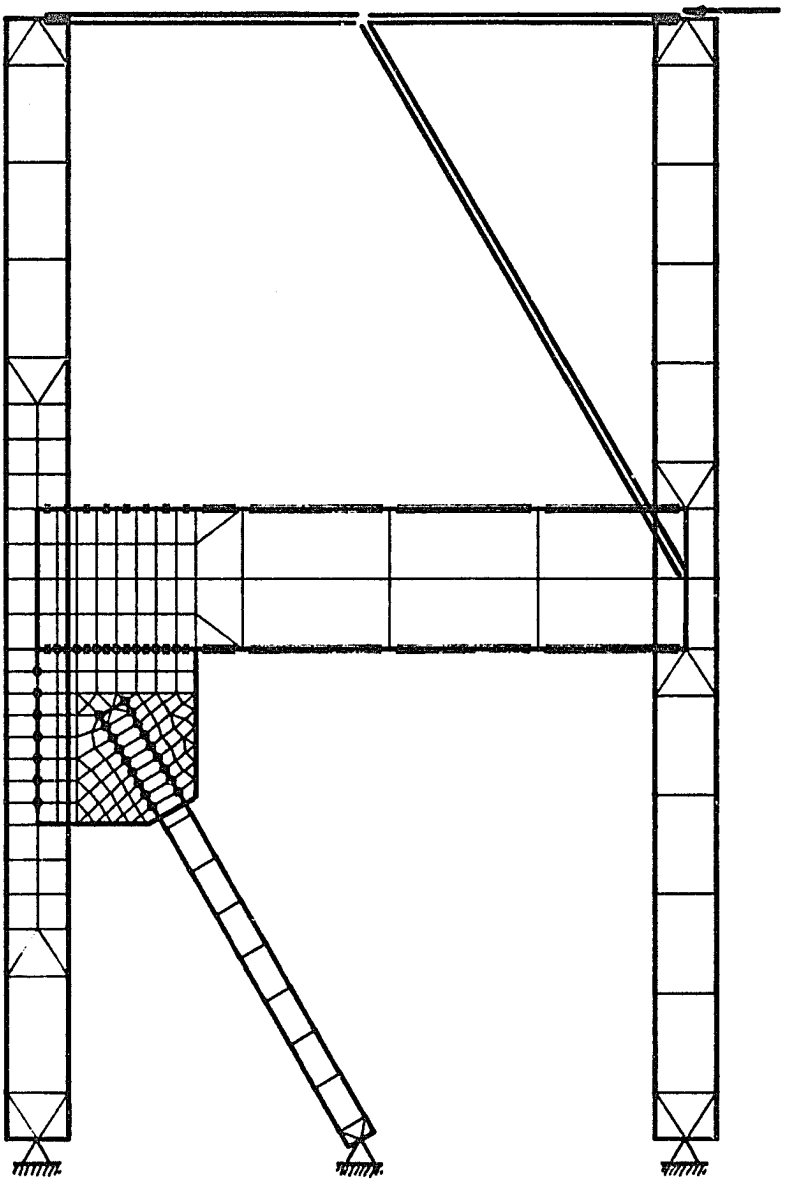

Figure 35. 60° Single Gusset Model (Weak Axis W12).

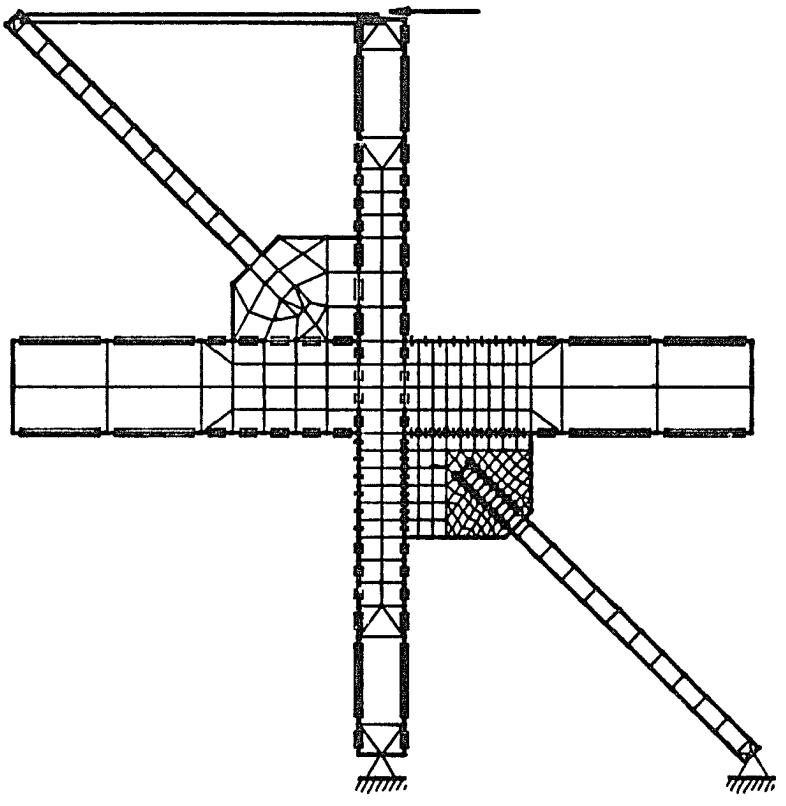

Figure 36. 45° Drag Through Gusset Model (Strong Axis W12).

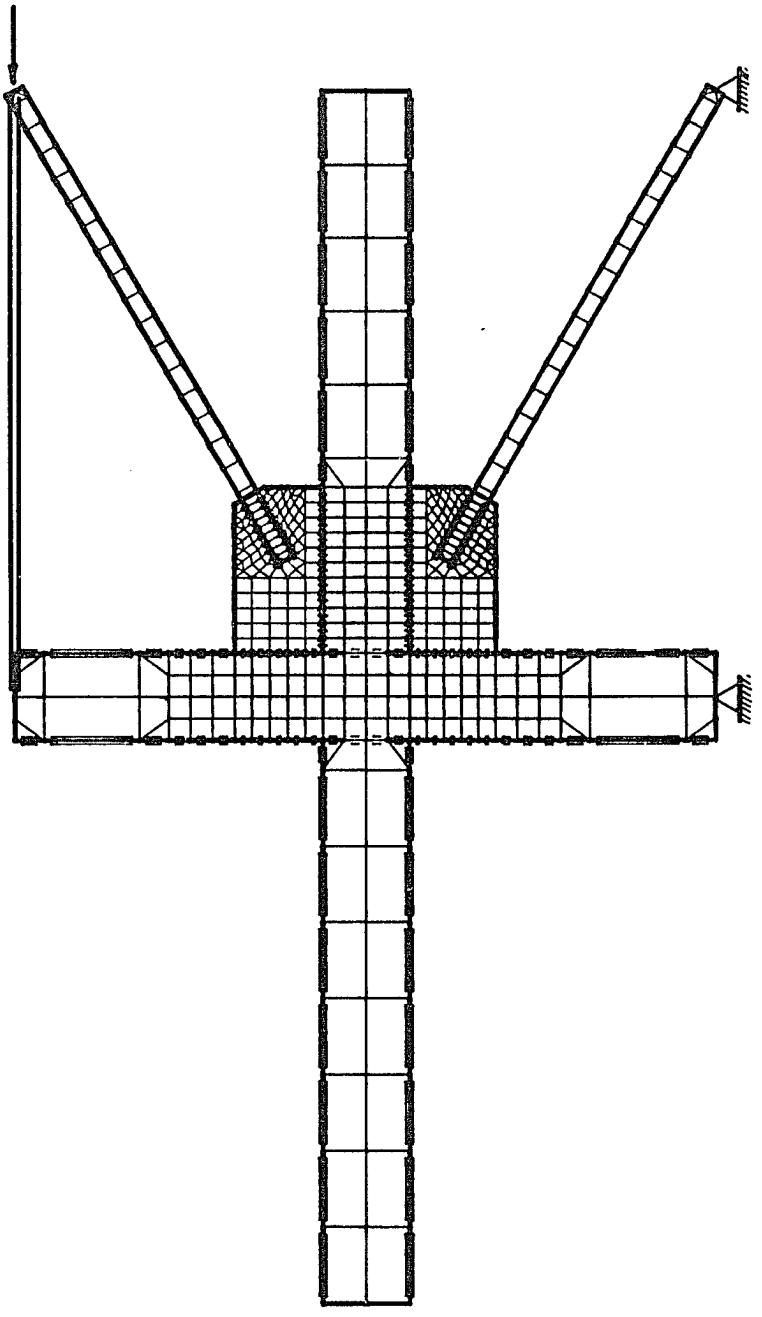

Figure 37. 30° Double Gusset Model (Strong Axis W24).

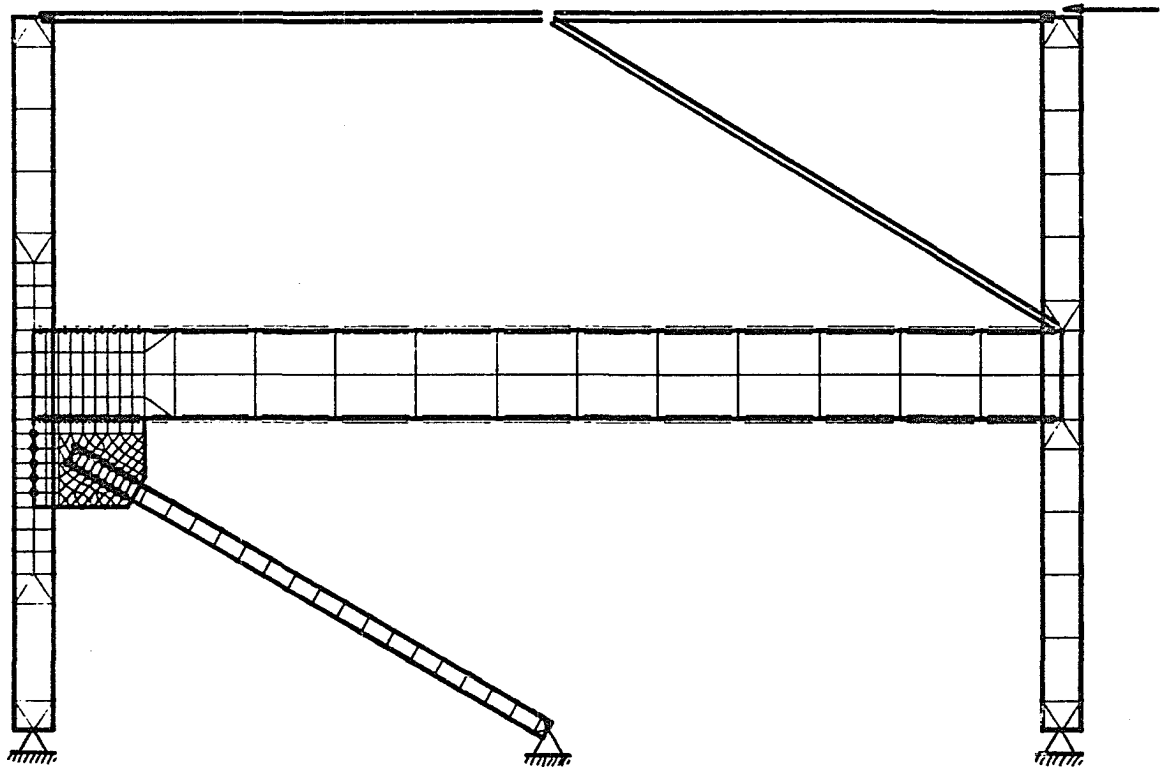

Figure 38. 30° Single Gusset Eccentric Model
(Weak Axis W12).

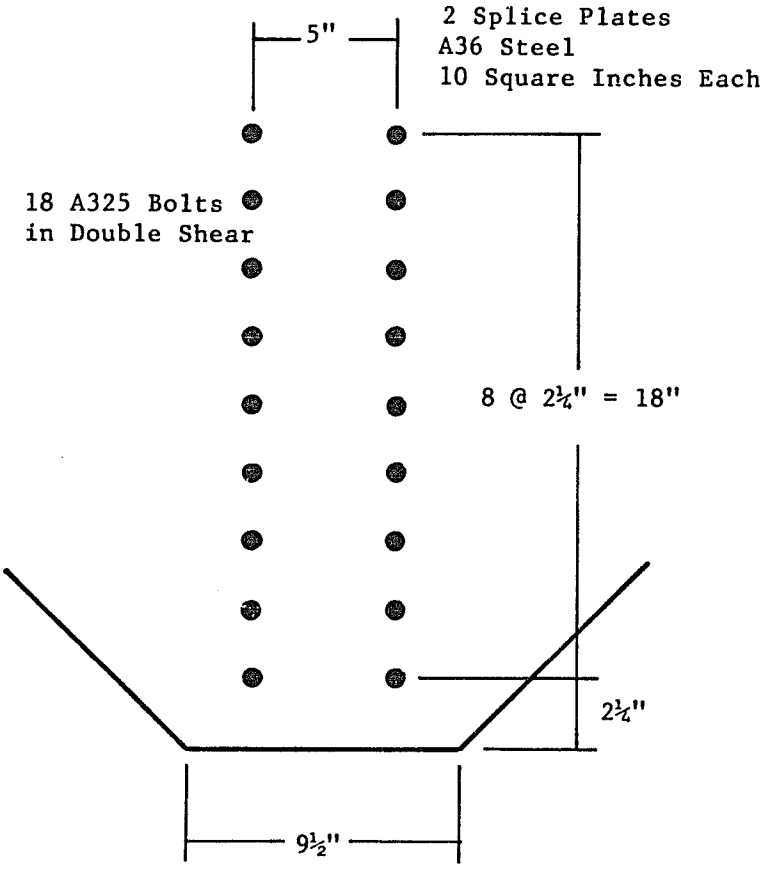

Figure 39. Splice Plate Bolt Details.

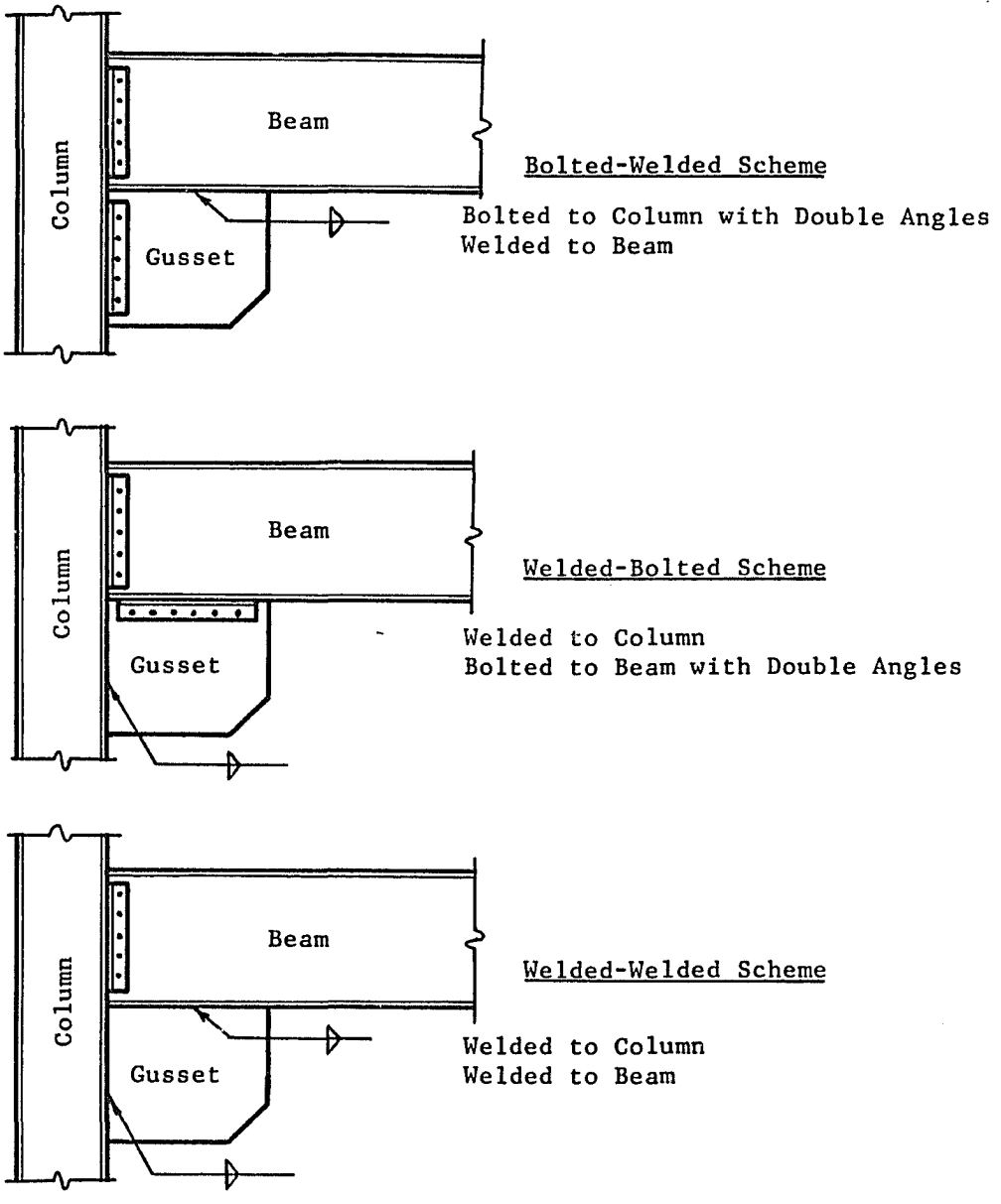

Figure 40. Gusset-to-Frame Connection Schemes.

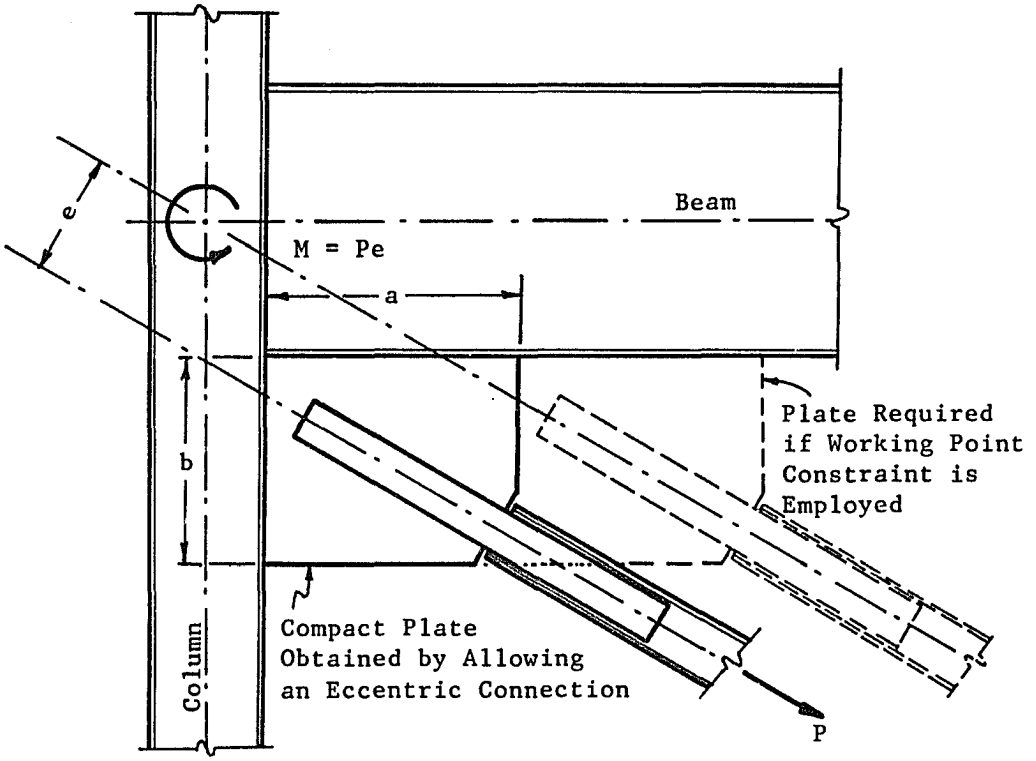

P = Brace Load

e = Eccentricity

M = Moment Caused by Eccentricity

Figure 41. Eccentric Connection.

Chapter 6

FINITE ELEMENT RESULTS

Several pre- and post-processing programs were generated to automate the analysis procedure. A summary of the computer programs used in this study is given in Appendix B. Each finite element model comprised approximately 400 elements and 350 nodes which were generated using program NODEM. The Runge Kutta nonlinear solutions were made using Program INELAS (28). Approximately 700 simultaneous equations with an optimized semi-bandwidth of approximately 70 were solved four times for each increment of load. Once Program INELAS was successfully executed, post-processing programs MODPLT and VECPLT were used to plot the deformed models and fastener force and displacement vectors, respectively.

A significant conclusion resulting from this study is the importance of frame action effects in the gusset-to-frame fastener force distributions. Deformed finite element meshes exaggerated are shown in Figures 42 through 45. In these models framing members pinch the gusset plate because the angle between the column and beam is reduced; and, as a result, the beam and column load the gusset, equally as much as the brace loads the gusset. Fastener force distributions are compared in Figure 46 for a model that includes the frame and a model that does not include the frame. To realistically simulate the

behavior of diagonal bracing connections, the frame must be incorporated in the finite element model.

As a result of the finite element analyses conducted, it was established that the following variables have relatively little effect on the gusset-to-frame fastener force distributions:

- compression vs. tension brace loads
- bracing configuration
- beam and column properties
- gusset-to-frame fastener type
- brace eccentricity

However, the gusset force distributions primarily depend on:

- plate aspect ratio
- brace load
- brace angle

These results were used to develop the design equations presented in Chapter 7.

As shown in Figures 47 through 49, the uniformity of the fastener force distributions is described at the gusset plate working, yield, and ultimate loads. As the brace load increases, the force distributions become more uniform. The nonuniformity of these fastener force magnitudes is of the same order as those of typical splice connections as shown in Figure 23. Therefore, designing gusset plate connections by assuming the total force is resisted uniformly by the

fasteners is consistent with current professional practice. Furthermore, in the compact gusset plates, in which the minimum required plate dimensions (those needed to accommodate the brace-to-gusset connection) are used, the force distributions are more uniform than for the noncompact plates. This explains why the range of fastener forces is narrowed for the eccentric connections. As illustrated in Figure 50 the fastener forces tend to become aligned with the brace as the brace load increases.

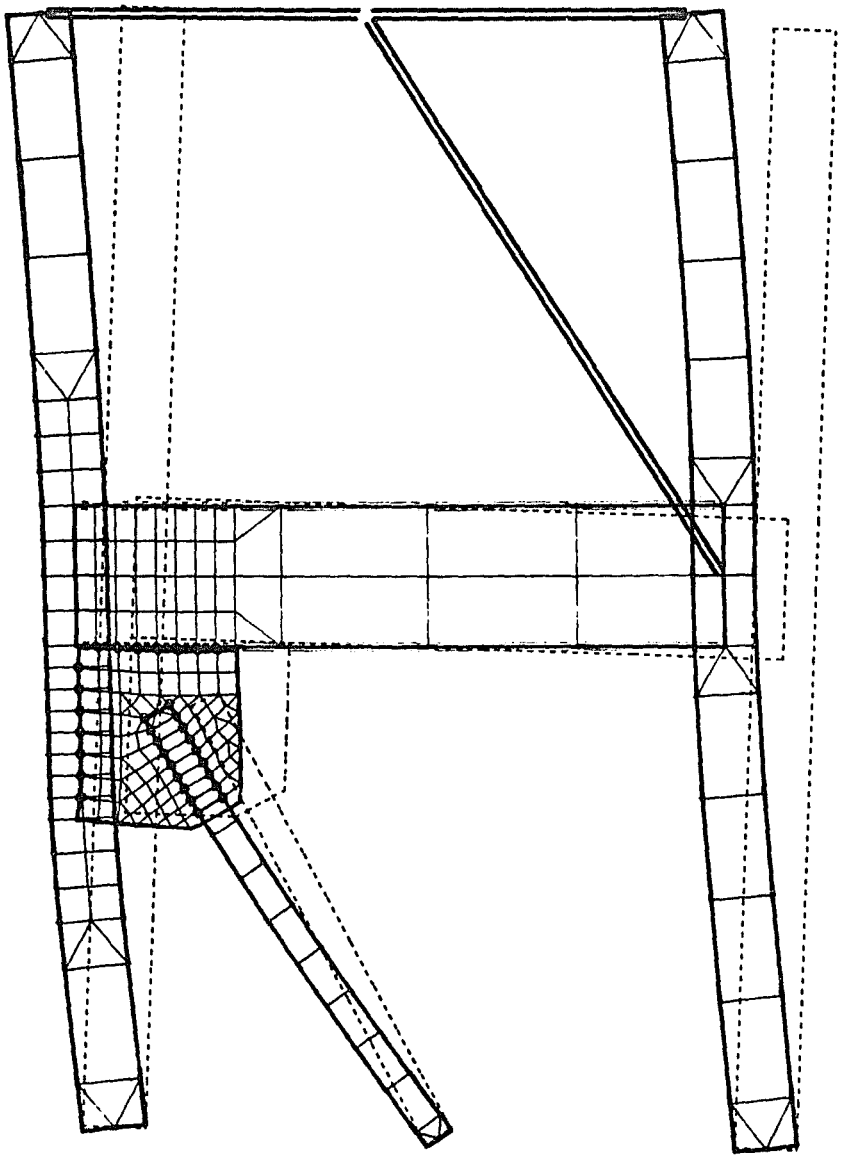

Figure 42. Deformed Mesh for 60° Single Gusset Model (Weak Axis W12).

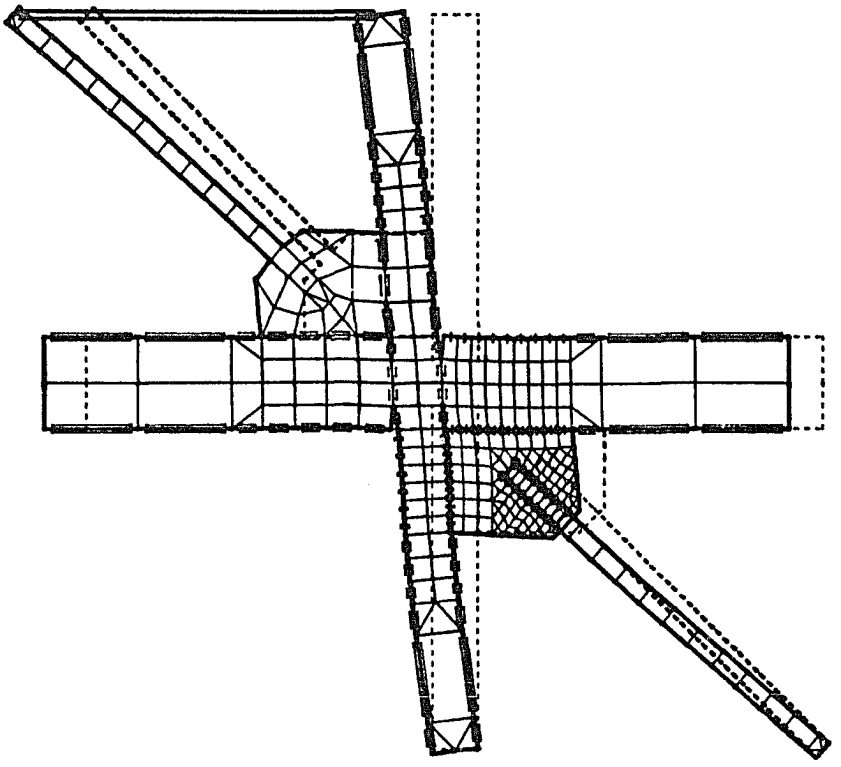

Figure 43. Deformed Mesh for 45° Drag Through Gusset Model (Strong Axis W12).

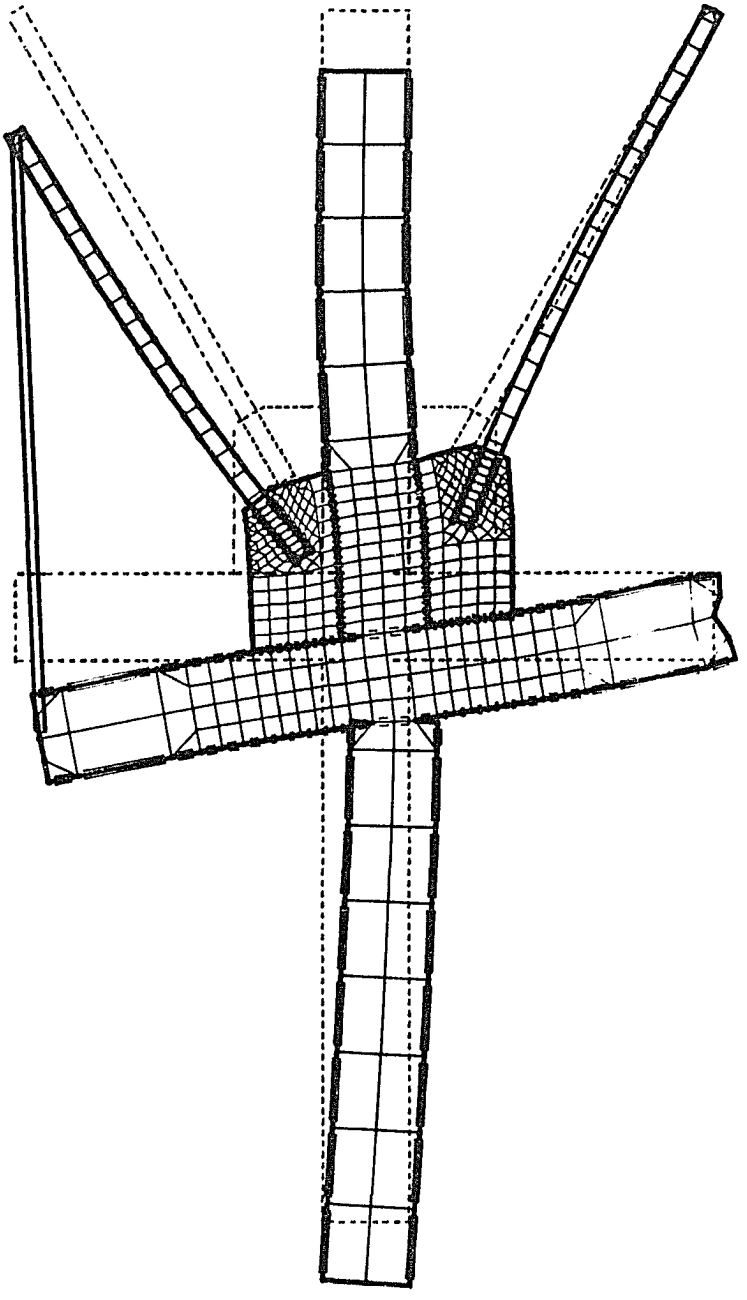

Figure 44. Deformed Mesh for 30° Double Gusset Model (Strong Axis W24).

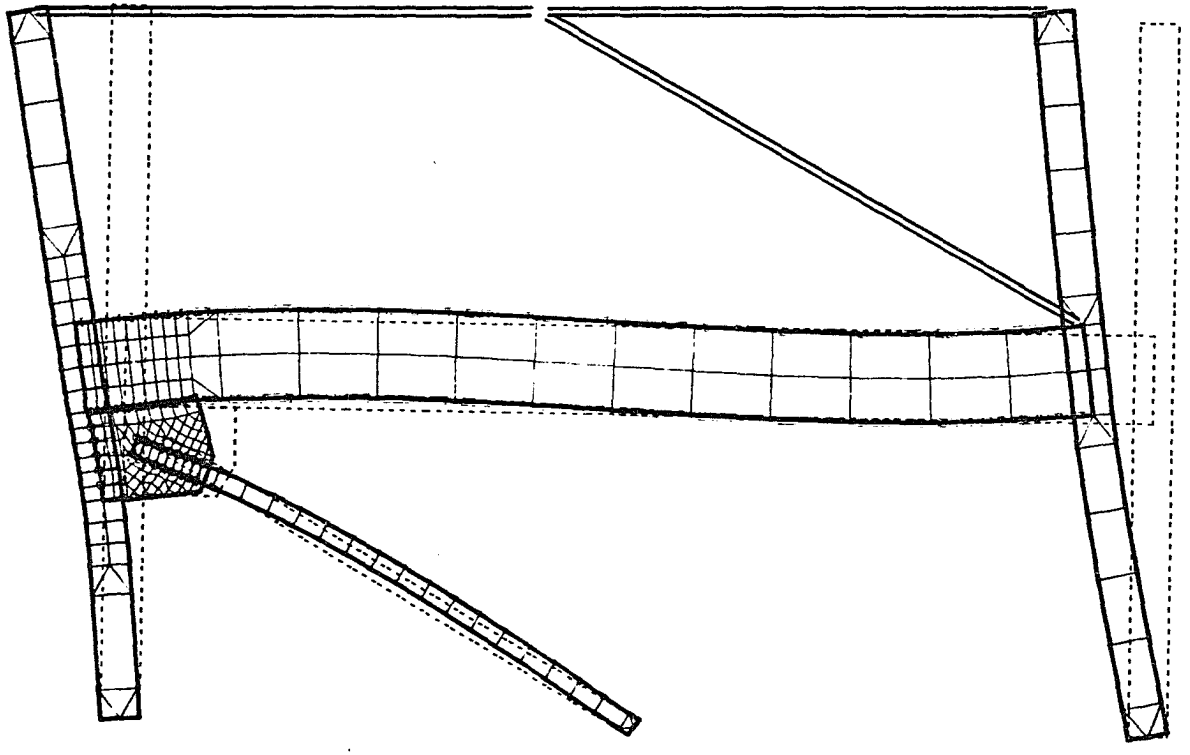

Figure 45. Deformed Mesh for 30° Single Gusset Eccentric Model (Weak Axis W12).

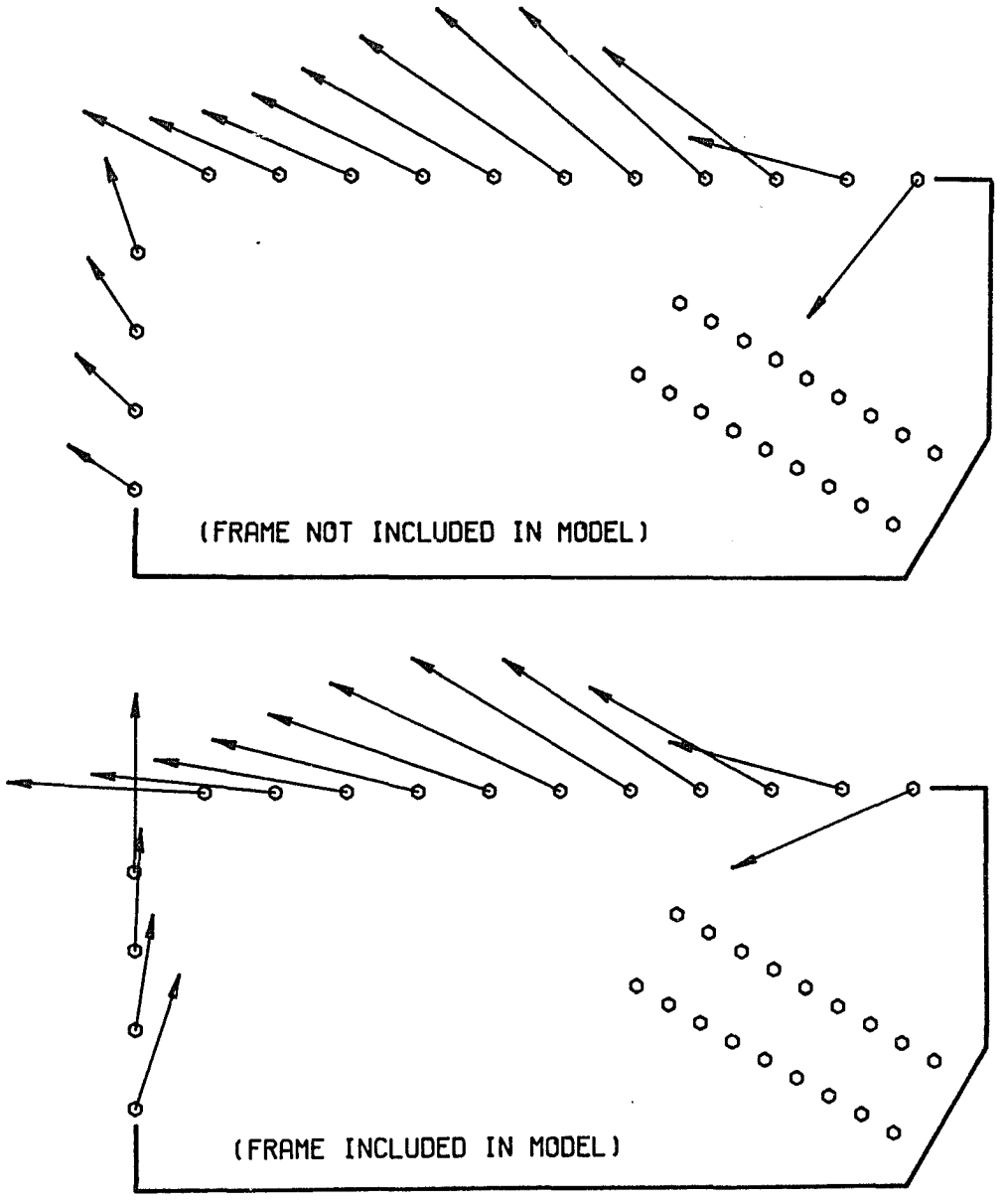

Figure 46. Gusset Plate Fastener Force Distributions.

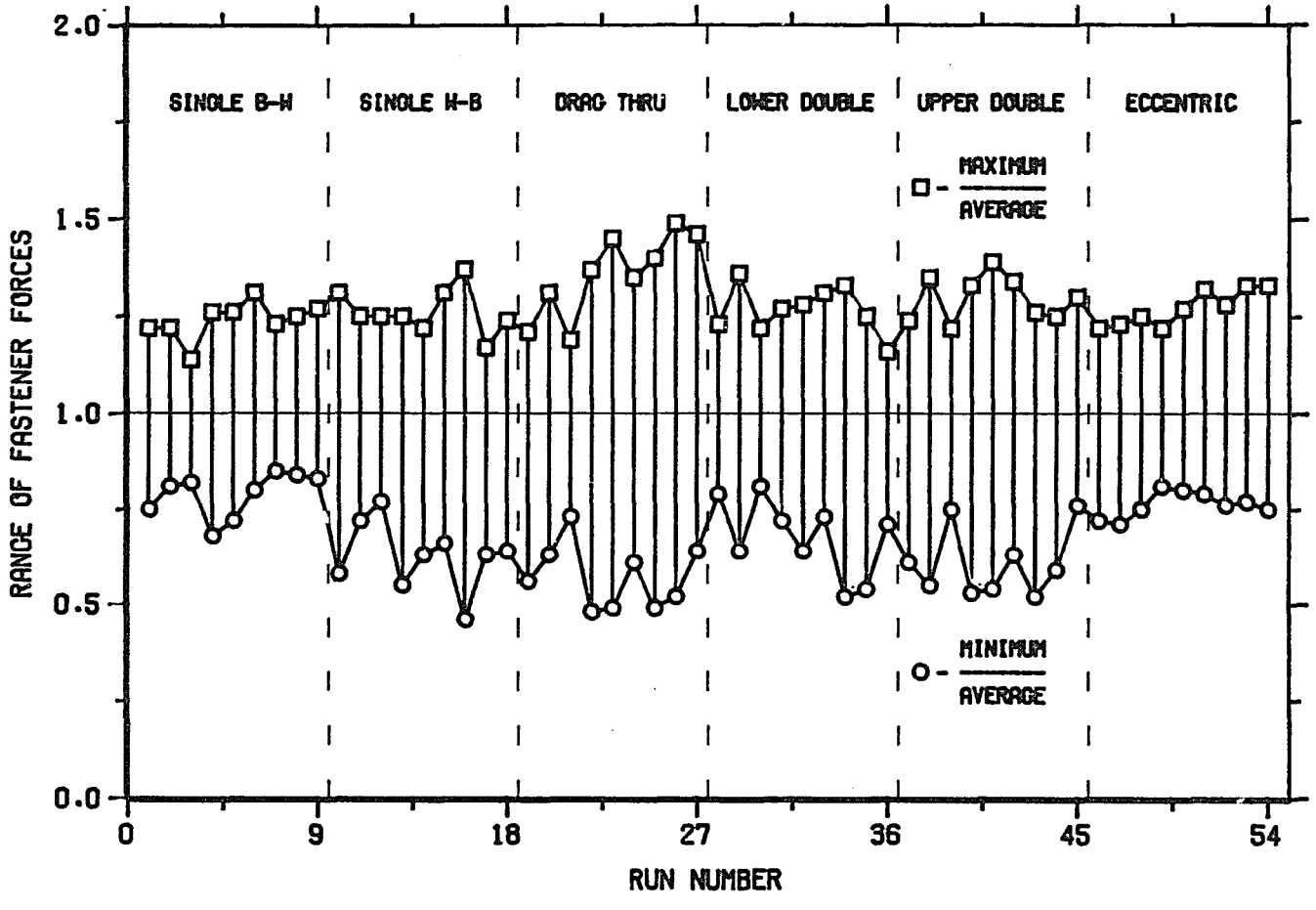

Figure 47. Uniformity of Fastener Force Distributions at Working Load.

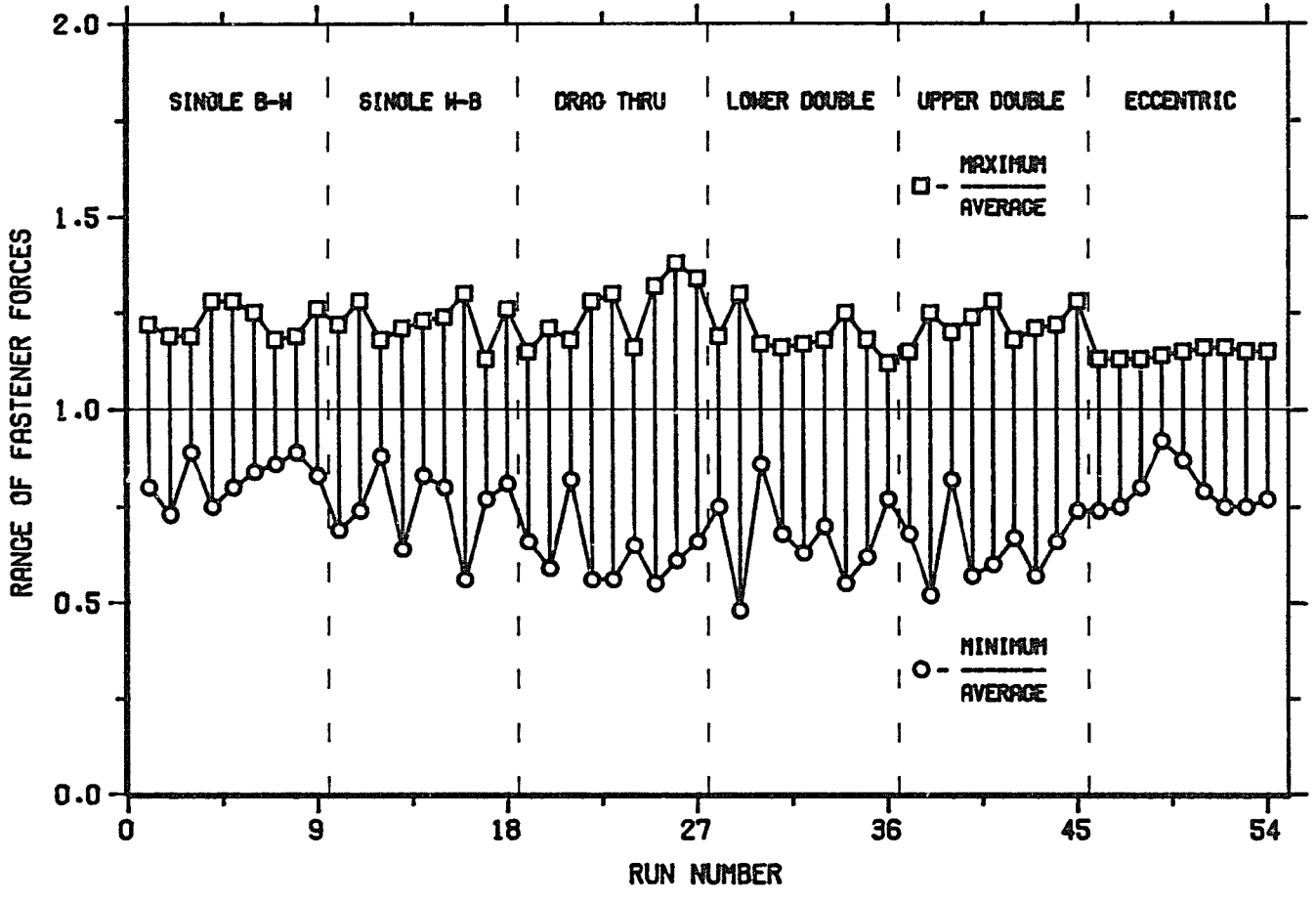

Figure 48. Uniformity of Fastener Force Distributions at Yield Load.

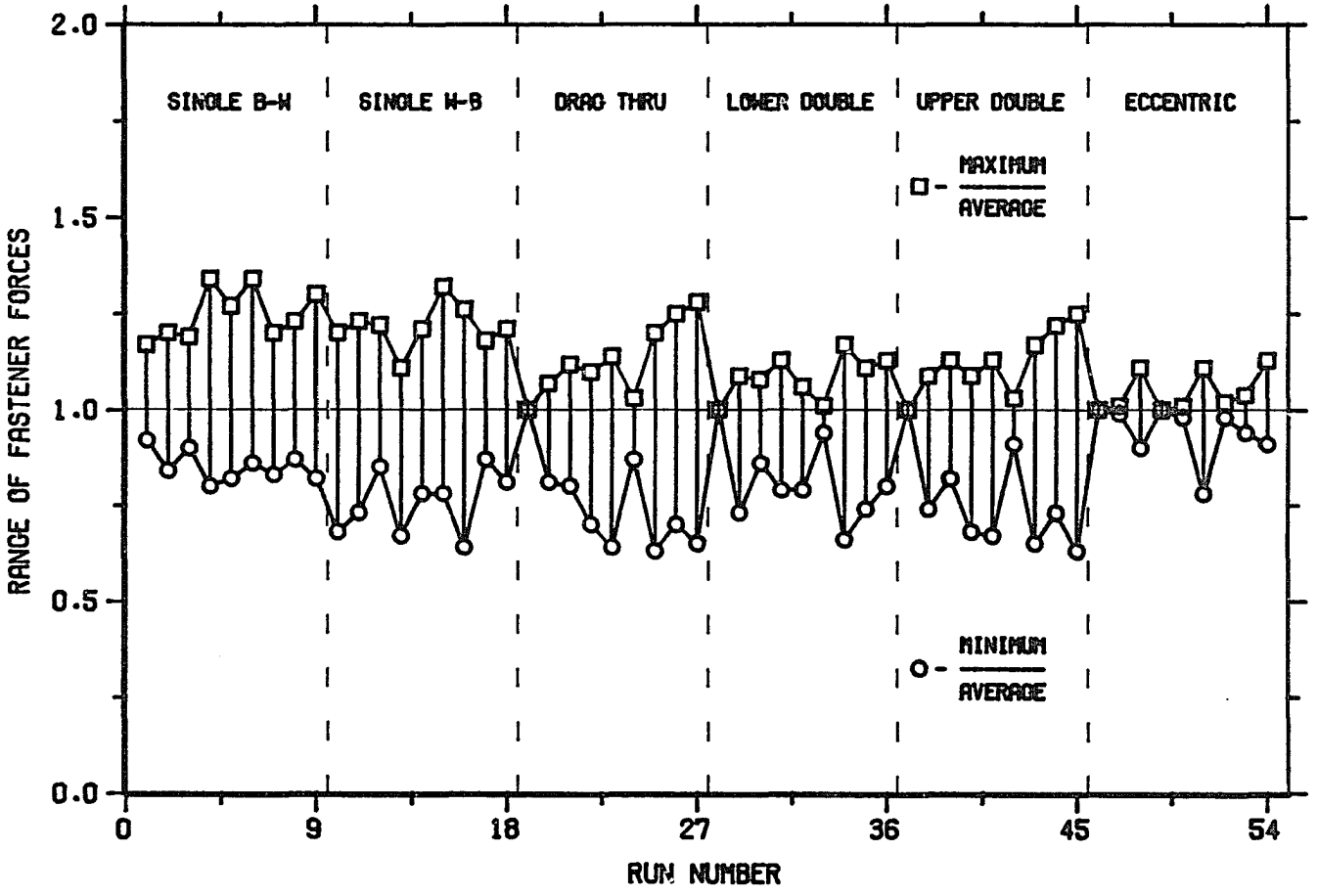

Figure 49. Uniformity of Fastener Force Distributions at Ultimate Load.

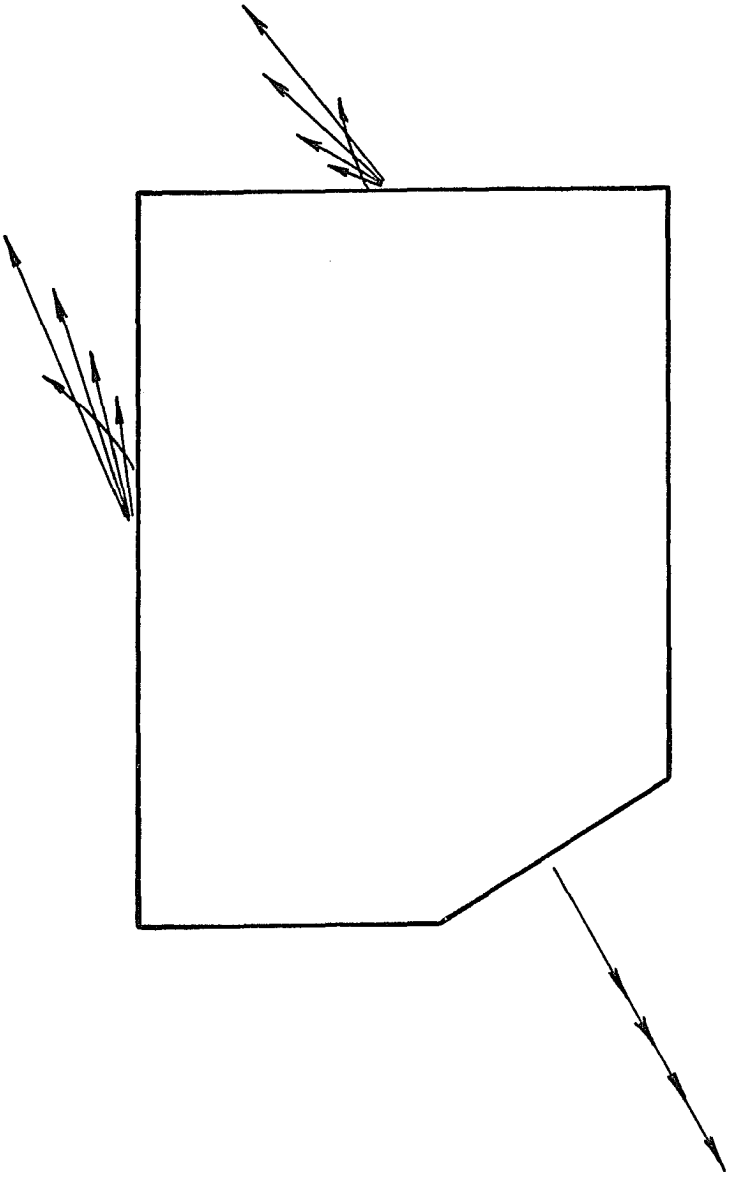

Figure 50. Alignment of Forces as Brace Load Increases.

Chapter 7

GUSSET FORCE DISTRIBUTION DESIGN EQUATIONS

To design the gusset-to-frame fasteners in a diagonal bracing connection, an estimate of the force distribution is required. Previous research on this subject does not exist. One major reason for this is the difficulty of experimentally determining the distribution of loads in the bolts, welds, and angles (fastener elements) in these complex connections. Current methods for predicting the fastener force distribution assume that the horizontal and vertical components of the brace load are transferred to the beam and column respectively (37). Therefore, fasteners are designed to resist the shear forces as shown in Figure 51.

Based on the parametric studies involving the 51 analytical models described in Chapter 5, the following design equations were developed to predict the gusset-to-frame fastener force distributions (refer to Figures 52 and 53):

$$R_B = [\ 1.4\ a/(a + b) - 0.1\ ]\ P$$

$$\theta_B = 0.6\ \theta \qquad (\theta < 45°)$$

$$\theta_B = 27 + [\ 8.5 - 20\ a/(a + b)\ ]\ (45 - \theta) \qquad (\theta > 45°)$$

$$P_{HB} = R_B \cos\theta_B$$

$$P_{VB} = R_B \sin\theta_B$$

$$P_{HC} = P \cos\theta - P_{HB}$$

$$P_{VC} = P \sin\theta - P_{VB}$$

where

R_B = force resultant on beam

θ_B = angle of beam resultant (degrees)

a = horizontal plate dimension

b = vertical plate dimension

P = brace load

θ = brace angle

P_{HB} = horizontal force component on beam

P_{VB} = vertical force component on beam

P_{HC} = horizontal force component on column

P_{VC} = vertical force component on column

These equations are based on the fastener force distributions which occur when the gusset plate is subjected to the block shear yield load. However, for design purposes these equations may be used to predict force distributions at any load level.

The gusset force distribution design equations were developed from the data shown in Figures 54 and 55. The amount of brace load distributed to the beam (R_B) depends only on the magnitude of the brace load (P) and the plate aspect ratio (a/b). Furthermore, the orientation of the force transferred to the beam (θ_B) is a function of the brace angle (θ) and the plate aspect ratio (a/b). Once the beam force components are calculated, the column force components can be

computed using equilibrium. These equations are independent of the following:

- fastener modes employed (bolts, welds...)
- bracing configuration (single, X-bracing...)
- beam and column properties (length, moment of inertia...)
- connection eccentricity

Plotted in Figures 56 through 59 are the analytical and design forces for the gusset plates considered in this study. The correlation between the design equation and the finite element results is excellent.

Compared in Figures 60 through 67 are the design formula and finite element values of various force distribution quantities. A study of the results shown in Figures 60 through 63 indicate that the larger shear components (P_{HB} and P_{VC}) are more accurately predicted than the smaller normal components (P_{VB} and P_{HC}). The resultant forces (R_B and R_C) are optimally predicted by the design formula, as shown in Figures 64 and 65. These resultants are the primary forces used to design the gusset-to-frame fasteners. The orientations of these connection resultants (θ_B and θ_C) are more accurately estimated for the beam than for the column, as illustrated in Figures 66 and 67.

Richard (27) has shown that for double framing angles with an A325 bolt in double shear, as illustrated in Figures 2 and 8, prying effects do not control bolt designs. Instead, the strength of the

double angles was either the bolt double shear value or the bolt-bearing value in the gusset plate. If bolted double angles are used in the diagonal bracing connections considered in this study, then the required number of 3/4" A325 bolts in double shear can be simply determined. The current design procedures conservatively estimate the number of required bolts along the beam and column for most cases, as shown in Figures 68 and 69. The number of bolts required by the proposed design formula is given in Figures 70 and 71. This formula is accurate to within one bolt for all but one gusset plate. A total of 16 bolts are required for all cases when the current design method is employed. However, if the design equations presented in this paper are utilized, only 13 to 15 bolts, depending on the plate and brace geometry, are required for the same brace load, a savings of 5% to 20%. The above observations explain why the current bolt and weld procedures for gusset plate designs are valid but generally conservative. It is noted that the proposed design method predicts a different distribution of forces from the current design method.

When designing a diagonal bracing connection, it is recommended that the entire length of the gusset edges should be fastened to the frame. The required number of bolts should be spaced to fill the complete length of the gusset. If the plate is welded to the framing member, the weld should cover the entire length of the plate. This

recommendation allows for an even transfer of load along the fasteners from the gusset to the frame.

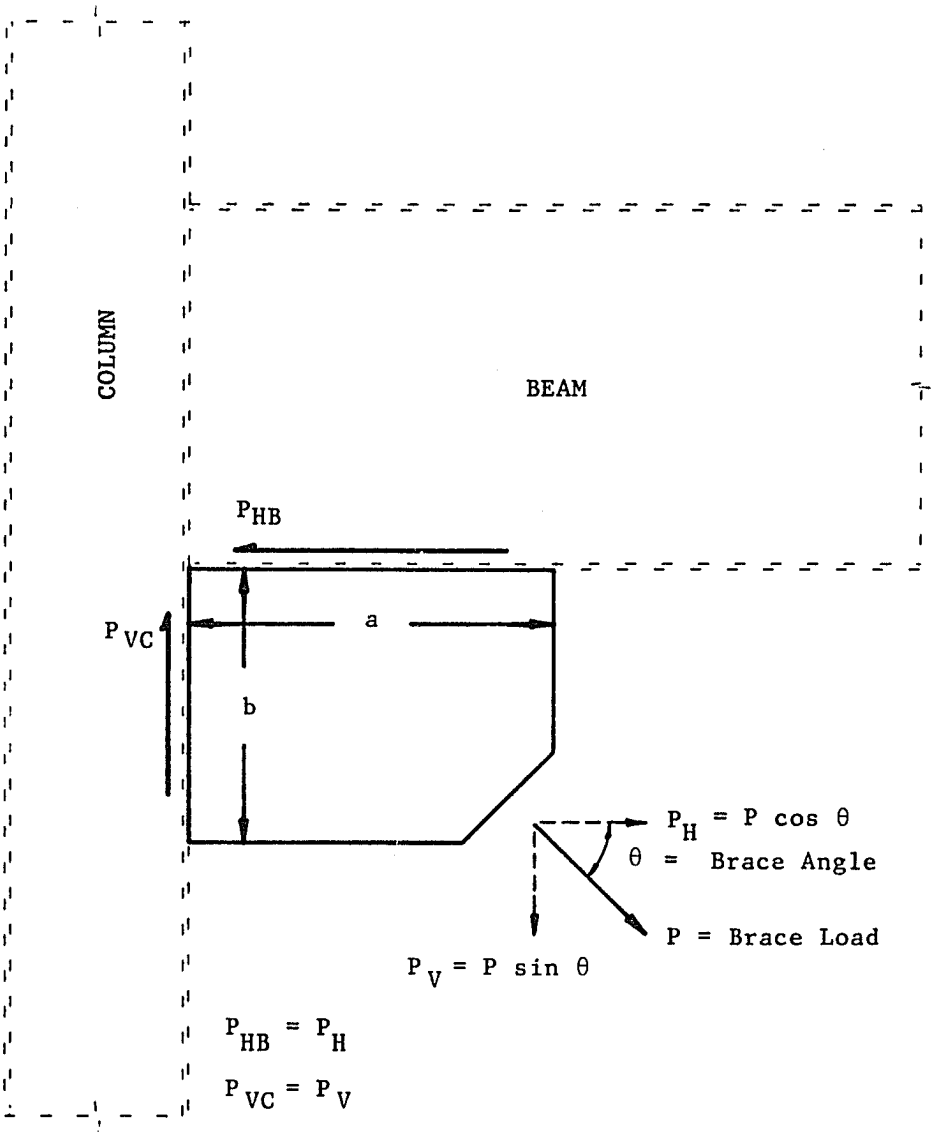

Figure 51. Current Method for Predicting Force Distributions.

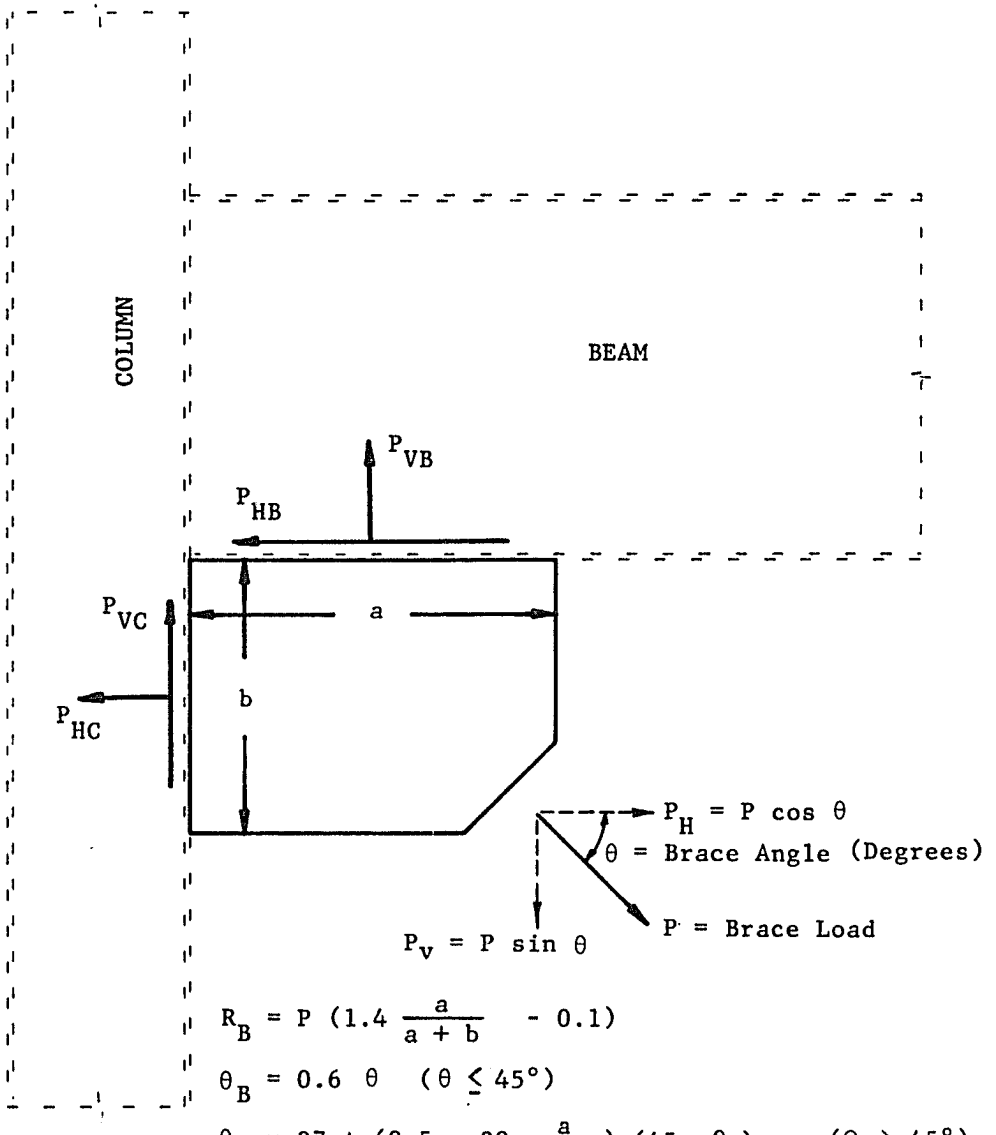

$$R_B = P\left(1.4 \frac{a}{a+b} - 0.1\right)$$

$$\theta_B = 0.6\ \theta \quad (\theta \leq 45°)$$

$$\theta_B = 27 + \left(8.5 - 20 \frac{a}{a+b}\right)(45 - \theta) \quad (\theta > 45°)$$

$$P_{HB} = R_B \cos \theta_B \qquad P_{HC} = P_H - P_{HB}$$

$$P_{VB} = R_B \sin \theta_B \qquad P_{VC} = P_V - P_{VB}$$

Figure 52. Force Components for Proposed Design Method.

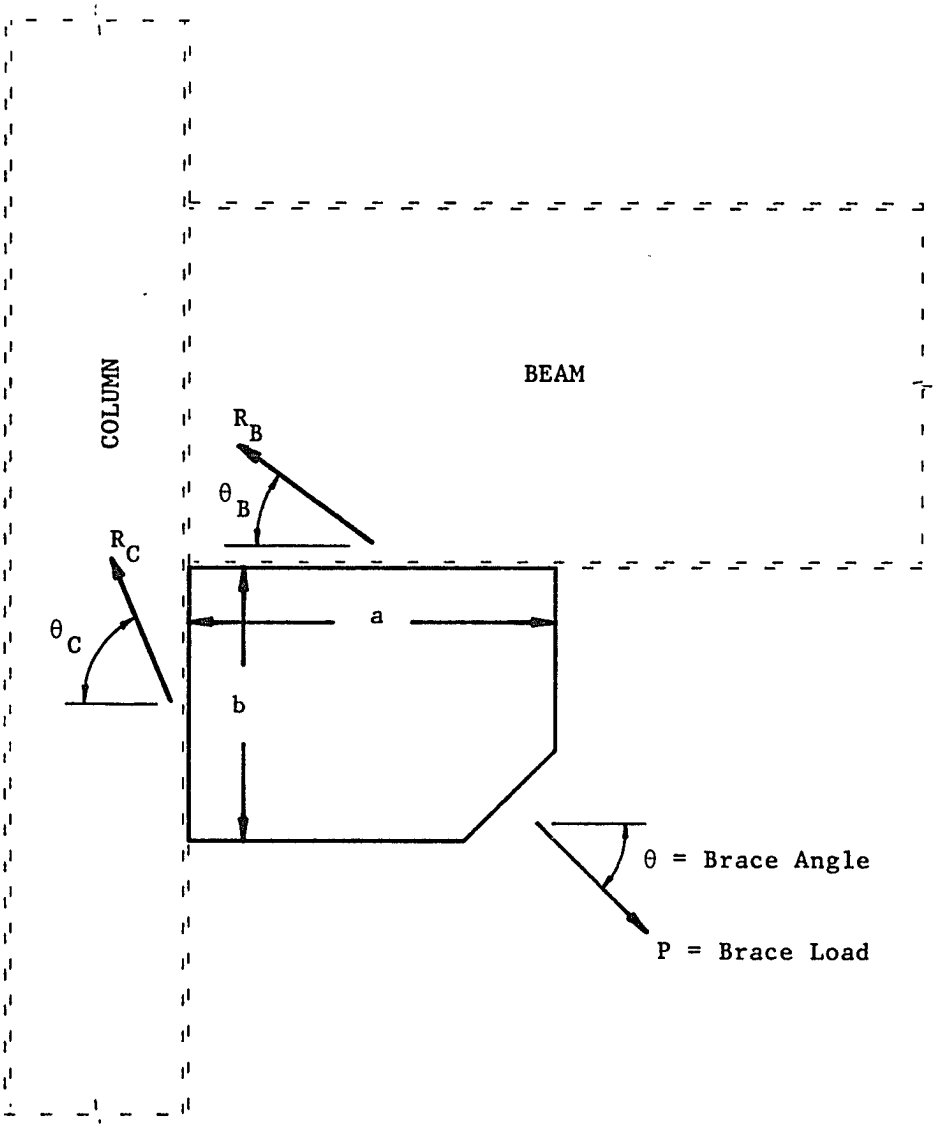

Figure 53. Force Resultants for Proposed Design Method.

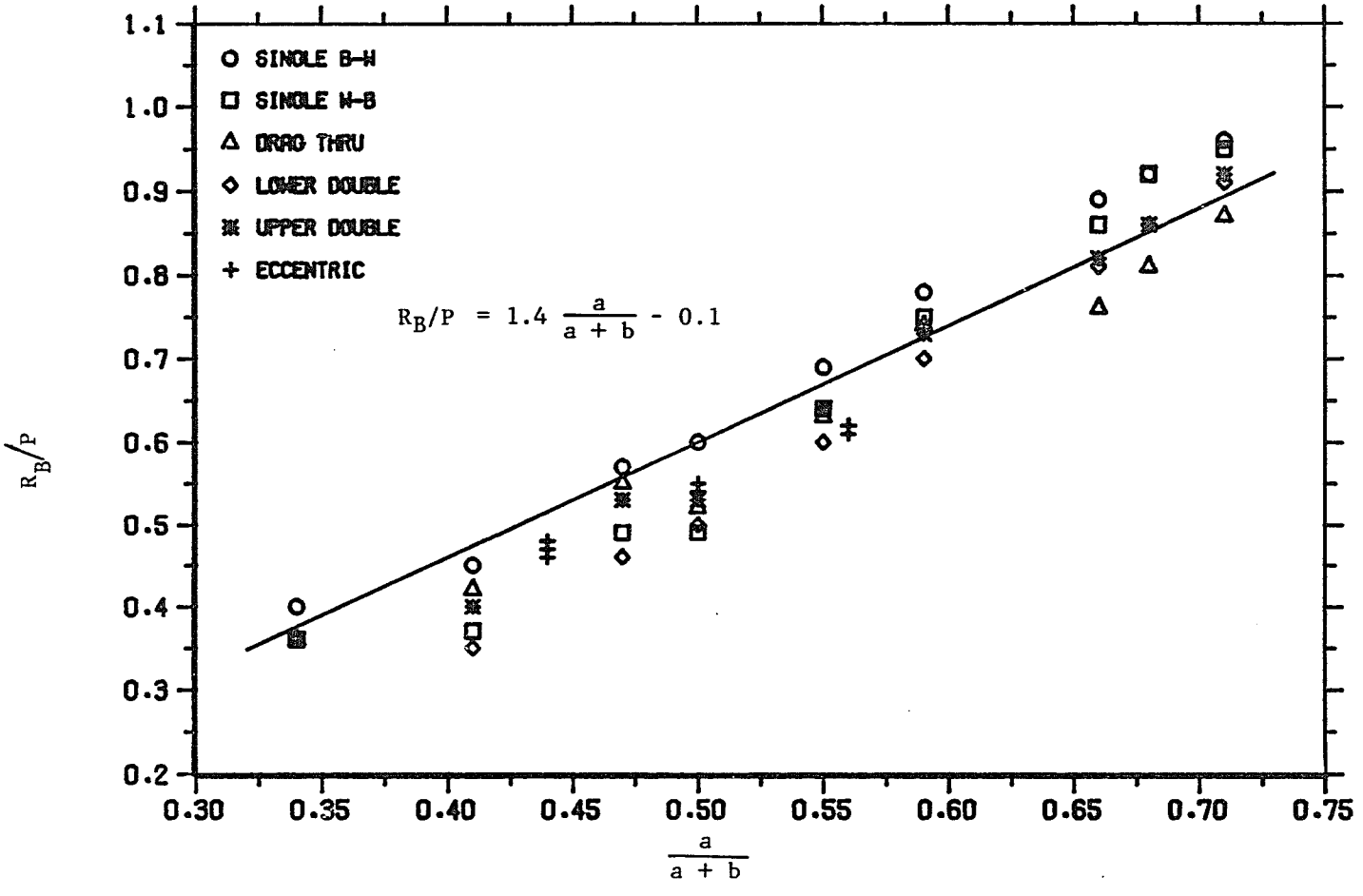

Figure 54. Origin of Design Equation for Resultant Force on Beam.

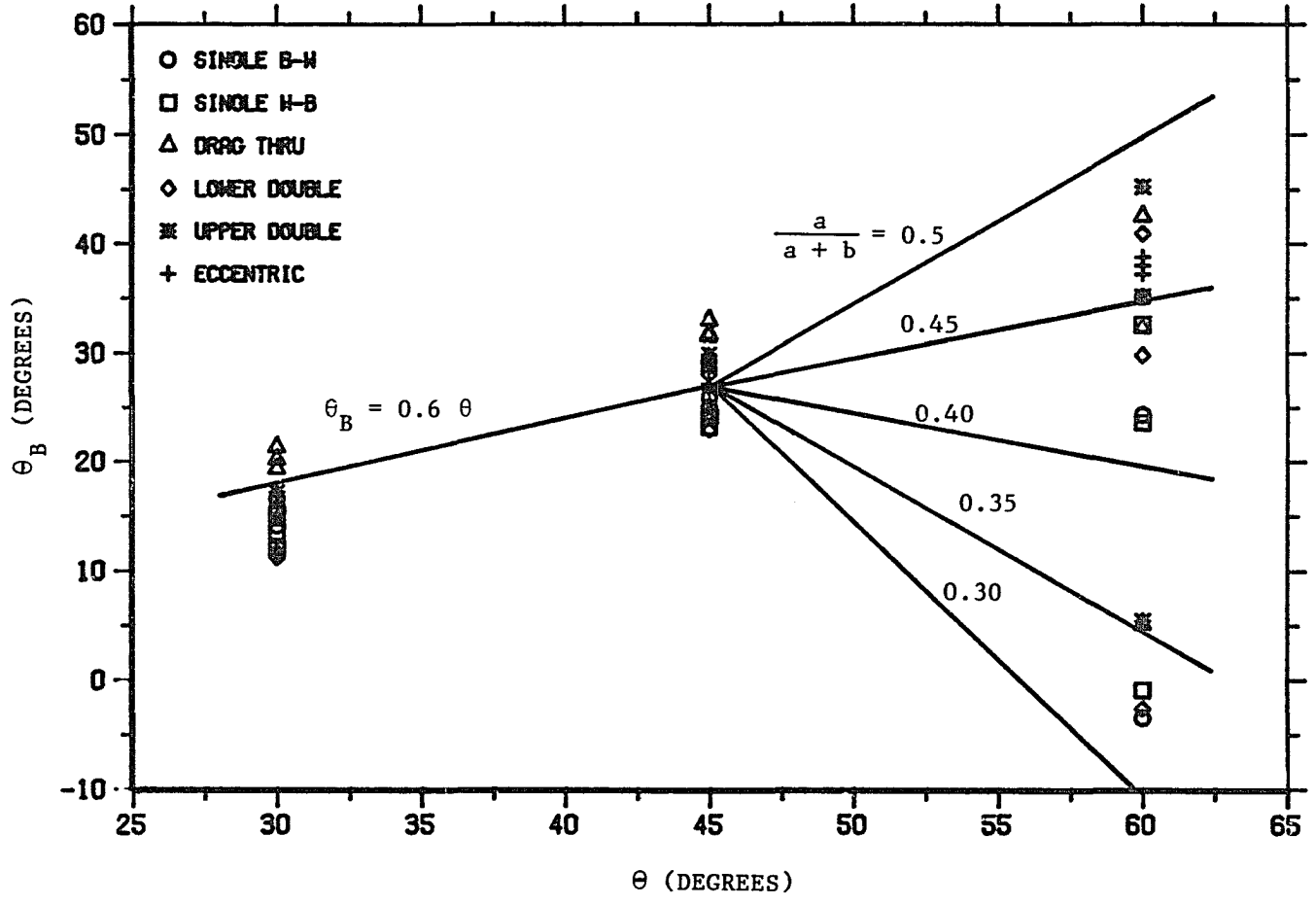

Figure 55. Origin of Design Equation for Angle of Resultant Force on Beam.

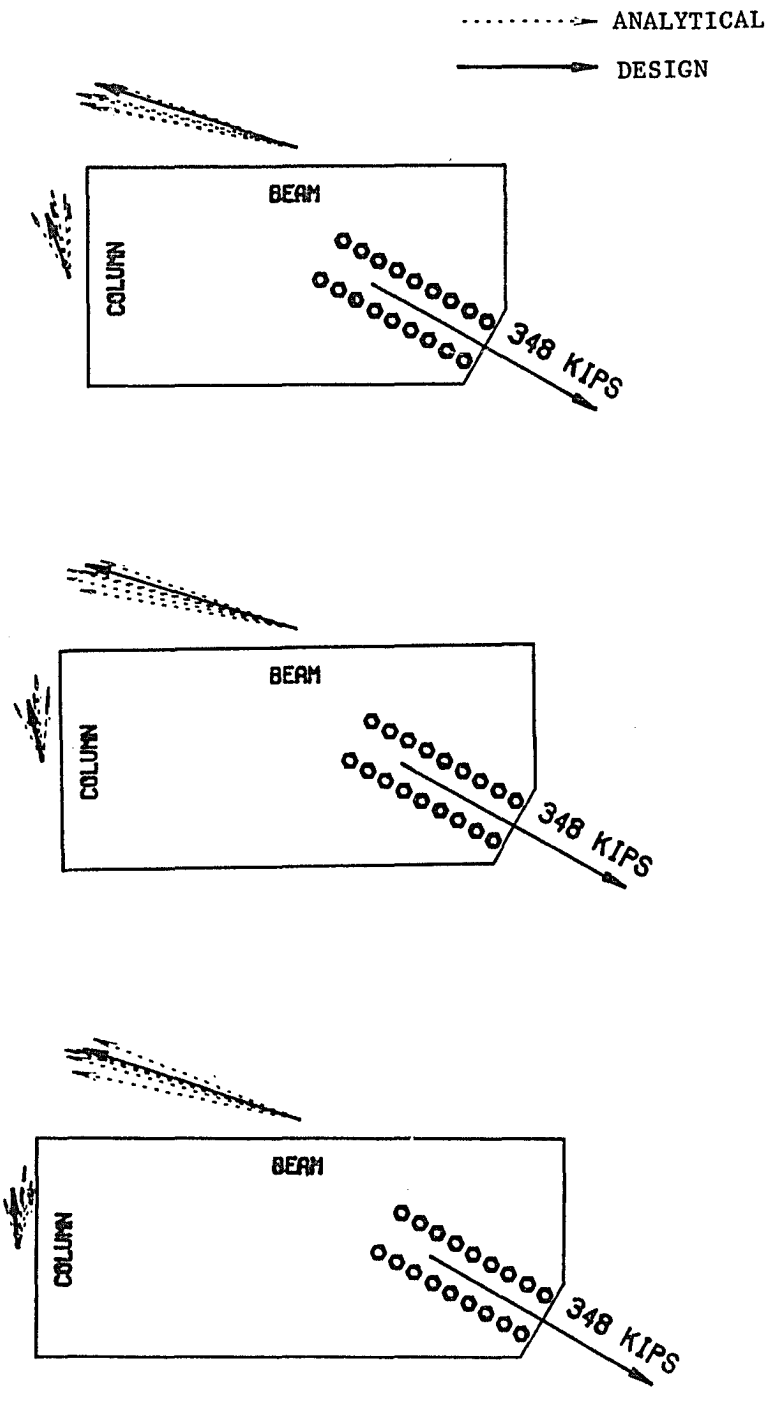

Figure 56. Analytical and Design Force Resultants for 30° Working Point Models.

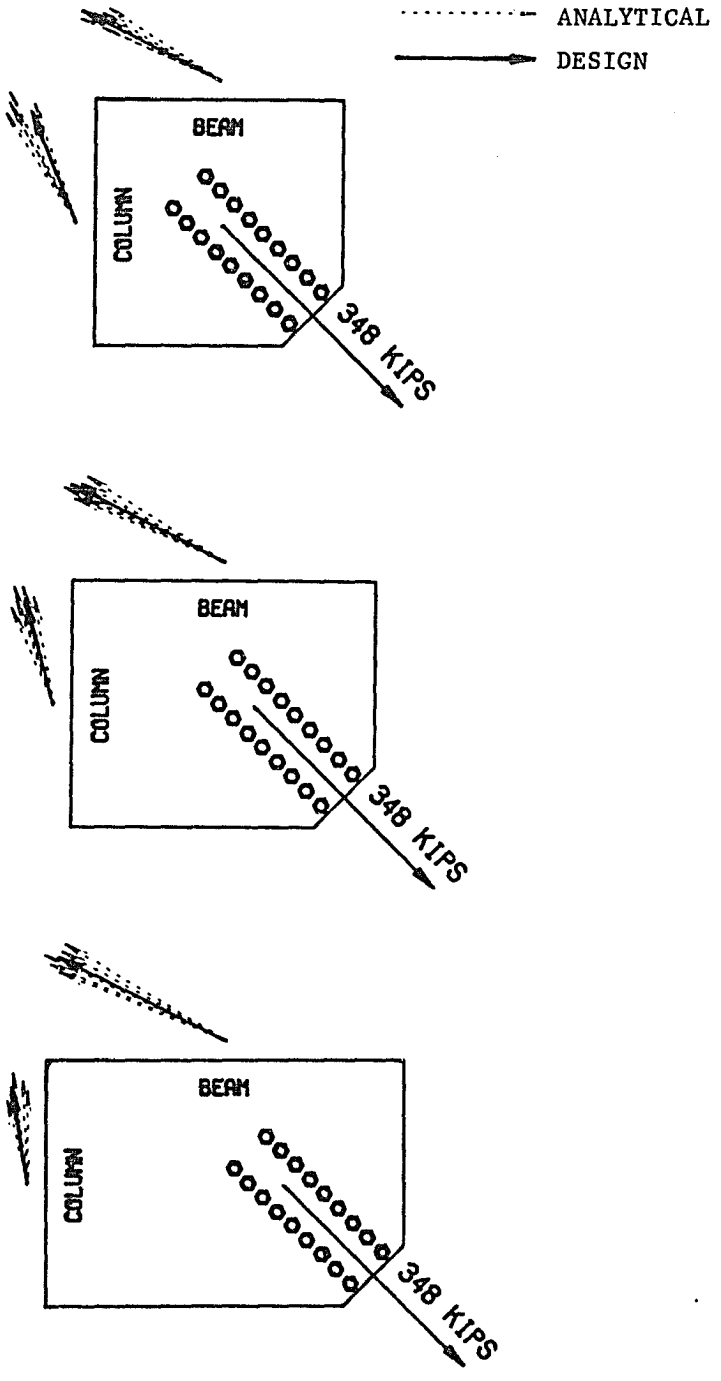

Figure 57. Analytical and Design Force Resultants for 45° Working Point Models.

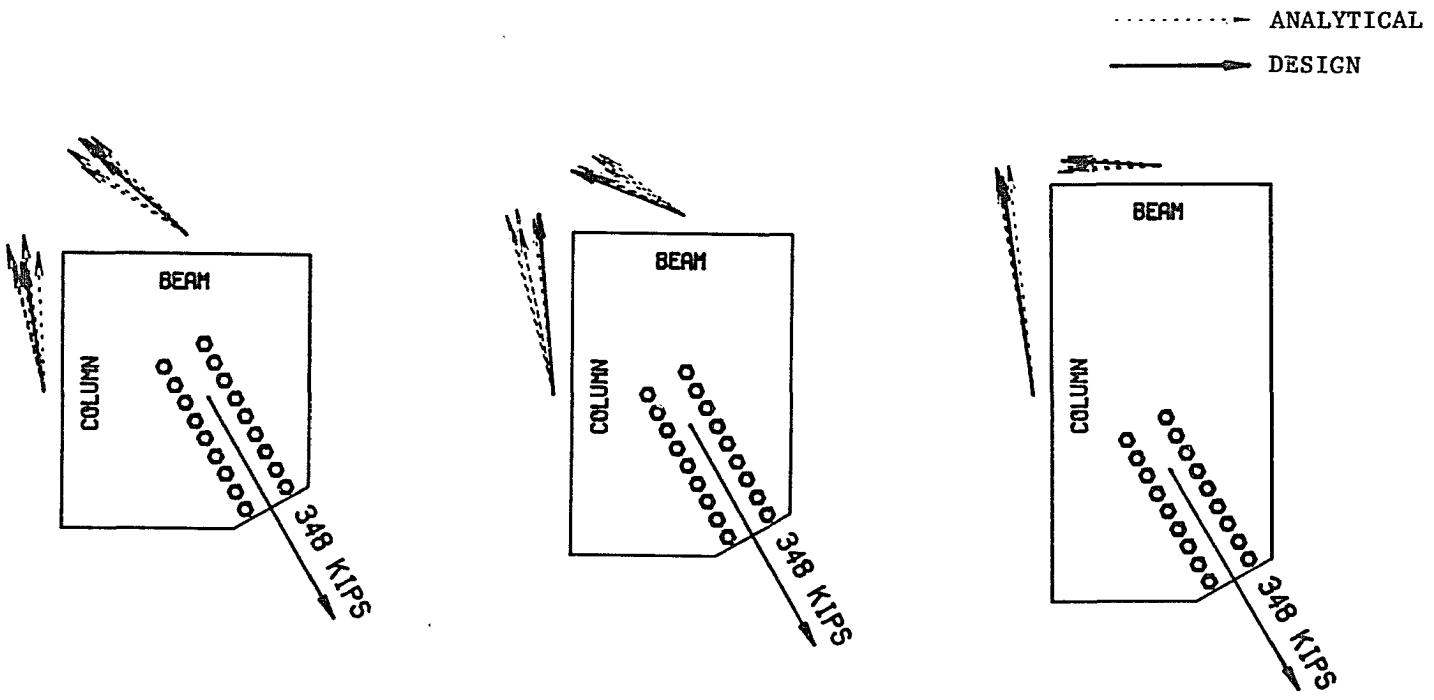

Figure 58. Analytical and Design Force Resultants for 60° Working Poing Models.

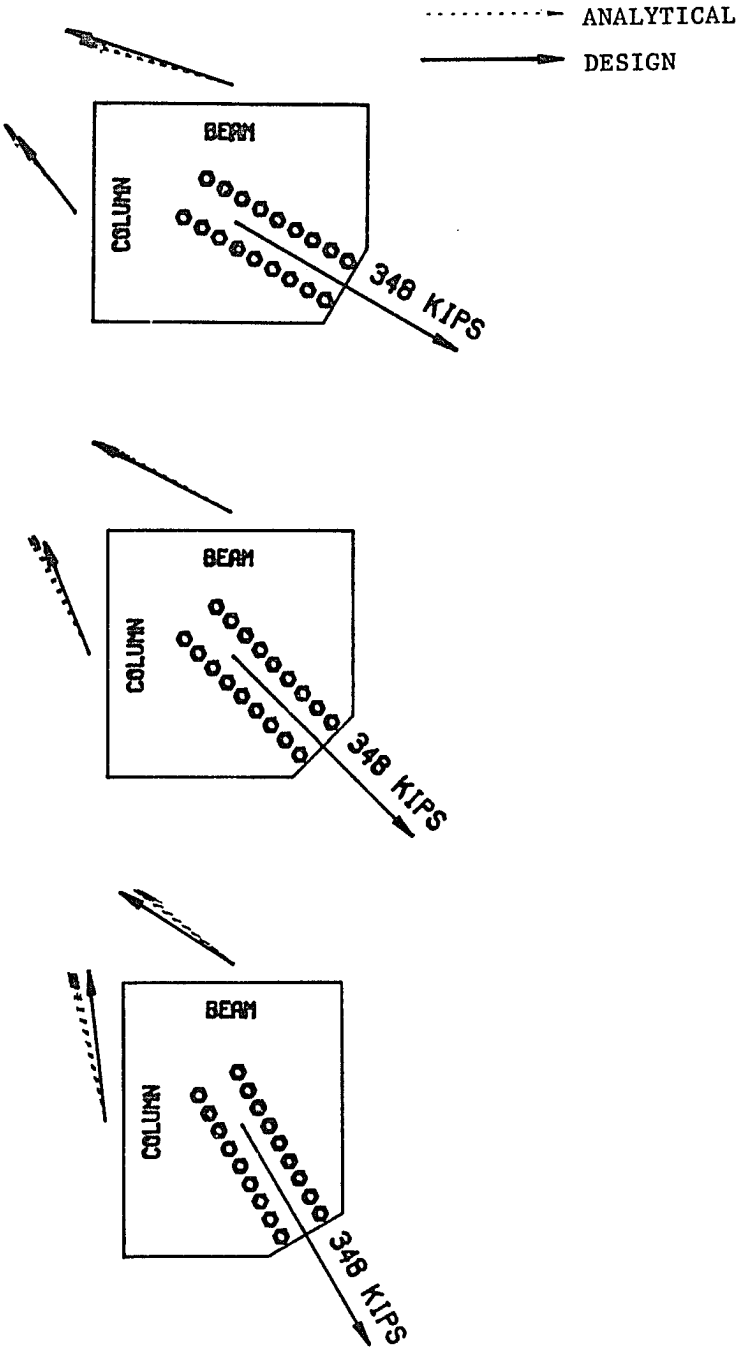

Figure 59. Analytical and Design Force Resultants for Eccentric Models.

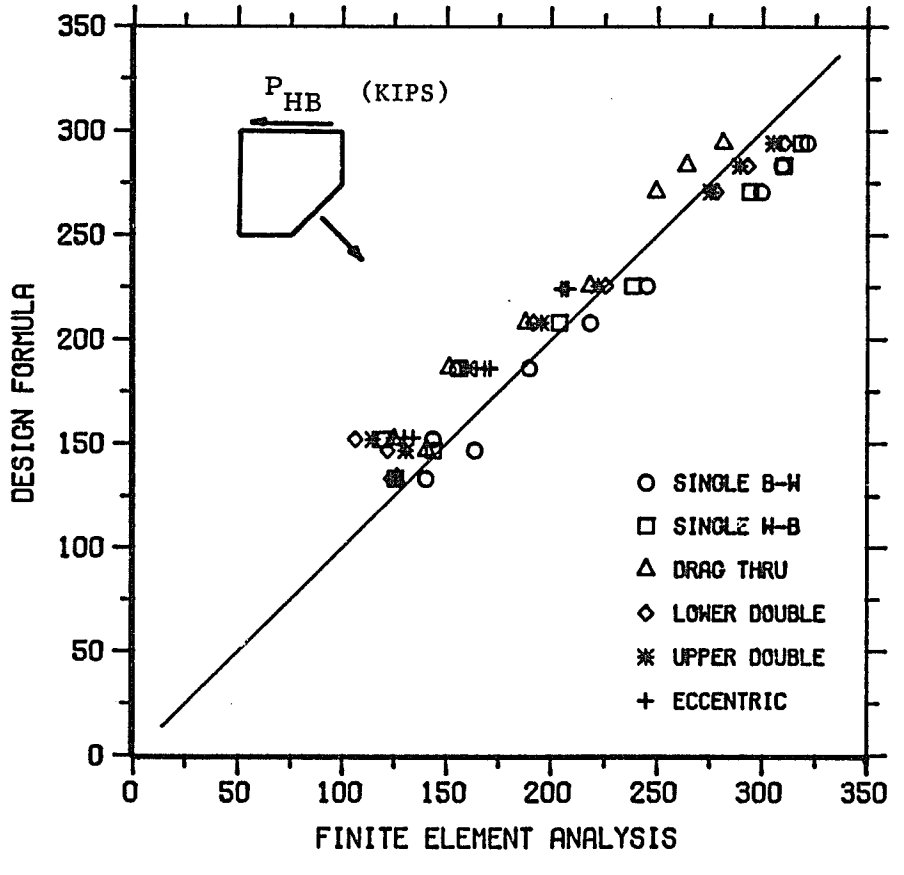

Figure 60. Design vs. Analysis for P_{HB}.

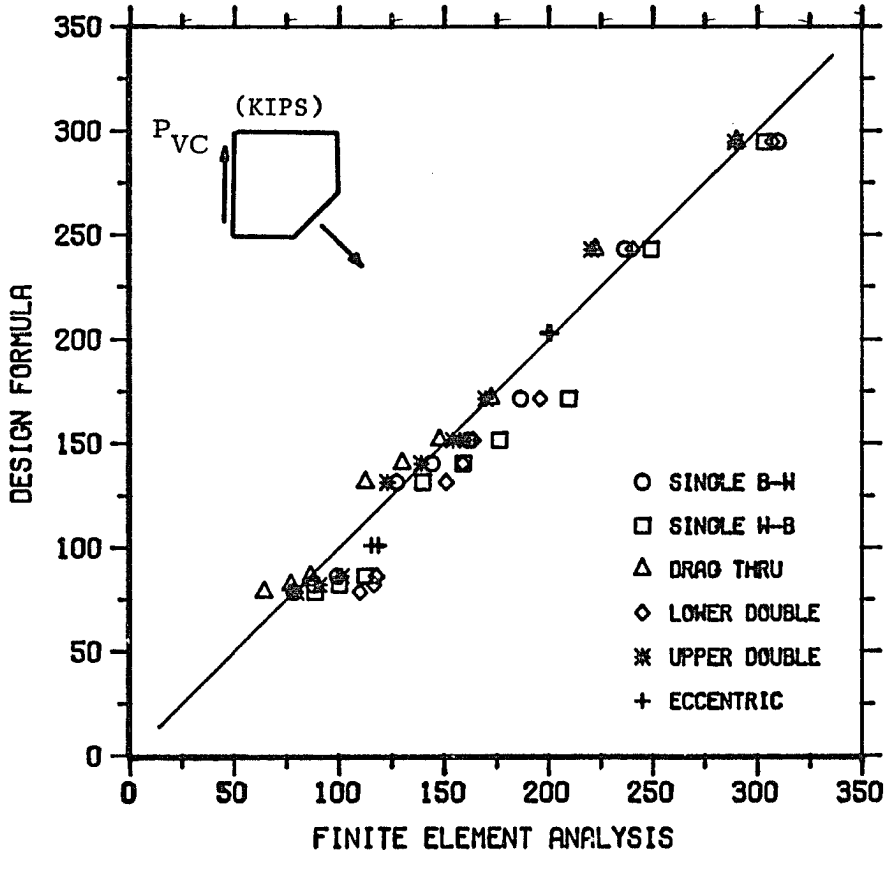

Figure 61. Design vs. Analysis for P_{VC}.

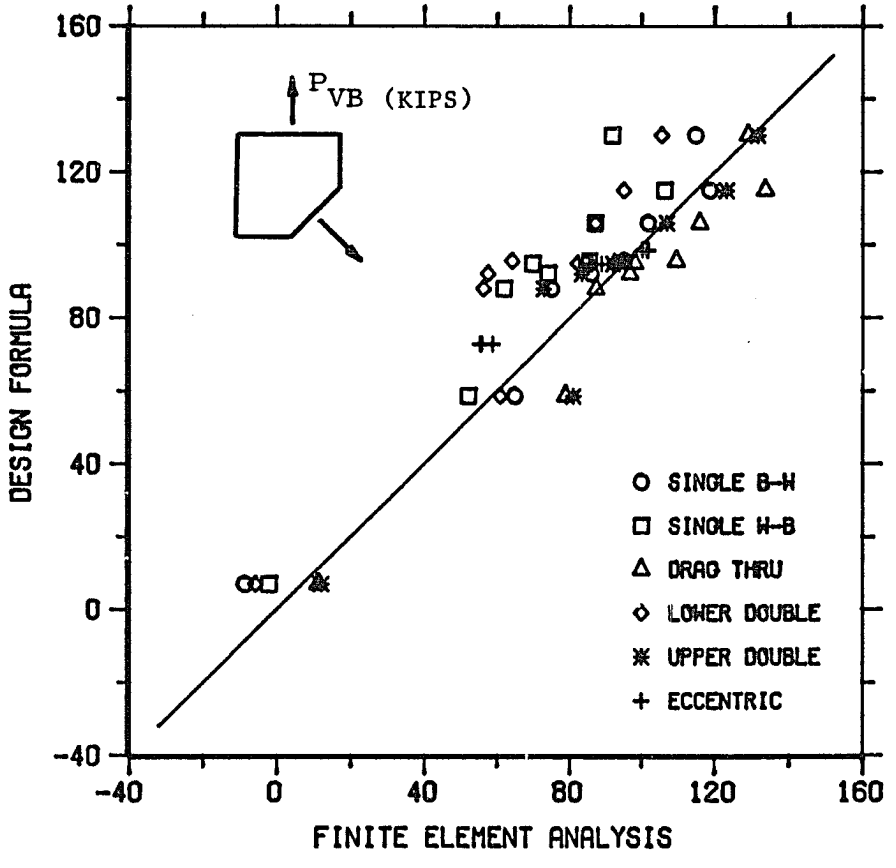

Figure 62. Design vs. Analysis for P_{VB}.

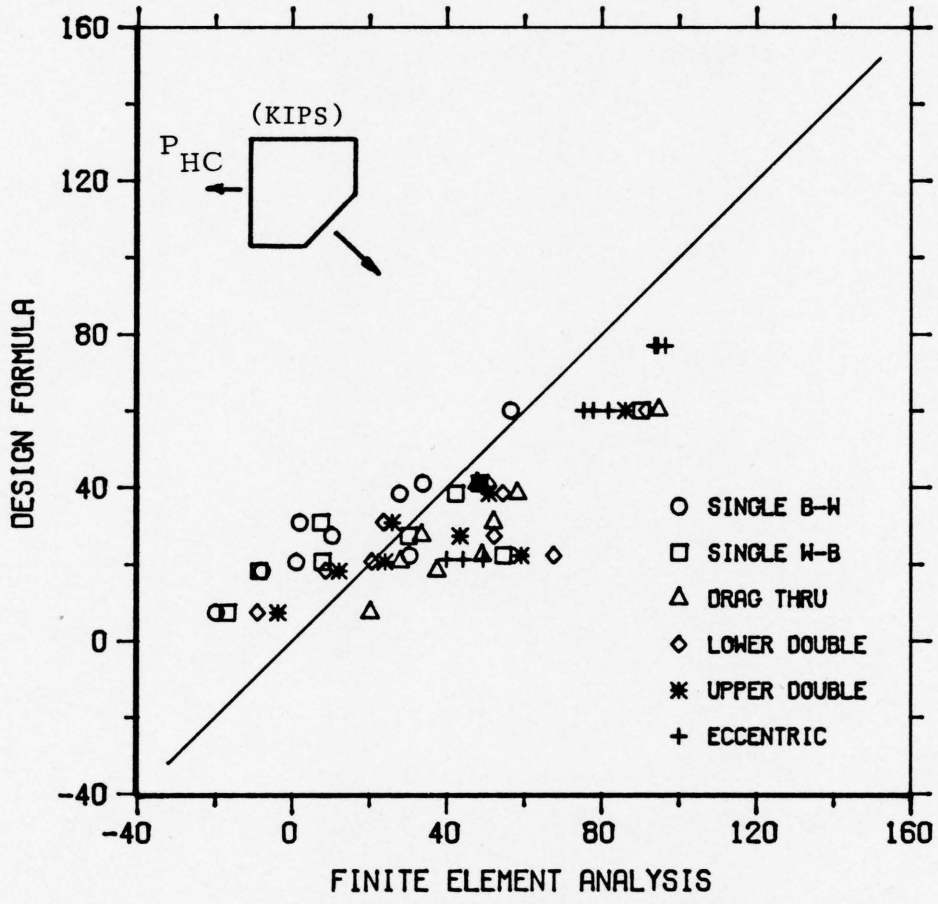

Figure 63. Design vs. Analysis for P_{HC}.

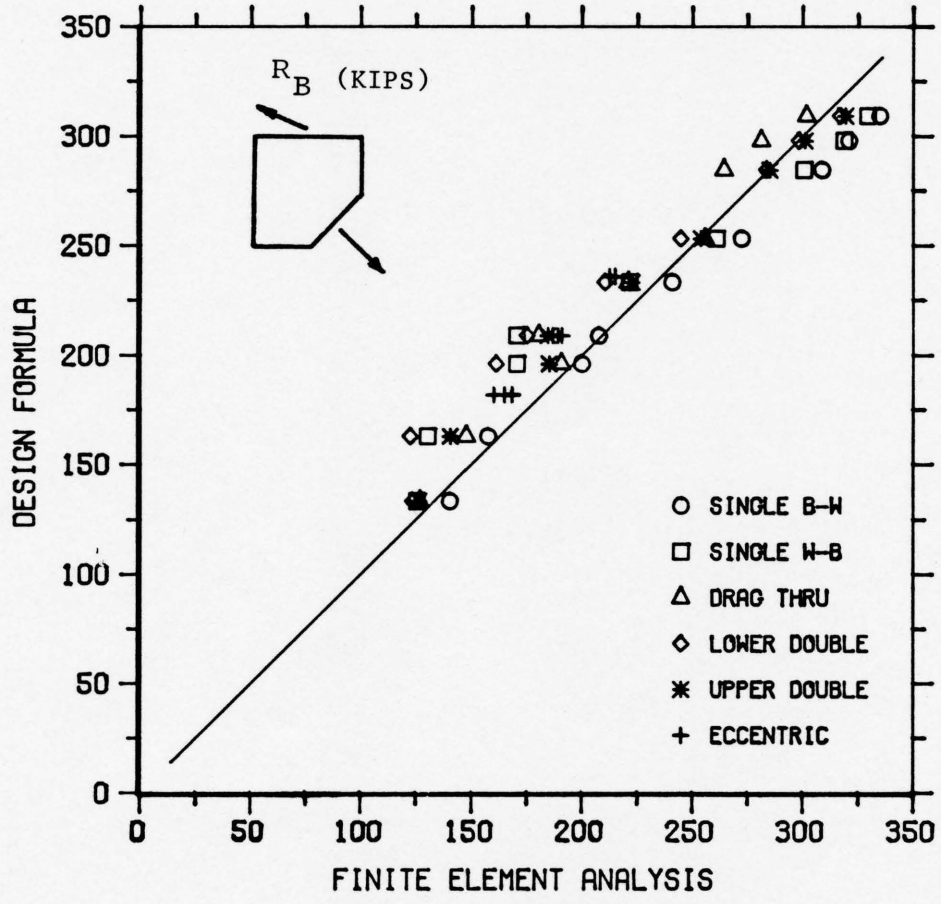

Figure 64. Design vs. Analysis for R_B.

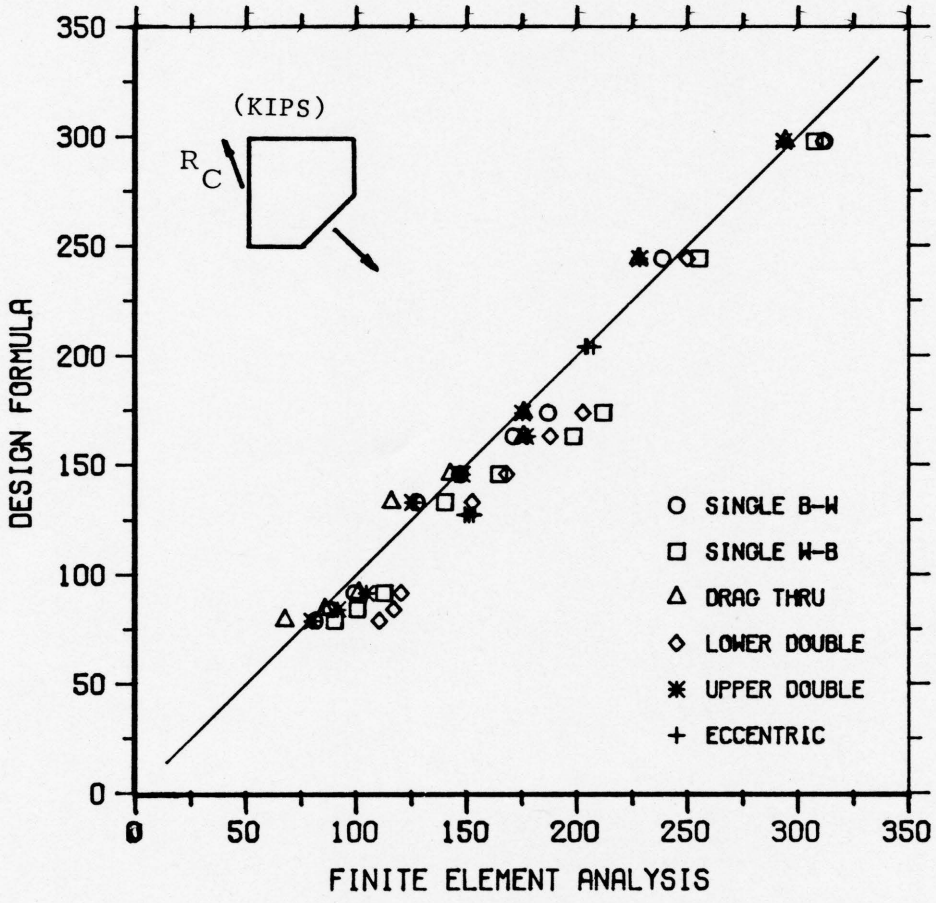

Figure 65. Design vs. Analysis for R_C.

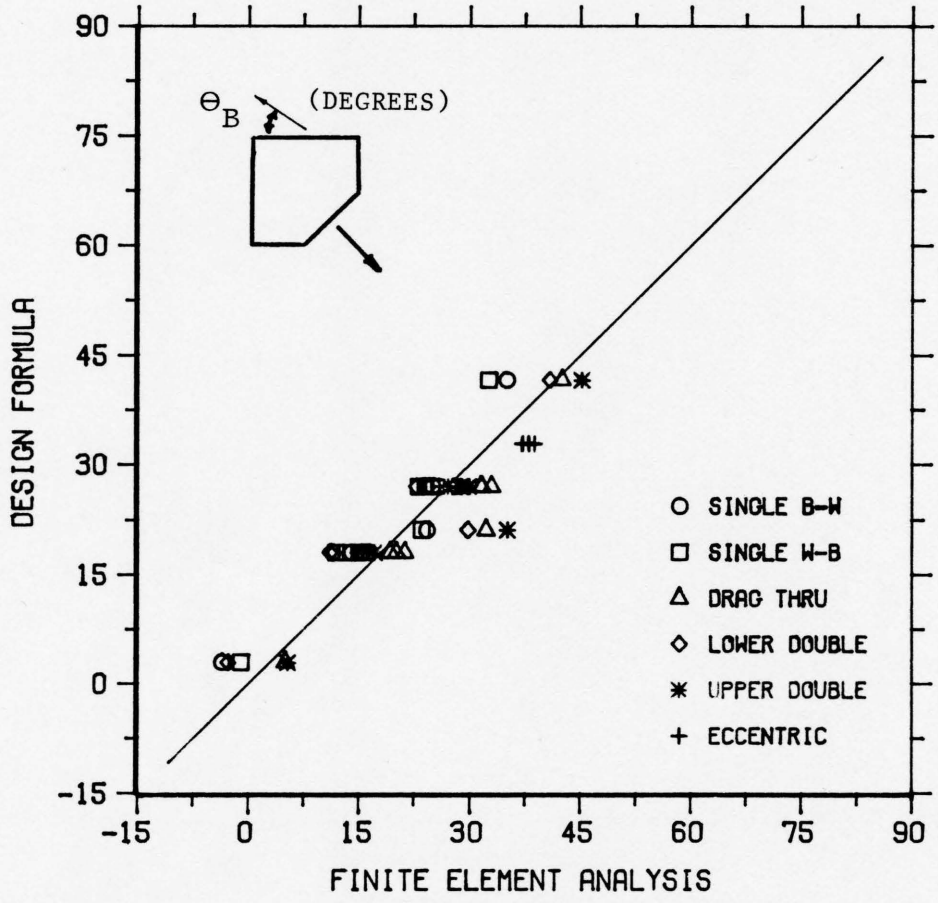

Figure 66. Design vs. Analysis for θ_B.

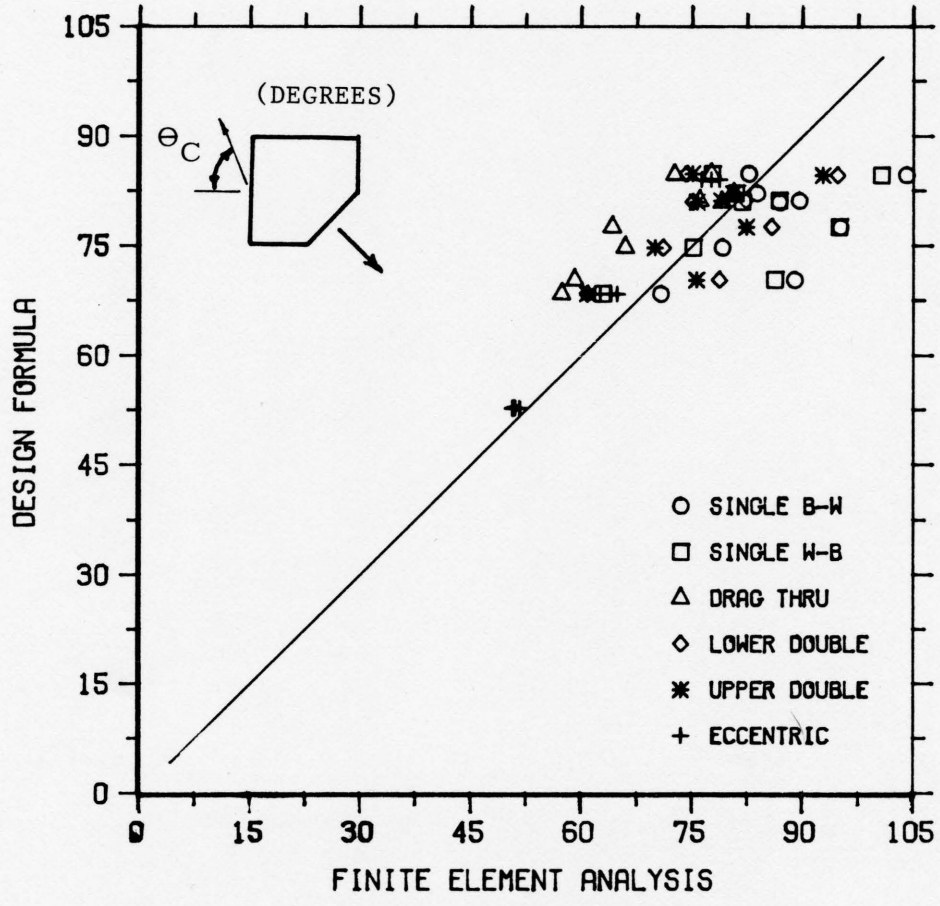

Figure 67. Design vs. Analysis for θ_C.

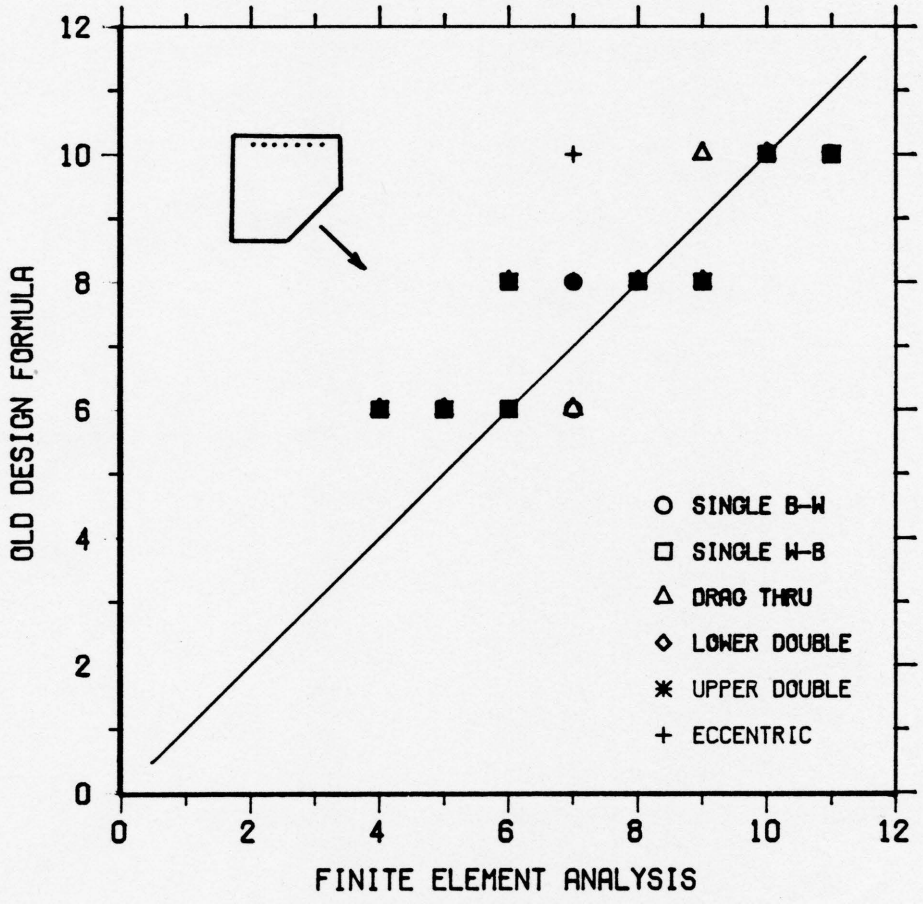

Figure 68. Current Design vs. Analysis for Number of Bolts Required Along Beam.

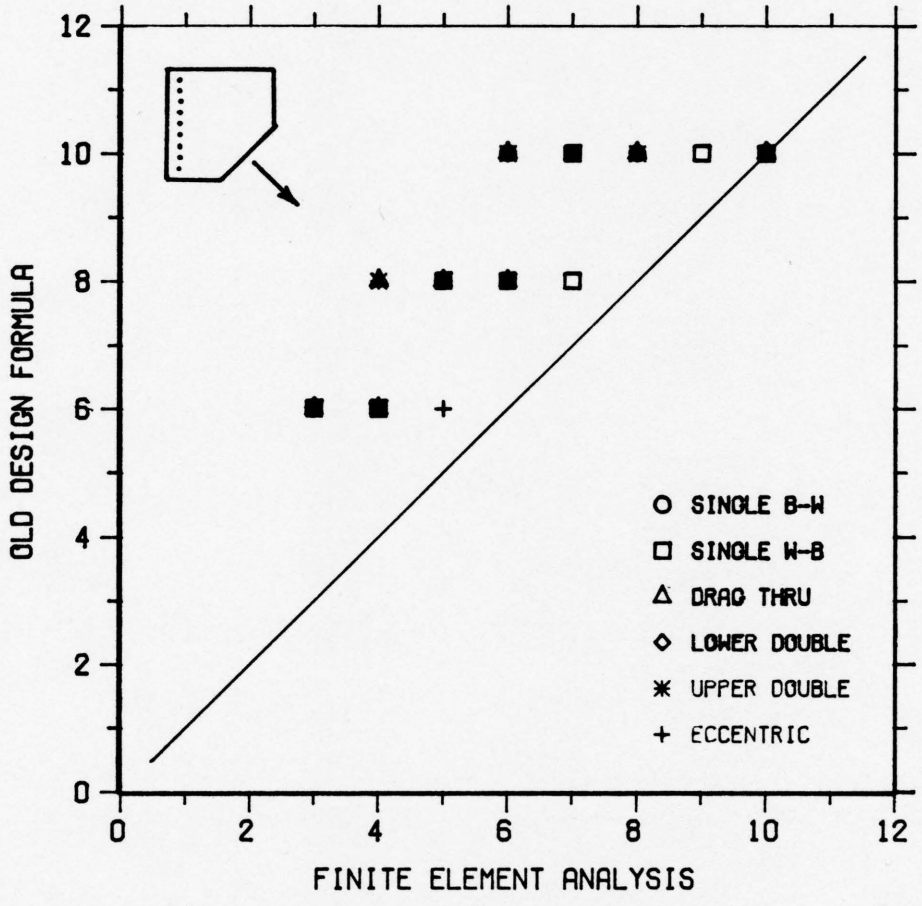

Figure 69. Current Design vs. Analysis for Number of Bolts Required Along Column.

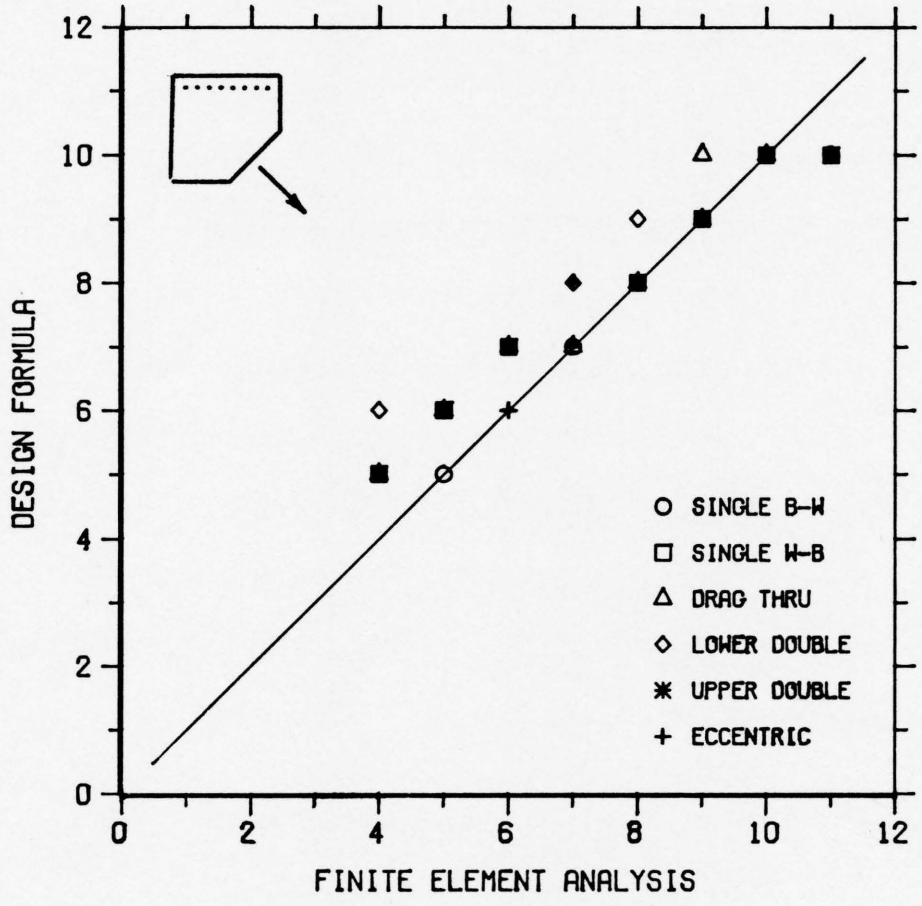

Figure 70. Proposed Design vs. Analysis for Number of Bolts Required Along Beam.

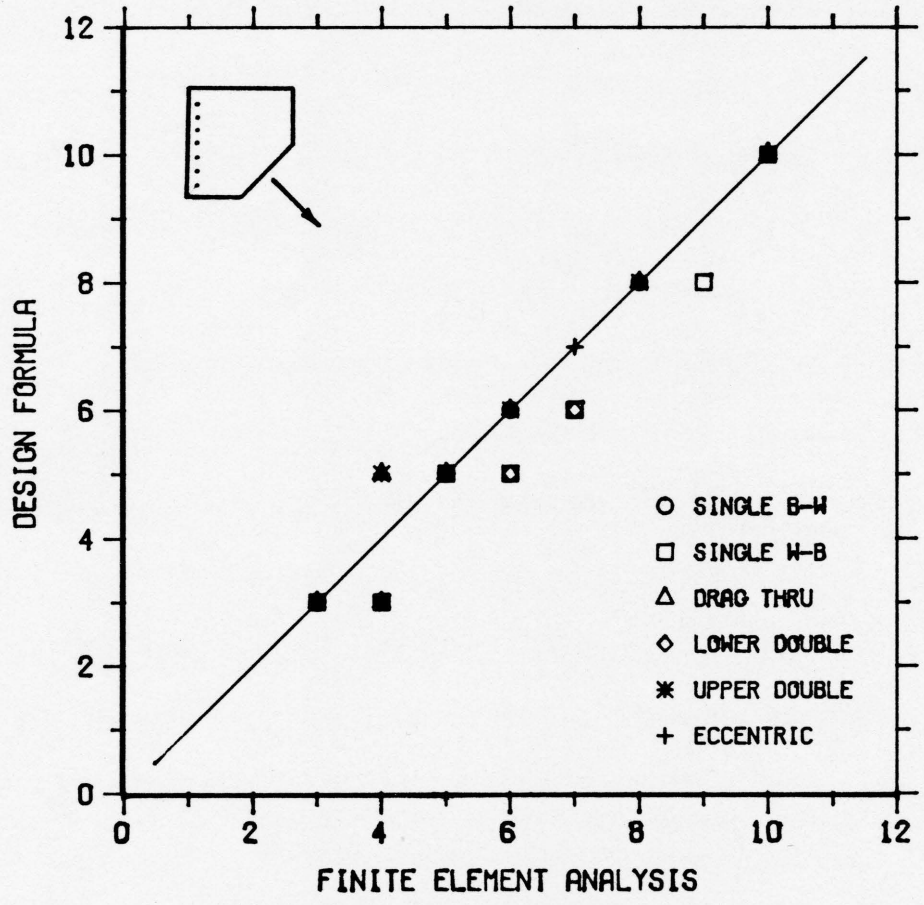

Figure 71. Proposed Design vs. Analysis for Number of Bolts Required Along Column.

Chapter 8

K-BRACING CONNECTIONS

Three bracing configurations were considered in Chapters 5, 6, and 7 to determine the gusset-to-frame connection force distributions. An additional bracing configuration shown in Figure 72 was analyzed to determine the structural behavior of these gusset plates used in K-bracing (or chevron) designs. Both the working point location and the beam-to-gusset force distributions were studied. The geometry of a typical K-bracing connection is shown in Figure 73. Brace angles of 30°, 45°, and 60° were considered for three different working point locations. All gusset plates were 3/8" thick and were welded to a 24 foot W24x100 simply supported beam. Summarized in Table 6 are the nine finite element models generated.

Illustrated in Figure 74 are the three working points considered. Currently used in practice, working point number one occurs when the axis of each bracing member and the neutral axis of the beam (without consideration of the effect of the gusset) intersect at a common point. The 30°, 45°, and 60° models with this working point are shown in Figure 77. As illustrated in Figure 75, the gusset plate contributes to the effective depth of the beam and causes the neutral axis to shift at the connection. The location of this revised neutral

axis can be calculated as shown in Figure 76. The axis of each bracing member and the revised neutral axis of the beam intersect to define working point number two, which is used in the three models plotted in Figure 78. If the minimal gusset dimensions required to accommodate the bracing are specified, then a third working point is defined. The three models using working point number three are illustrated in Figure 79.

The displacements of all models shown in these figures were magnified using the same scale to allow for comparisons of the deformed shapes. Illustrated in Figures 80 through 82 are the exaggerated deflected shapes of the 30°, 45°, and 60° models which employ the three working points. As shown in Figure 75, when working point number 1 is utilized, a negative moment (right-hand rule) acts on the part of the beam to which the gusset is attached. However, the remaining part (without the gusset attached) does not bend. If the working point (number 2) is located at the revised neutral axis, then the deformations are the smallest of the three defined working points. In contrast, the deformations are greatest when the plate dimensions are minimized (working point number 3). For working points 2 and 3, the beam should be designed to withstand the additional moment generated in the connection.

Illustrated in Figure 83 are typical weld force distributions for the gusset-to-beam connections. Two major conclusions can be drawn

from the results shown in these figures. First, the weld forces are not uniform; and second, the weld forces do not act in pure shear (parallel to the edge of the plate). Each of these behaviors cause the maximum weld force to be 20% to 50% greater than a uniform weld force acting in pure shear. However, because of material ductility, the force distribution will become uniform as ultimate load is achieved. Since the weld forces do not act in pure shear, it is recommended that the gusset-to-beam fasteners be designed to withstand 1.3 times the brace components which act parallel to the beam. That is,

$$V = (1.3)(2)\ P \cos\theta = 2.6\ P \cos\theta$$

where

V = design load to be resisted by fasteners

P = brace design load

θ = brace angle

In summary, utilizing the minimum gusset plate dimensions required to accommodate the bracing members will:

- produce an economic connection
- result in greater uniformity in the gusset-to-beam fastener loads
- increase the buckling strength of the plate (see Chapter 9)
- create a small moment in the eccentric connection

Table 6. Finite Element Models Generated to Study the Structural Behavior of K-Bracing Gusset Plates

Brace Angle	Plate Dimensions 2a	b	Working Point Location, h
30°	104.8"	21"	0"
45°	72.0"	24"	0"
60°	54.0"	30"	0"
30°	88.2"	21"	4.8"
45°	60.6"	24"	5.7"
60°	42.9"	27"	6.6"
30°	54.0"	21"	14.7"
45°	48.0"	24"	12.0"
60°	42.0"	27"	7.4"

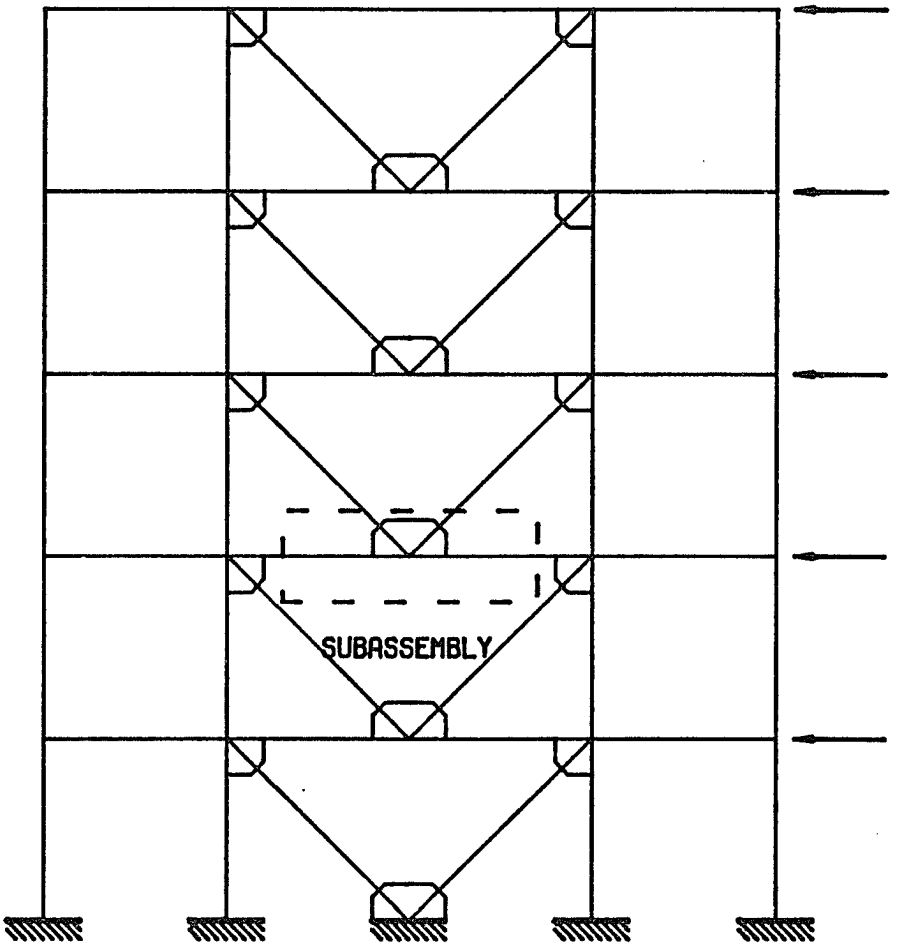

Figure 72. K-bracing Configuration.

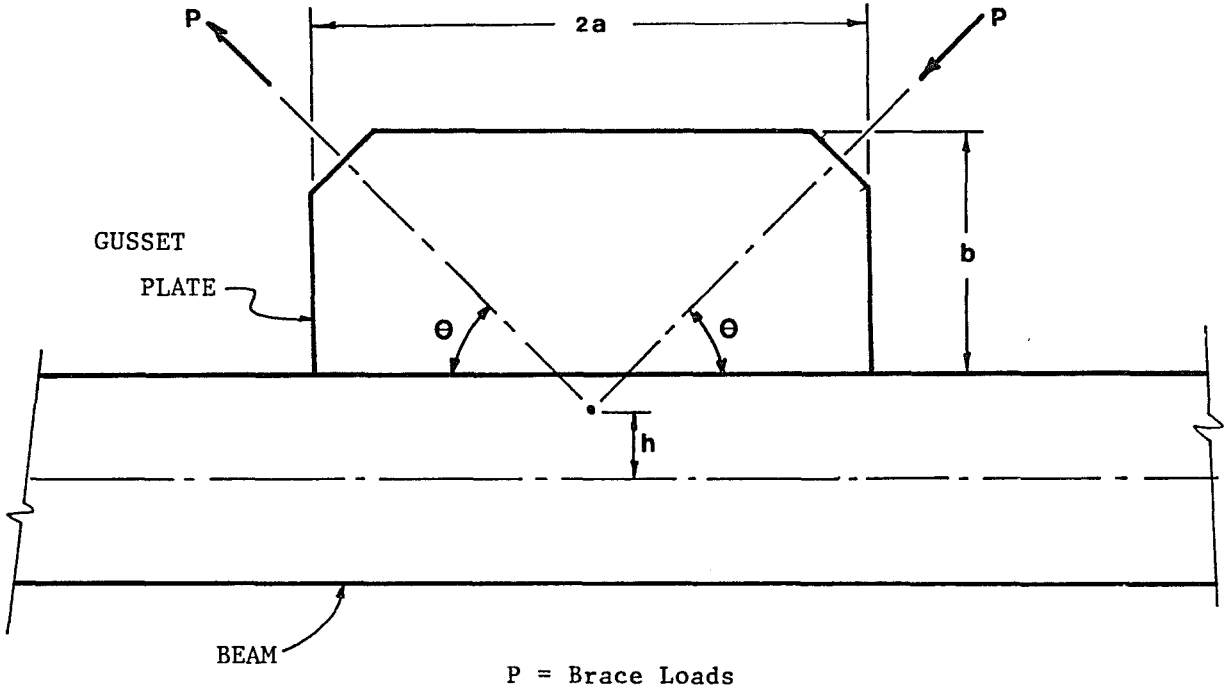

P = Brace Loads

θ = Brace Angle

2a x b = Plate Dimensions

h = Working Point Location

Figure 73. K-bracing Connection Geometry.

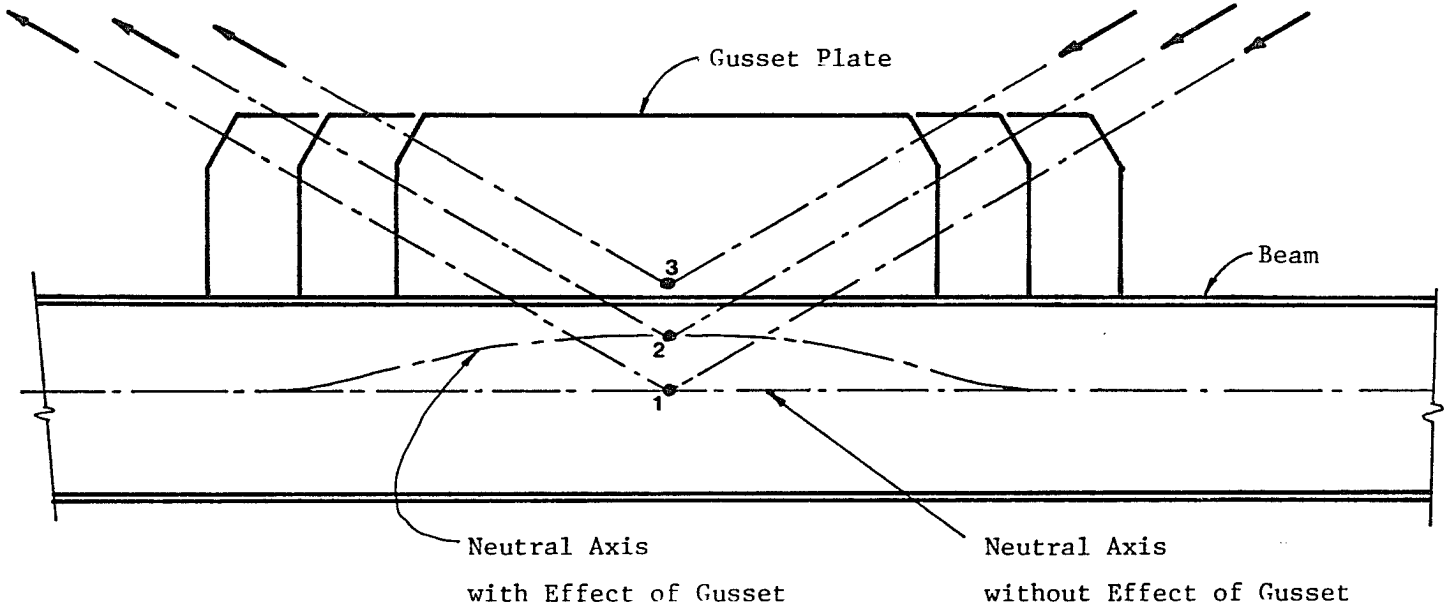

Figure 74. K-bracing Connection Working Points.

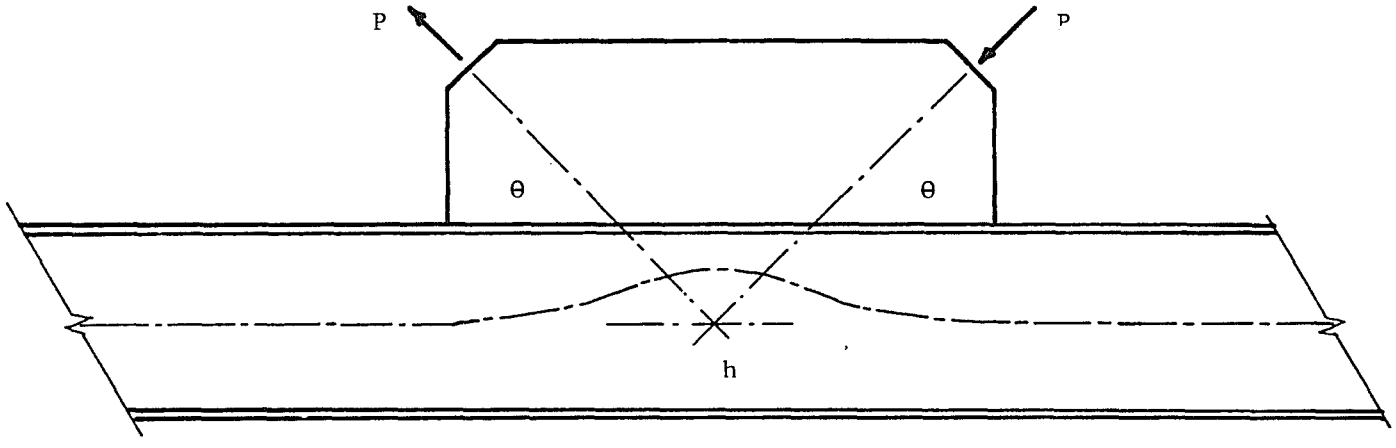

BEAM WITH GUSSET PLATE FOR K-BRACING

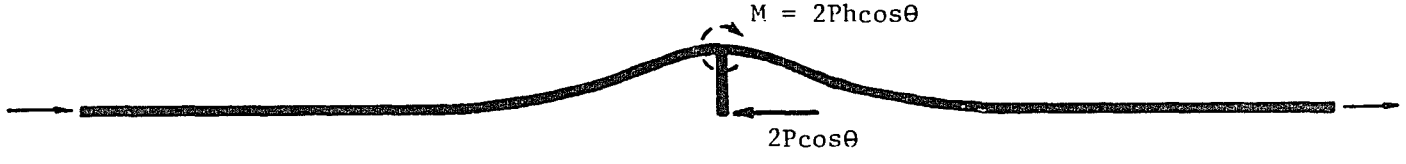

LINE MODEL

Figure 75. Effects of Gusset Plate on Beam.

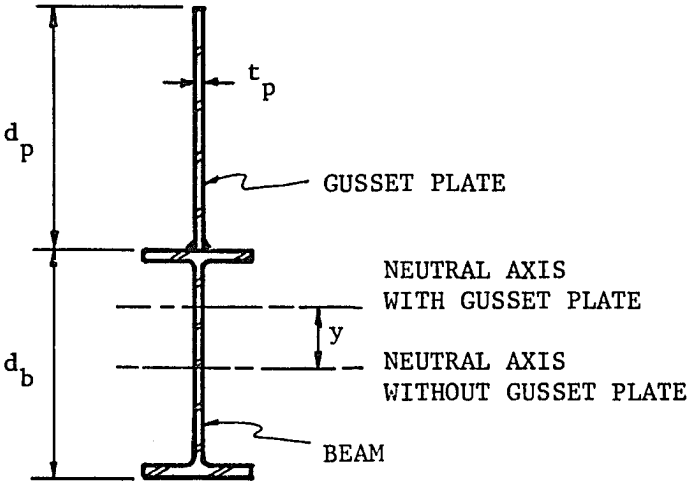

$$y = \frac{0.5\ t_p d_p (d_p + d_b)}{A_b + t_p d_p}$$

t_p = GUSSET PLATE THICKNESS

d_p = GUSSET PLATE DEPTH

d_b = BEAM DEPTH

A_b = BEAM CROSS SECTIONAL AREA

Figure 76. Calculation of Revised Beam Neutral Axis.

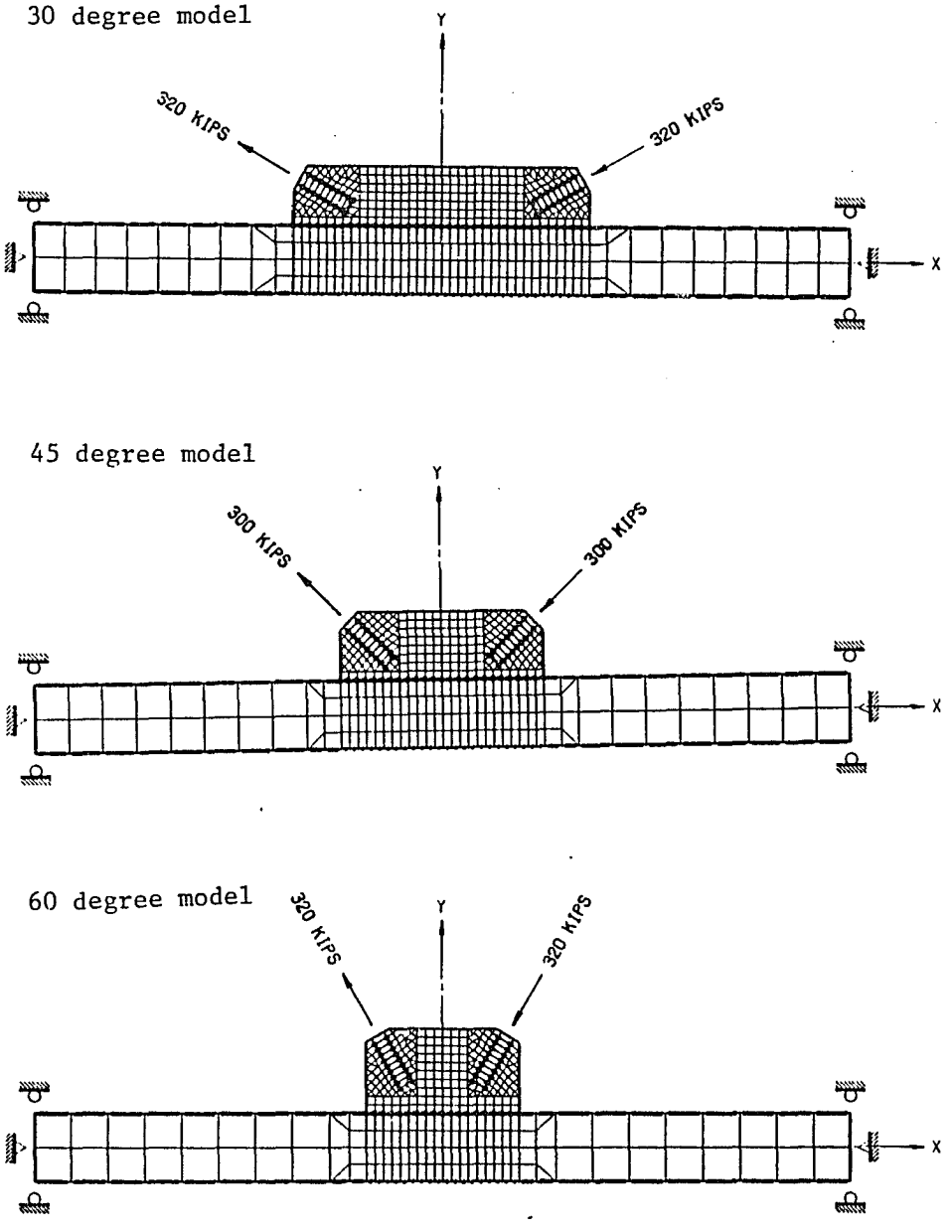

Figure 77. K-bracing Connection Models Utilizing Working Point Number 1.

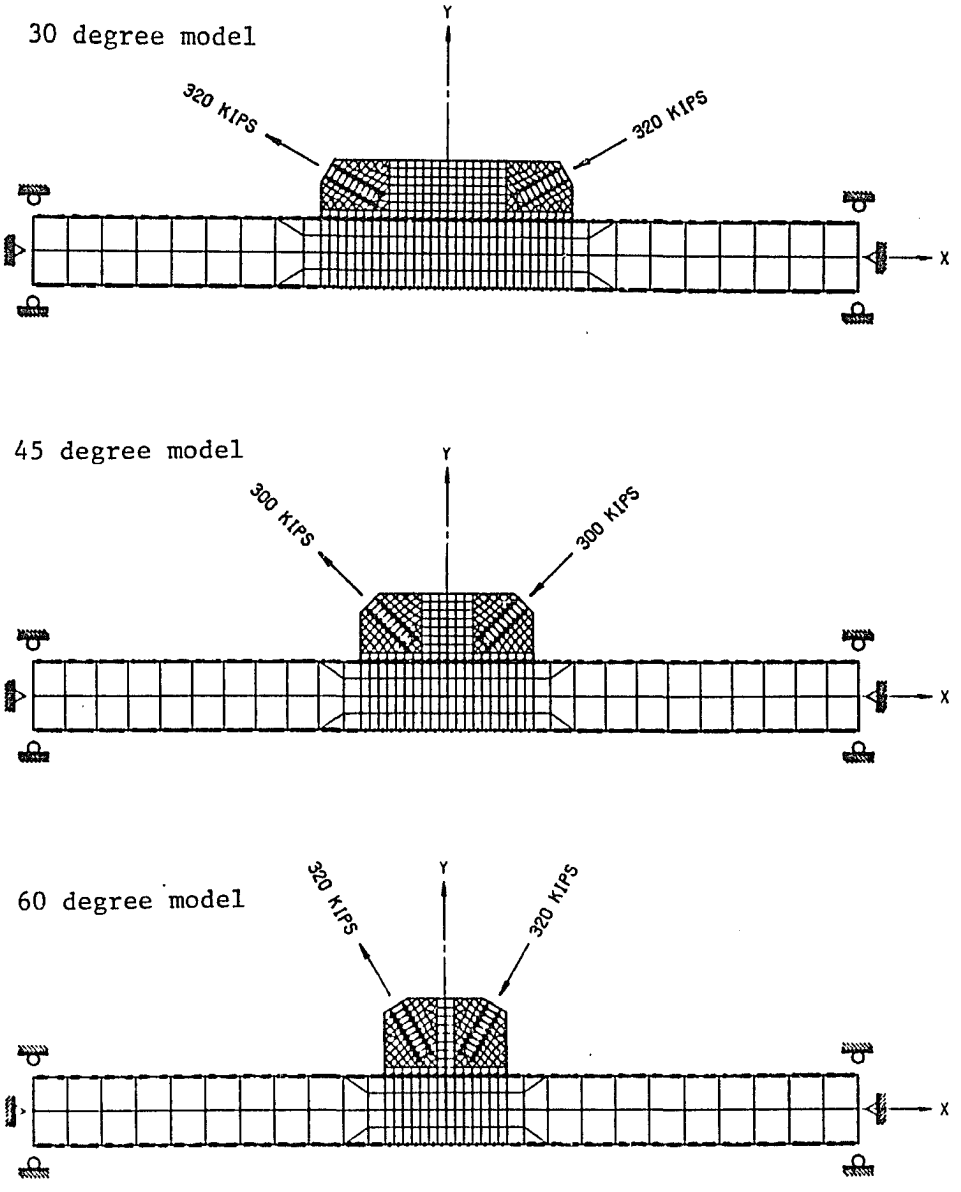

Figure 78. K-bracing Connection Models Utilizing Working Point Number 2.

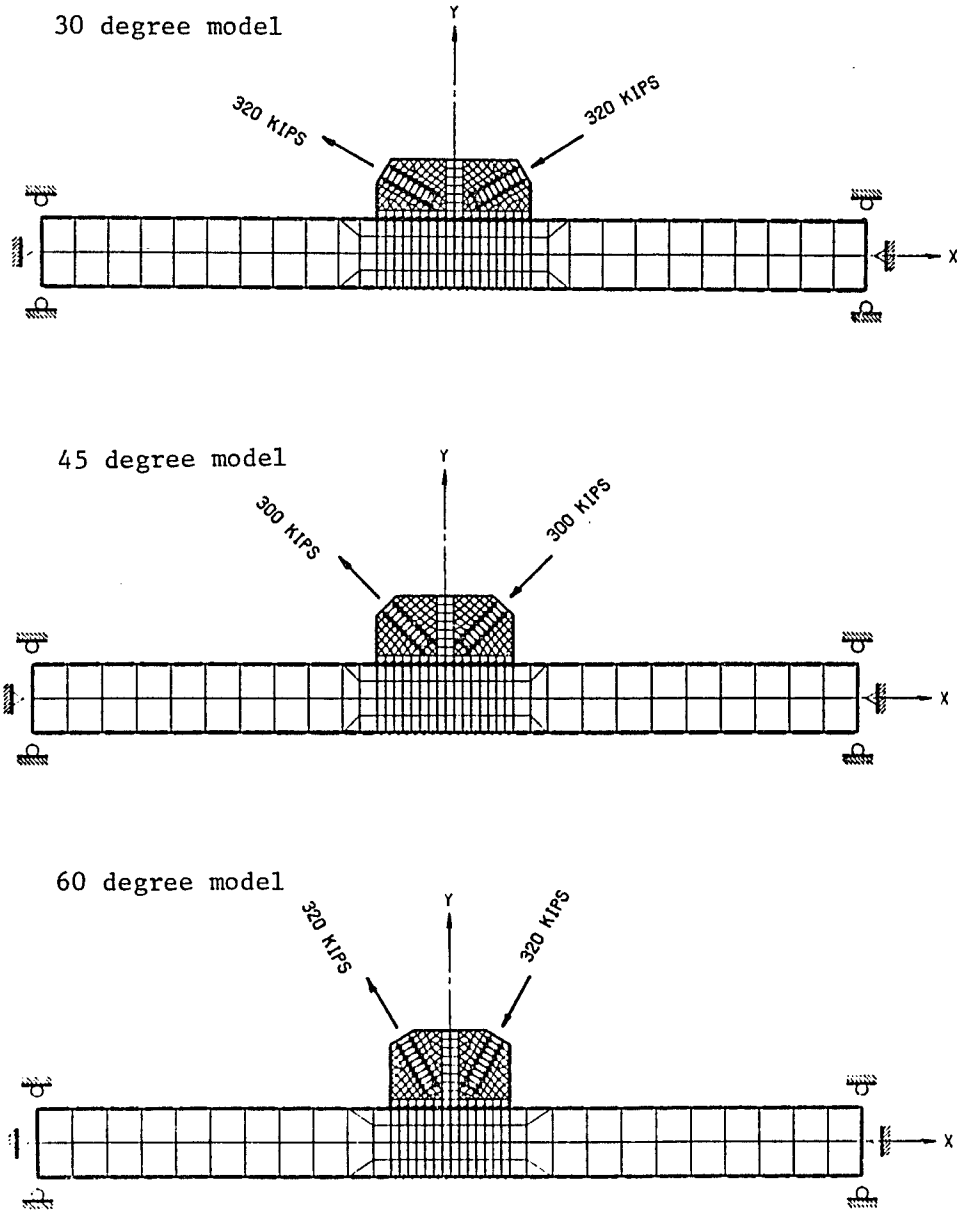

Figure 79. K-bracing Connection Models Utilizing Working Point Number 3.

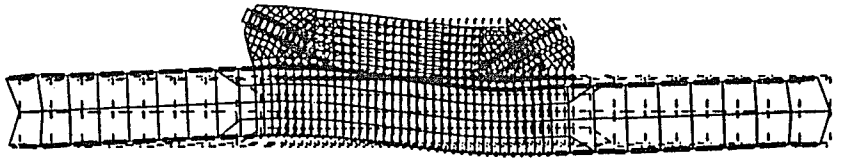

30 degree model

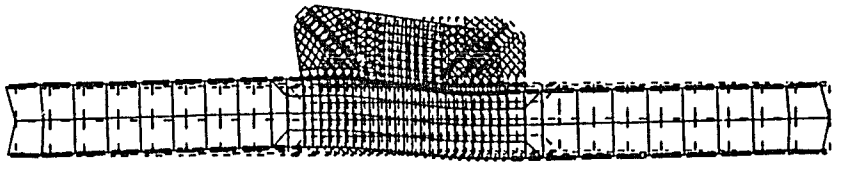

45 degree model

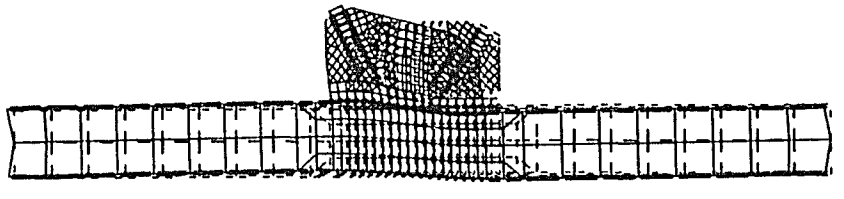

60 degree model

Figure 80. Exaggerated Deflected Shapes of the Working Point Number 1 Models.

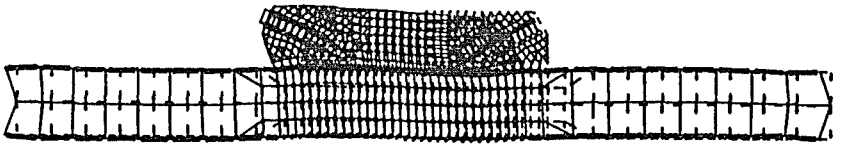

30 degree model

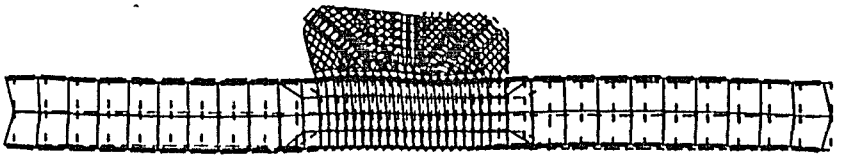

45 degree model

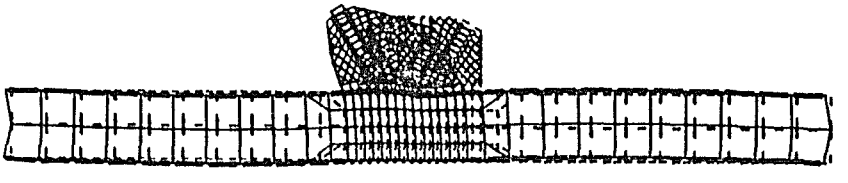

60 degree model

Figure 81. Exaggerated Deflected Shapes of the Working Point Number 2 Models.

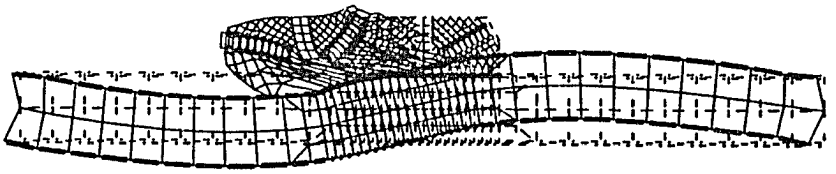

30 degree model

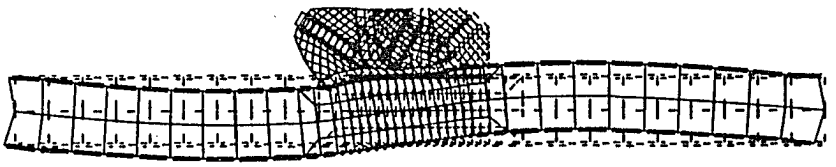

45 degree model

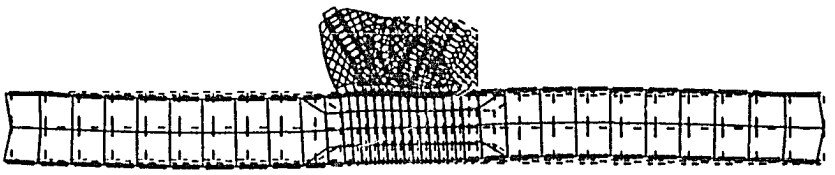

60 degree model

Figure 82. Exaggerated Deflected Shapes of the Working Point Number 3 Models.

30° WORKING POINT NO. 1

BRACE LOAD = 320 KIPS

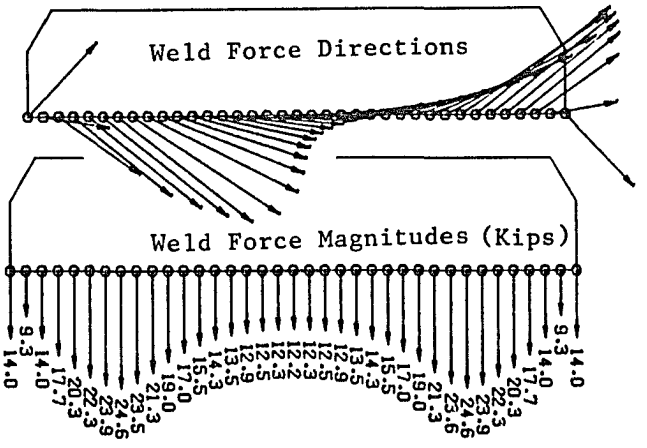

30° WORKING POINT NO. 2

BRACE LOAD = 320 KIPS

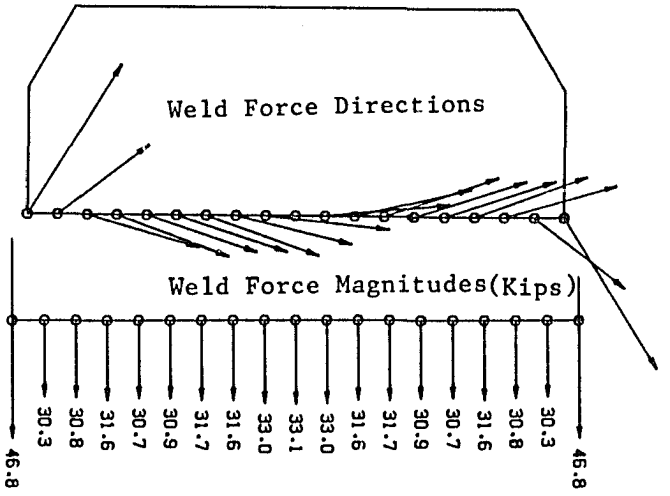

Figure 83. Typical Weld Force Distributions in K-bracing Connections.

Chapter 9

BUCKLING STRENGTH OF GUSSET PLATES

Illustrated in Figure 84 are two braced frames subjected to lateral loads which cause compressive stresses in the bracing members and gusset plates. When the load in a diagonal member is compressive, the gusset plate can fail by buckling. To study the buckling strength of gusset plates, the general purpose finite element program NASTRAN was utilized. All of these analyses were restricted to linearly elastic assumptions, and no estimate was made of the post-buckling strength.

Finite Element Analyses

Summarized in Table 7 are the 17 finite element models generated for the buckling analyses. The gusset plate geometry is defined in Figure 85. To isolate the buckling behavior of the gusset plate, the beam and column framing members were not included in these models. In addition, the bracing member was assumed to be stiff enough not to buckle; therefore, the gusset plate at the brace-to-gusset connection was restrained from out-of-plane translations. All gussets were modeled as 3/8" steel plates. The following connection parameters were studied:

- number of bracing members attached to the gusset: single brace, double brace (K-brace)
- brace angles: 45°, 60° (same as 30°)
- edge supports: simple, fixed
- mesh sizes: coarse, fine
- plate dimensions: from 39" x 27" to 24" x 48"

The elastic buckling load and the buckled shape for the first mode of buckling was obtained for each model. Finite element meshes are shown in Figures 86 through 90.

The analytically determined buckling loads obtained from the NASTRAN analyses are summarized in Table 8. The buckled shapes for each model are illustrated in Figures 91 through 97. The following conclusions can be drawn from these results.

1. The buckling loads obtained from the coarse mesh are within 6% of the loads obtained from the fine mesh; therefore, these meshes adequately predict the buckling behavior of the gusset plates.
2. The fixed edge support condition yields buckling loads that are approximately 80% greater than for the simple support edge condition.
3. The buckling loads for these K-bracing gussets are 50% to 150% greater than the buckling loads for the single bracing gussets.

4. The single bracing gusset buckling modes show maximum displacement along the longest unsupported edge.
5. The K-brace gusset buckling modes show maximum displacement along the longest unsupported edge, as well as, in the interior of the plate. This is because of the greater complexity of the connection, and the presence of the tensile brace load.

Design Procedures

The Whitmore pattern can be utilized to determine the buckling strength of diagonal bracing connections (37). The unsupported lengths L_1, L_2, and L_3 can be calculated as shown in Figure 98. For the K-bracing configuration only half of the gusset plate should be considered as shown. A modified Euler critical buckling load (38) can be calculated for elastic design purposes:

$$P_{cr} = \pi^2 EI/(kL)^2$$

where,

E = Young's Modulus

$I = dt^3/12$

d = effective Whitmore length (see Chapter 4)

t = gusset plate thickness

k = 0.65, for single bracing gussets

= 0.45, for K-bracing gussets

L = maximum of L_1, L_2, and L_3

The modified Euler loads for the analytical models considered in this study are listed in Table 9.

As illustrated in Figure 99, the elastic analytical and Euler loads compare favorably for the simply supported gusset plates. However, when fixed edge supports are employed, the modified Euler formula is conservative by an approximate factor of two. Therefore, since the true boundary conditions for the gusset plate edge support is between the simple and fixed conditions, the modified Euler formula is conservative for predicting the elastic buckling load of gusset plates. However, in real connections gusset plates may buckle inelastically.

To calculate inelastic buckling loads, the following procedure is recommended (37).

1. Consider a 1-inch strip of length L to be a fixed-fixed column (k=0.65, or k = 0.45 for K-bracing gussets) where L is the maximum of L_1, L_2, and L_3 (refer to Figure 98).
2. Calculate the radius of gyration of the one-inch strip: $r = \sqrt{I/A} = t/\sqrt{12}$, where t is the gusset plate thickness (inches).
3. Compute kL/r = 2.25 L/t (= 1.56 L/t for K-bracing gussets).
4. Find the allowable compressive stress F_a corresponding to kL/r in the AISC specification Table 3-36 (21).

5. If the normal stress on the Whitmore effective area (see Chapter 4) is less than F_a then the gusset will not buckle.

This procedure is conservative because it ignores the post-buckling strength of plates. Further research is required to study inelastic buckling of gusset plates.

To increase the buckling strength of a given gusset plate, several options are available:

- increase the plate thickness
- reduce the plate dimensions
- add stiffeners to long unsupported plate edges

As discussed in Chapter 10, the frame must be designed to withstand the additional moments caused by connection eccentricities that may result from reducing the plate dimensions. The buckled shapes shown in Figures 91 through 97 show why the stiffener should be added to the longer plate edge. Further studies are required to develop a criterion for designing gusset plate stiffeners.

Table 7. Finite Element Models for Buckling Analysis

Plate No.	Brace Angle	Plate Dimensions a	b	Case 1	2	3	4
1	45°	27"	27"	X	X		X
2	45°	37"	27"	X			X
3	45°	39"	27"	X		X	X
4	60°	24"	30"	X	X		X
5	60°	24"	39"	X		X	X
6	60°	24"	48"	X		X	X

Case	Gusset Type	Edge Supports	Mesh Size
1	Single Brace	Simple	Coarse
2	Single Brace	Simple	Fine
3	Single Brace	Fixed	Coarse
4	K-Brace	Simple	Coarse

Table 8. Elastic Analytical Buckling Loads (Kips) for the Gusset Plate Models

Plate No.	Case 1	2	3	4
1	738	697	-	1146
2	450	-	-	771
3	268	-	491	597
4	537	526	-	1014
5	232	-	429	570
6	127	-	237	337

(Buckling Load)/(Buckling Load for Case 1)

Plate No.	Case 1	2	3	4
1	1.00	0.94	-	1.55
2	1.00	-	-	1.71
3	1.00	-	1.83	2.23
4	1.00	0.98	-	1.89
5	1.00	-	1.85	2.46
6	1.00	-	1.87	2.65

Table 9. Elastic Euler Buckling Loads

Plate No.	L_1	L_2	L_3	Critical Load (Kips) Single Brace	K-Brace
1	13.2"	0.3"	0.3"	457	937
2	13.2"	8.8"	0.3"	457	937
3	13.2"	17.3"	0.3"	267	545
4	11.7"	-2.8"	4.2"	585	1192
5	19.5"	-2.8"	14.6"	209	429
6	19.5"	-2.8"	25.0"	127	261

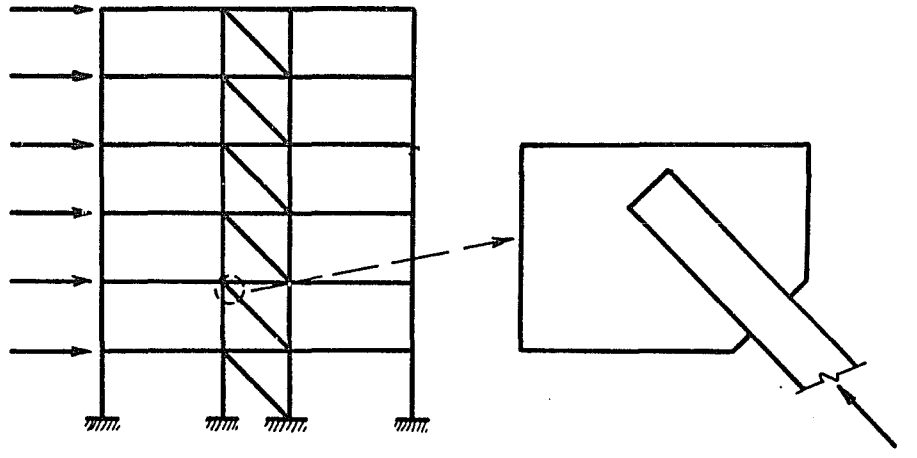

Single Brace Gusset Plate

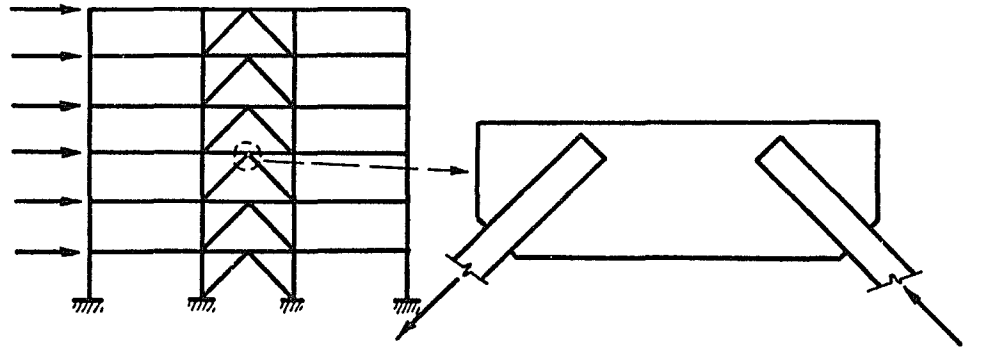

K-Brace Gusset Plate

Figure 84. Braced Frames with Compressive Brace Loads.

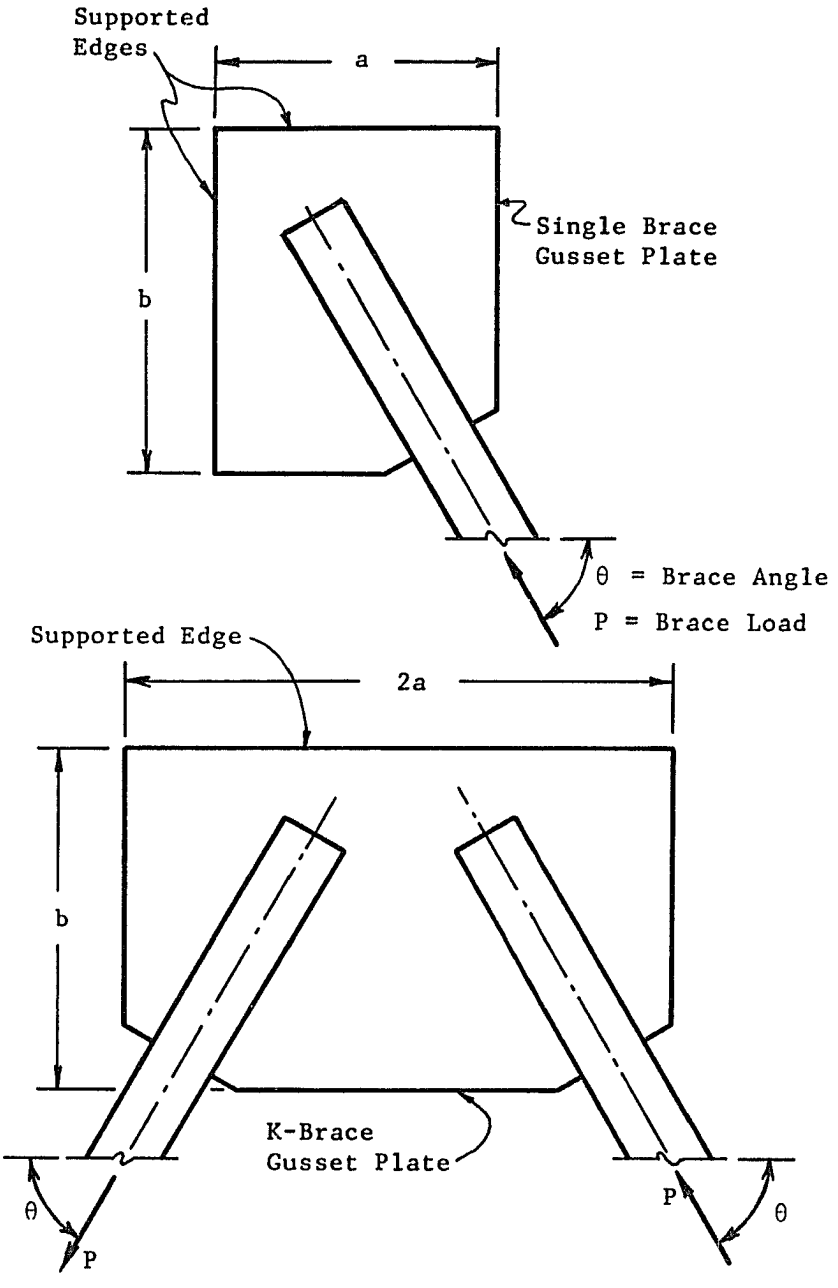

Figure 85. Gusset Plate Geometry for Buckling Analyses.

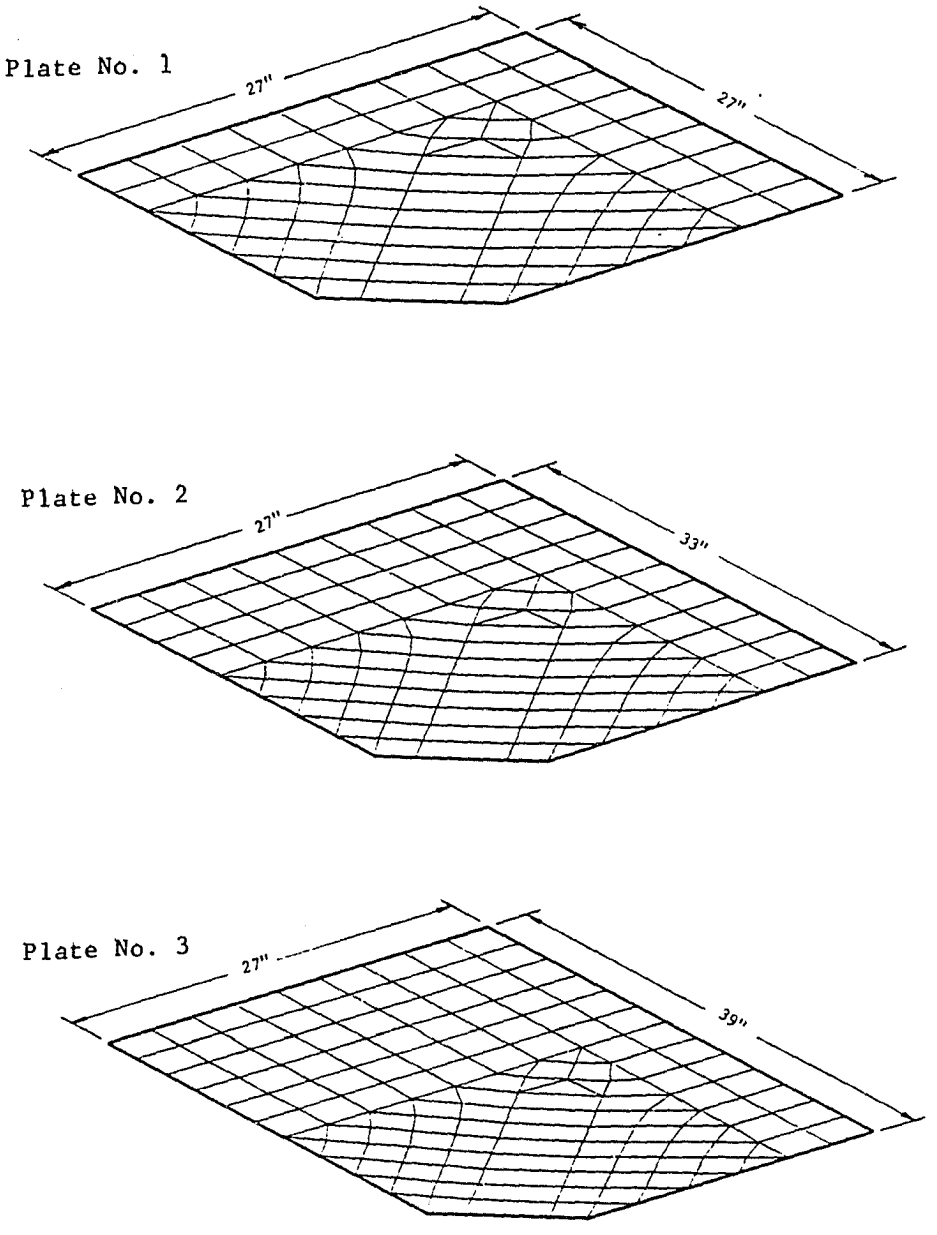

Figure 86. 45° Single Bracing Gusset Models for Buckling Analysis.

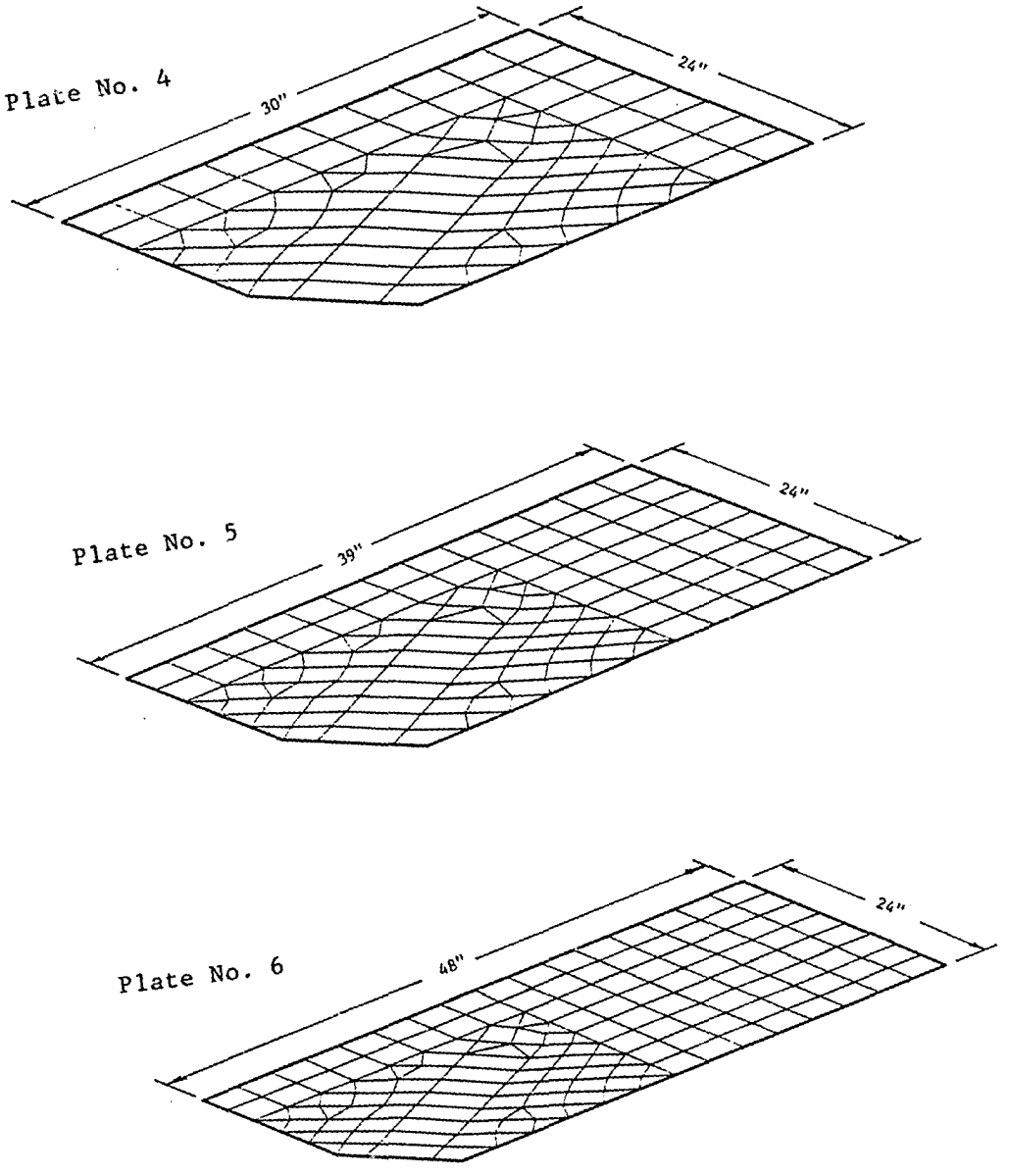

Figure 87. 60° Single Bracing Gusset Models for Buckling Analysis.

Plate No. 1

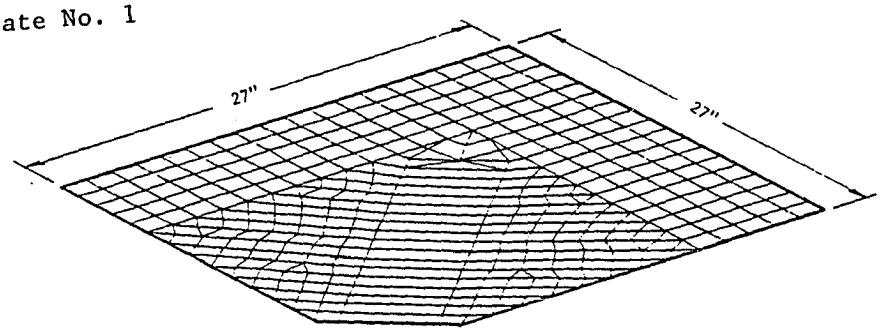

Plate No. 4

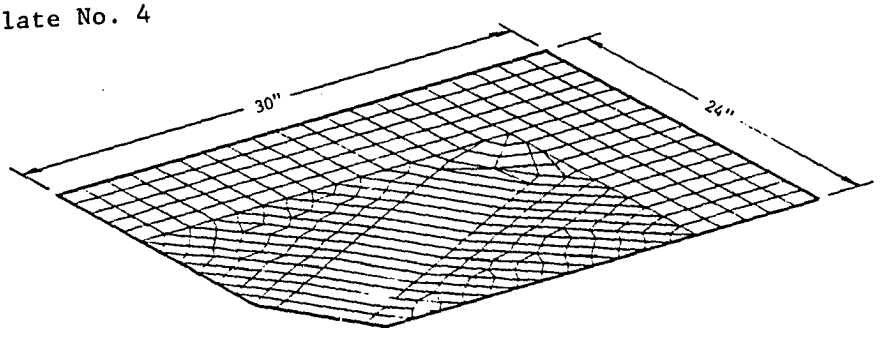

Figure 88. Fine Mesh Models for Buckling Analysis.

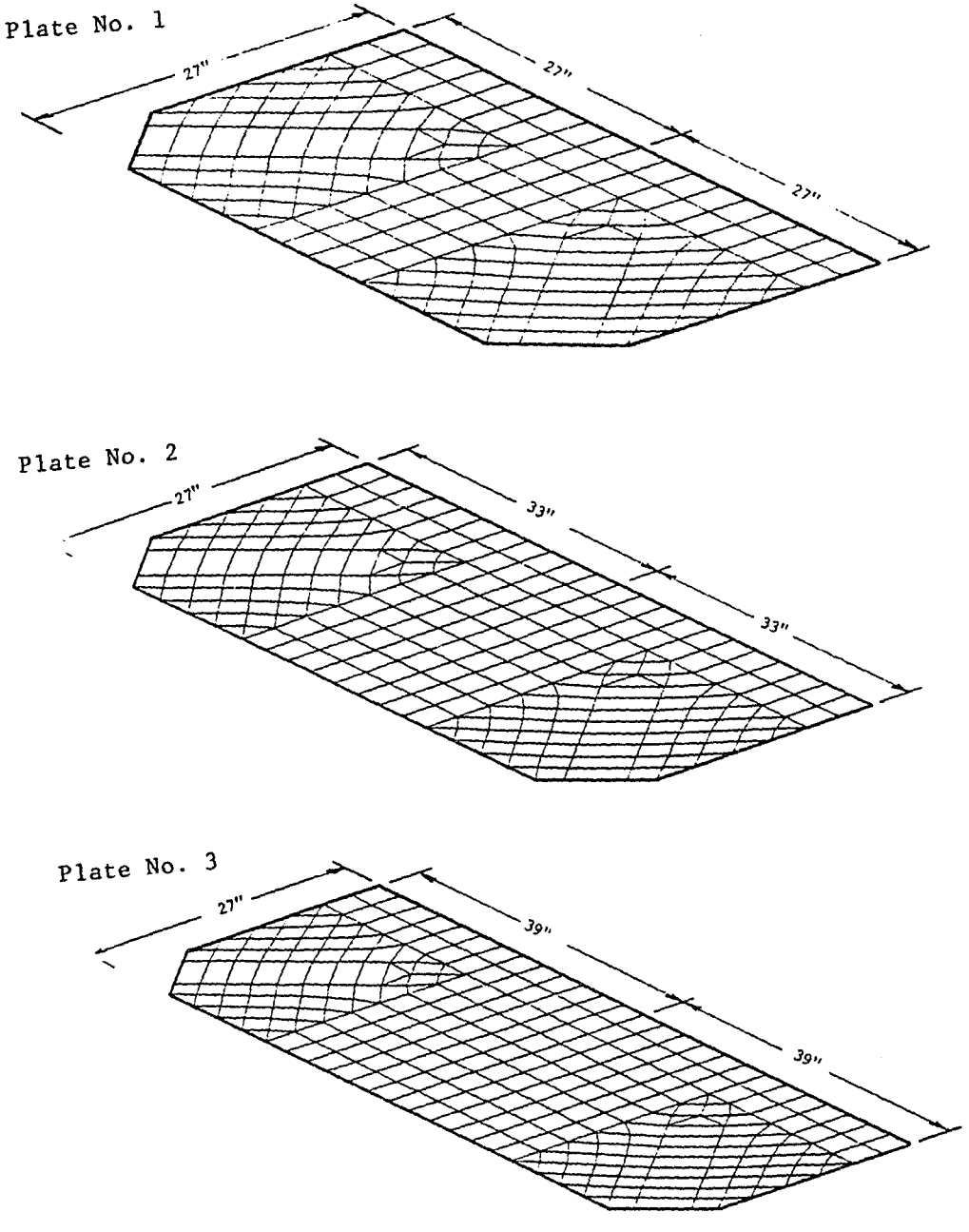

Figure 89. 45° K-Bracing Gusset Models for Buckling Analysis.

Plate No. 4

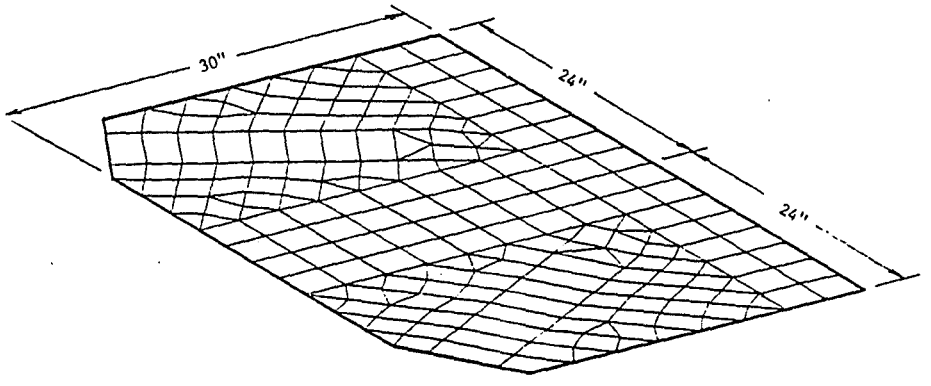

Plate No. 5

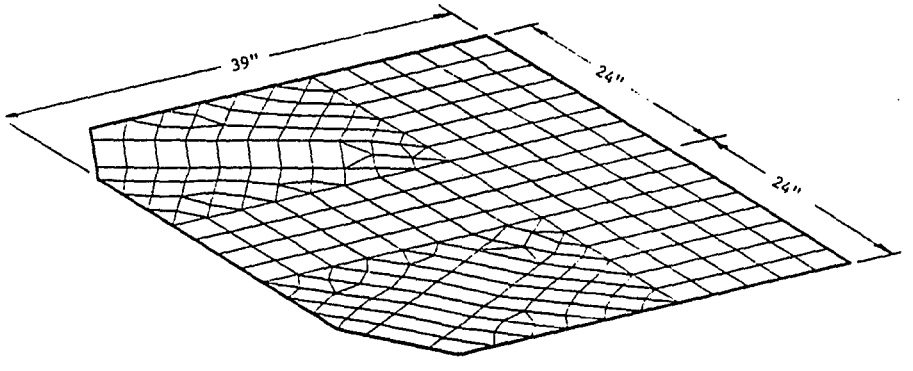

Plate No. 6

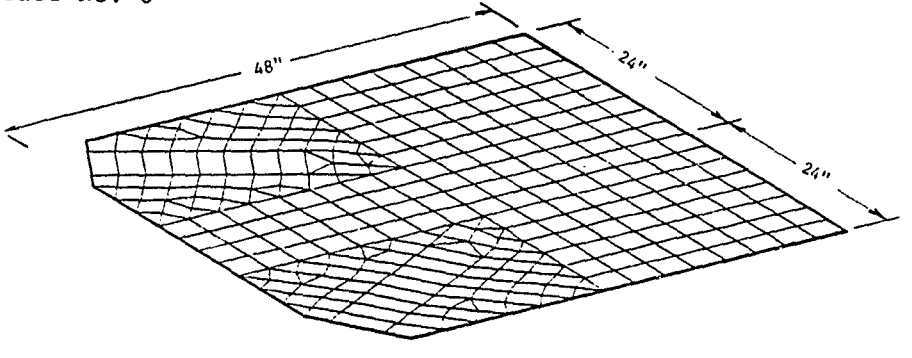

Figure 90. 60° K-Bracing Gusset Models for Buckling Analysis.

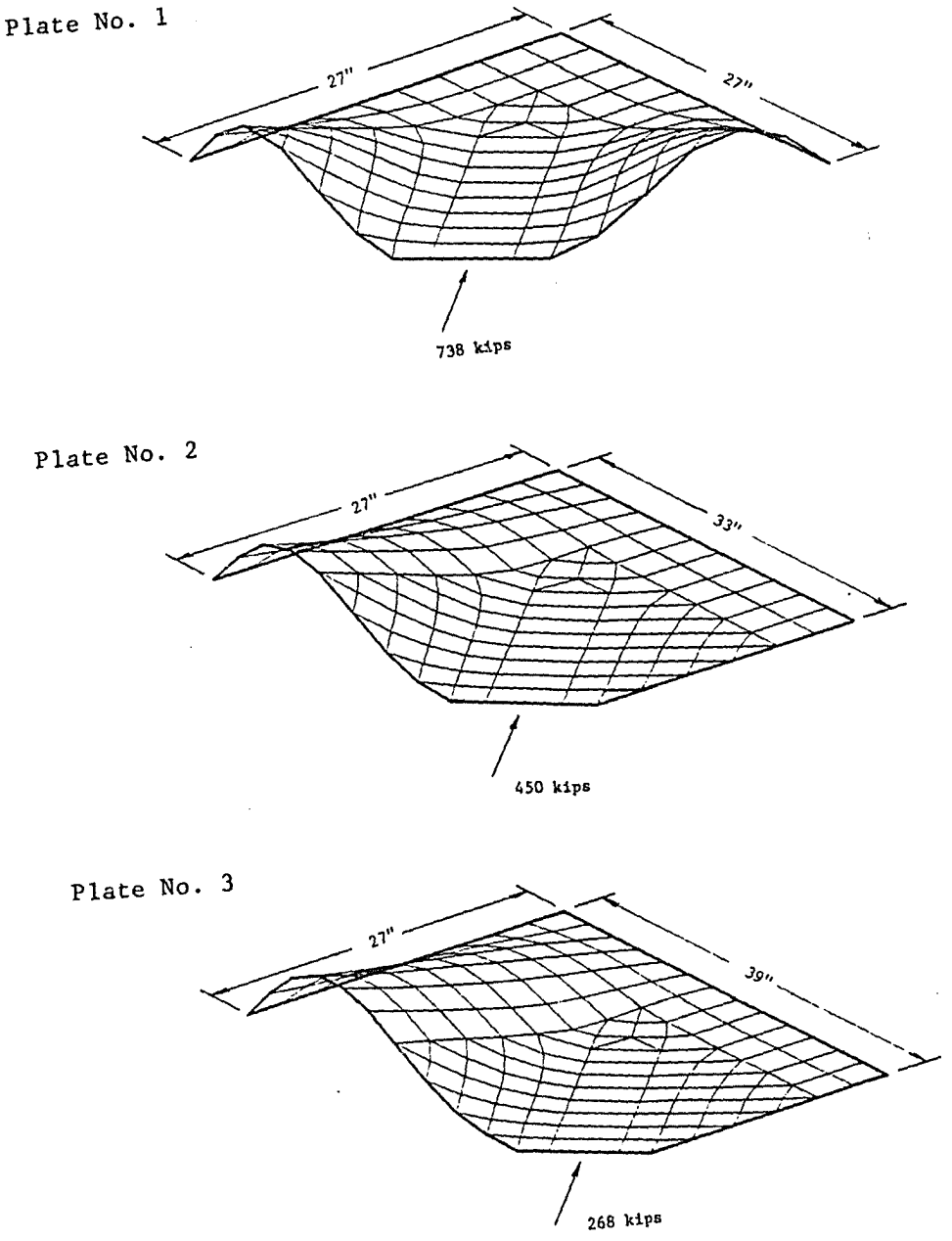

Figure 91. 45° Single Bracing Gusset Buckled Shapes (Simple Supports).

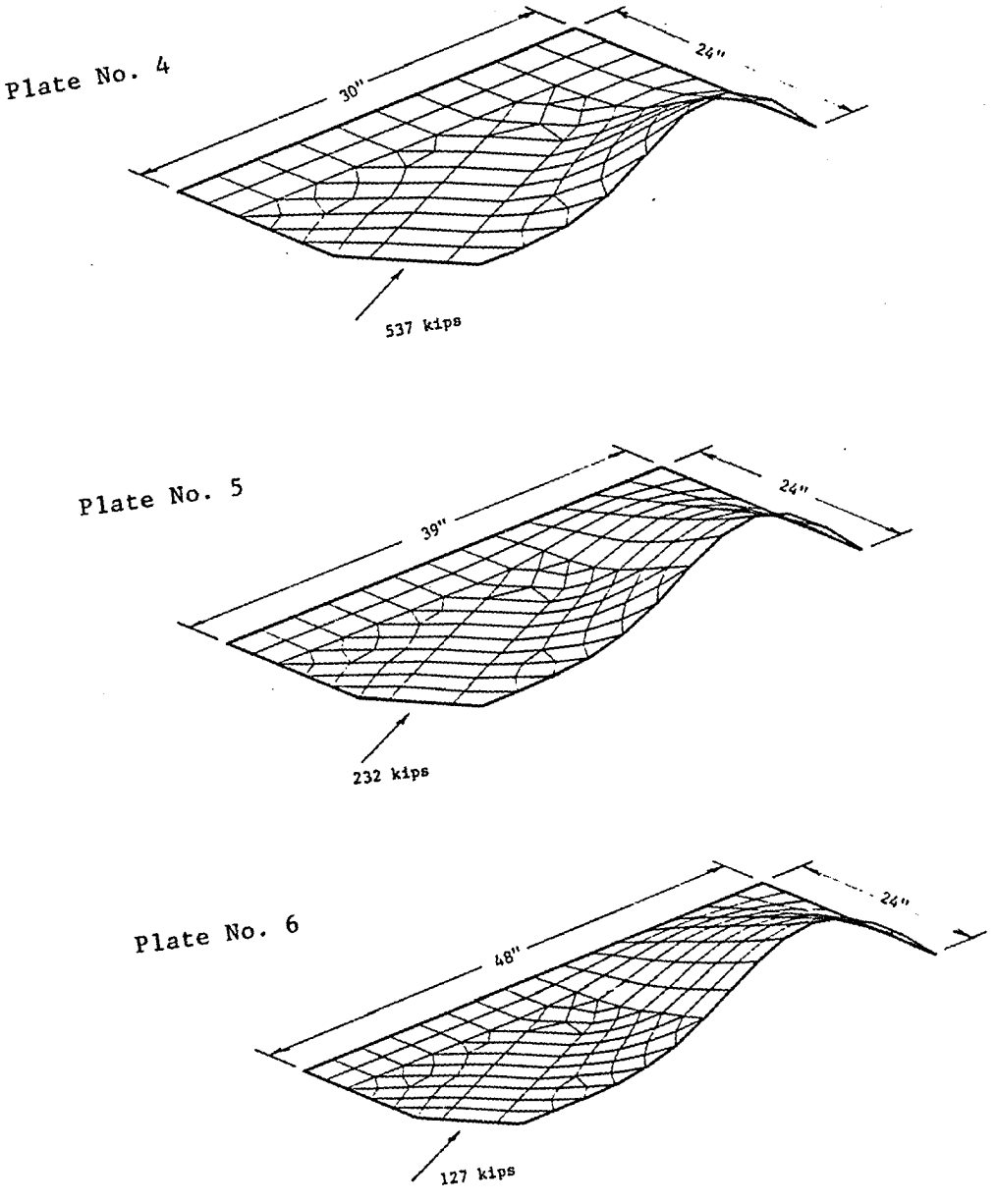

Figure 92. 60° Single Bracing Gusset Buckled Shapes (Simple Supports).

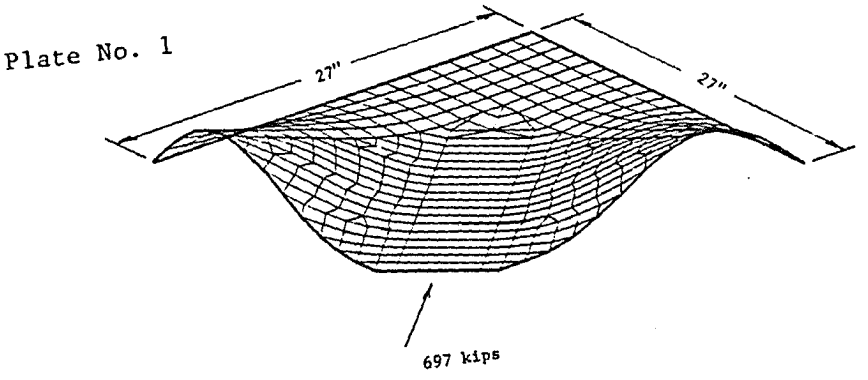

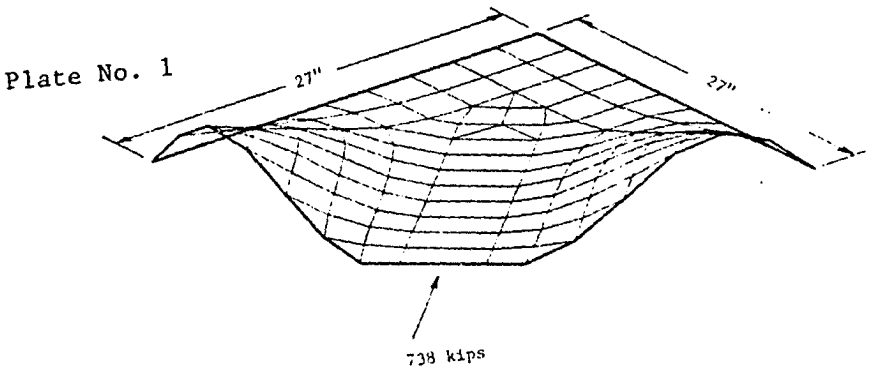

Figure 93. 45° Single Bracing Buckled Shape (Coarse and Fine Meshes).

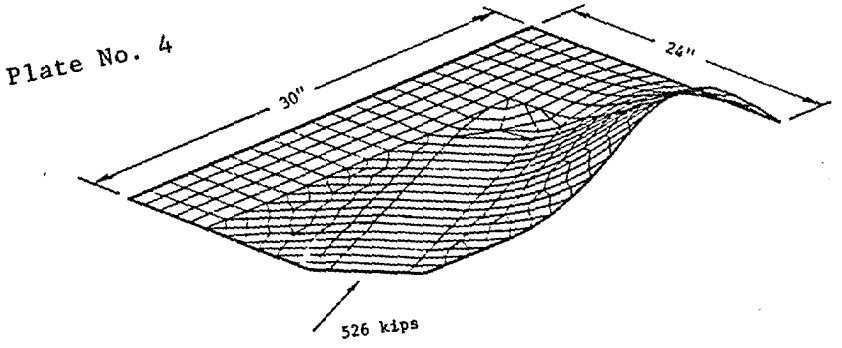

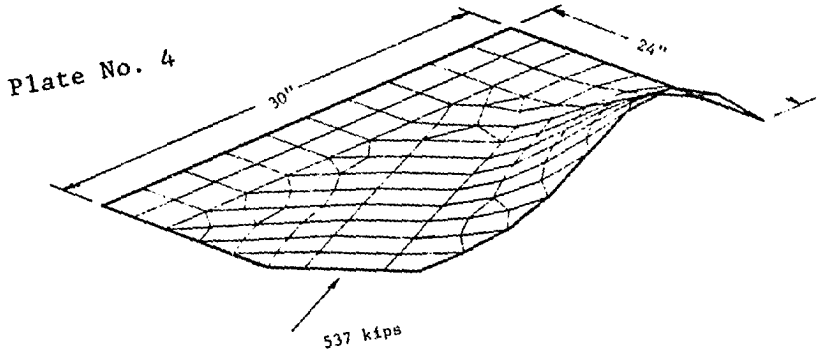

Figure 94. 60° Single Bracing Buckled Shape (Coarse and Fine Meshes).

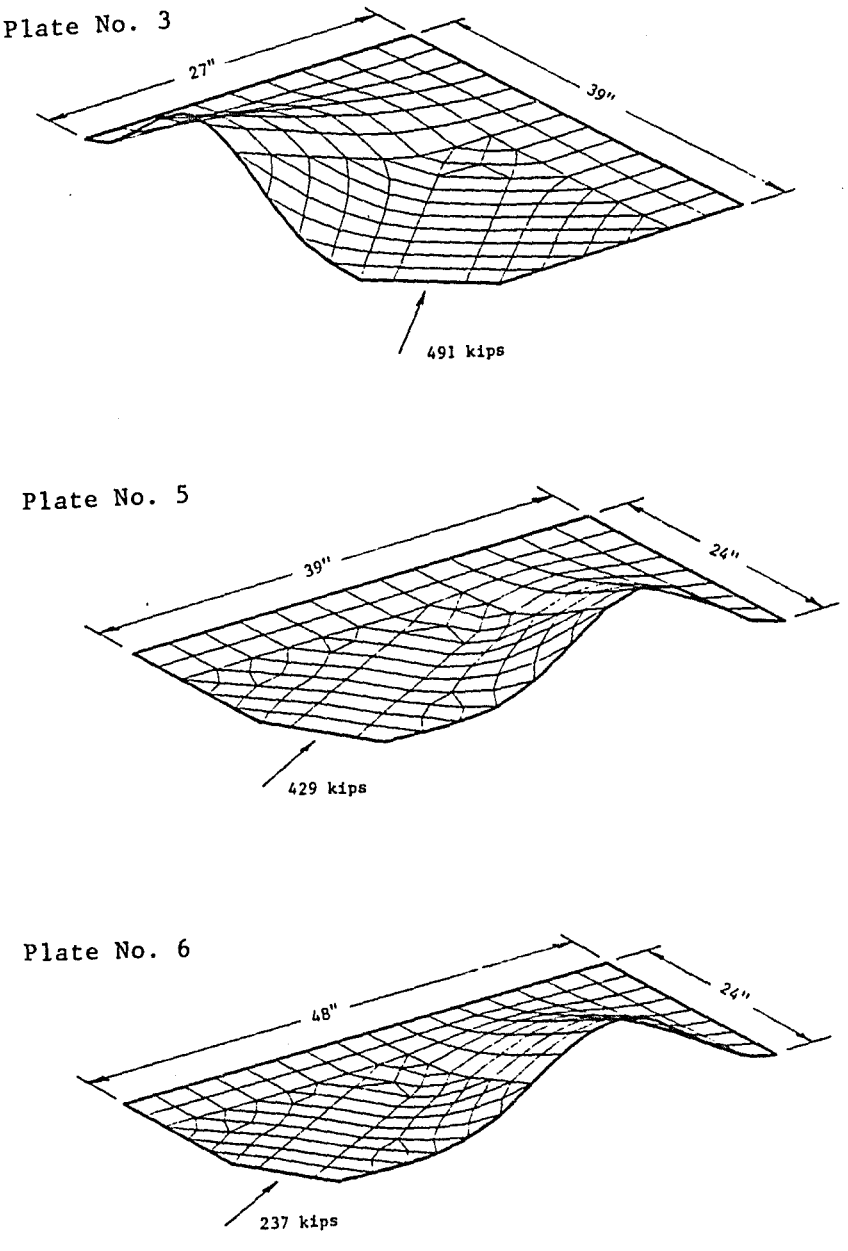

Figure 95. Single Bracing Gusset Buckled Shapes (Fixed Supports).

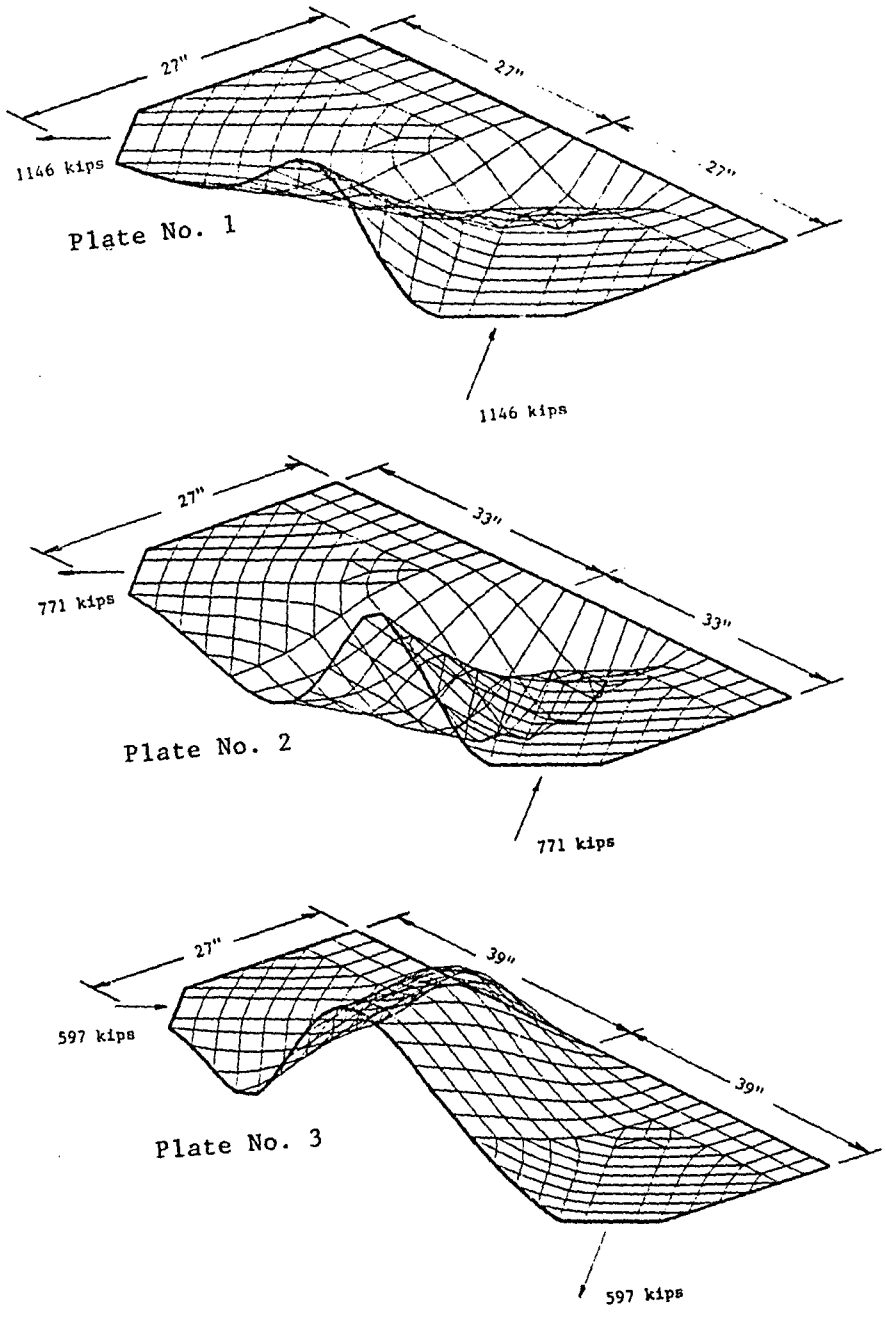

Figure 96. 45° K-Bracing Gusset Buckled Shapes.

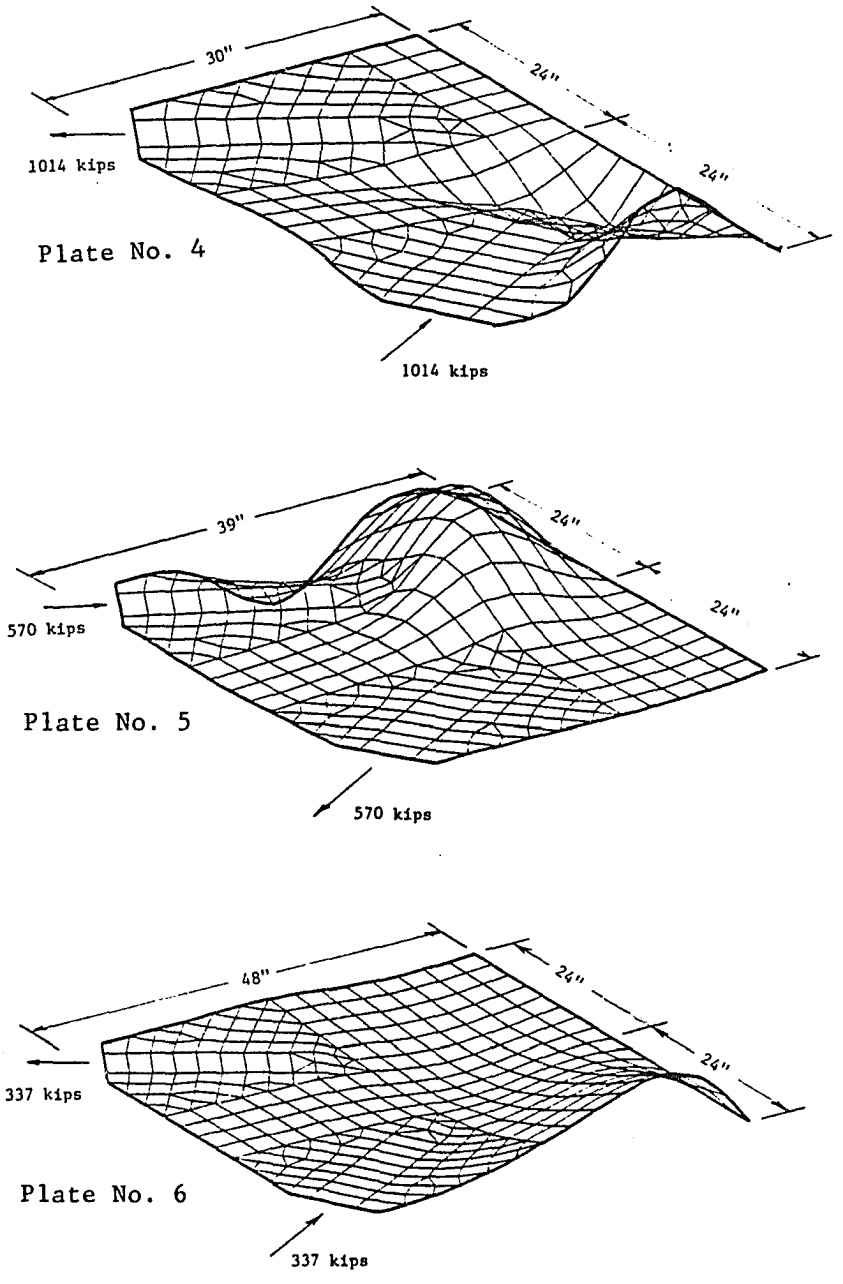

Figure 97. 60° K-Bracing Gusset Buckled Shapes.

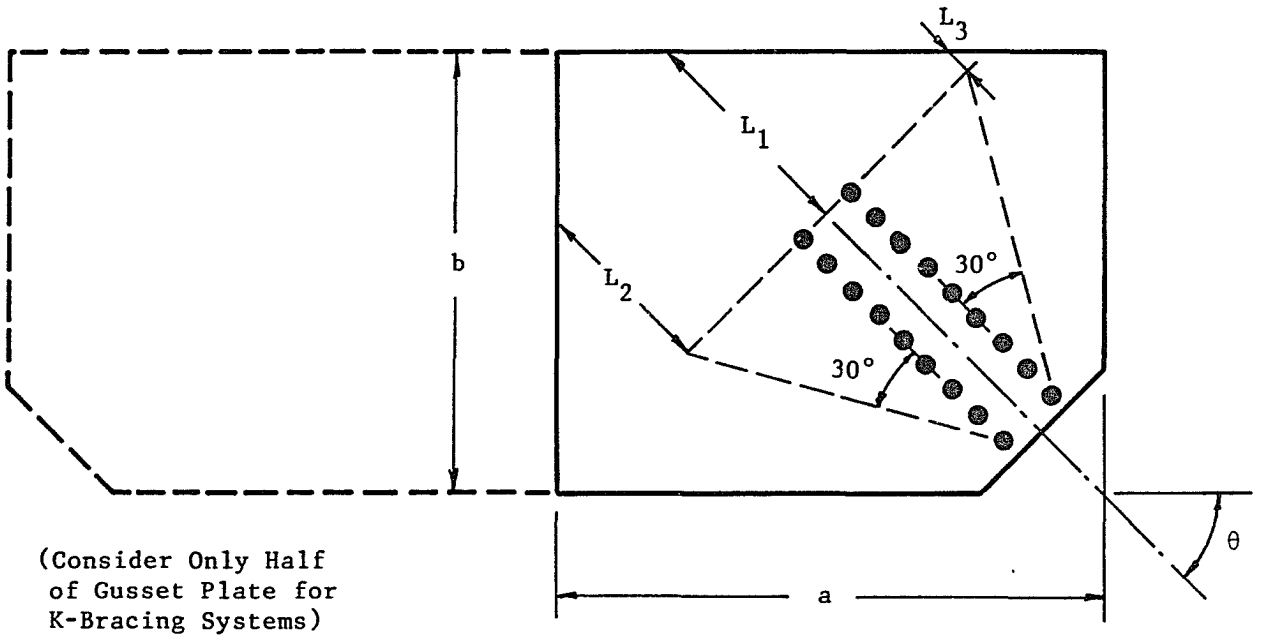

Figure 98. Whitmore Pattern for Buckling Strength Design.

CASE	BRACE	SUPPORTS	MESH
○ - 1	SINGLE	SIMPLE	COARSE
□ - 2	SINGLE	SIMPLE	FINE
△ - 3	SINGLE	FIXED	COARSE
◇ - 4	K	SIMPLE	COARSE

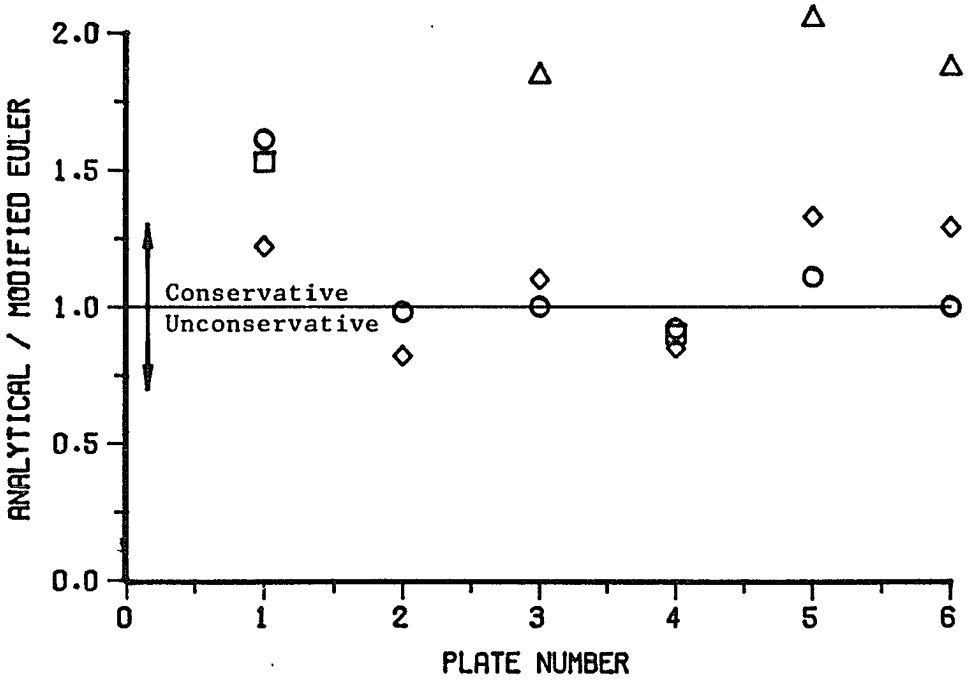

Figure 99. Comparison of Elastic Analytical and Elastic Euler Buckling Loads.

Chapter 10

ADDITIONAL DESIGN CONSIDERATIONS

When the line of action of the bracing member does not go through the beam-column working point, a moment is introduced into the connection which must be resisted by the frame. Two methods are available to check the frame for this moment. If the frame is being analyzed with a computer program, a short beam link can be inserted into the frame model at each eccentric connection as shown in Figure 100. The beams and columns can be sized directly from the resulting member loads. An alternative method can be used where the bracing member axis is assumed to intersect with the beam and column axes at a common point. This frame model can be analyzed to determine the primary member forces. As shown in Figure 100, a moment distribution can then be performed to determine the secondary member forces resulting from the moment caused by the eccentric connection. The frame members are then designed using the combined primary and secondary member forces.

Illustrated in Figure 101 are the effective stress contours for a typical gusset plate (0.375" thick) and the adjacent beam web (0.468" thick) and column web (0.390" thick). These contours indicate that the brace load significantly contributes to the beam and column web stresses. Therefore, if the web thickness of an adjacent framing

member is less than the gusset plate thickness, then web stiffeners should be provided for that member.

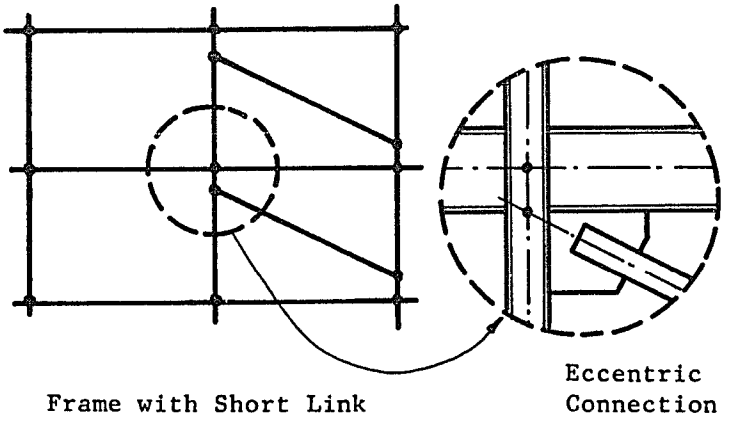

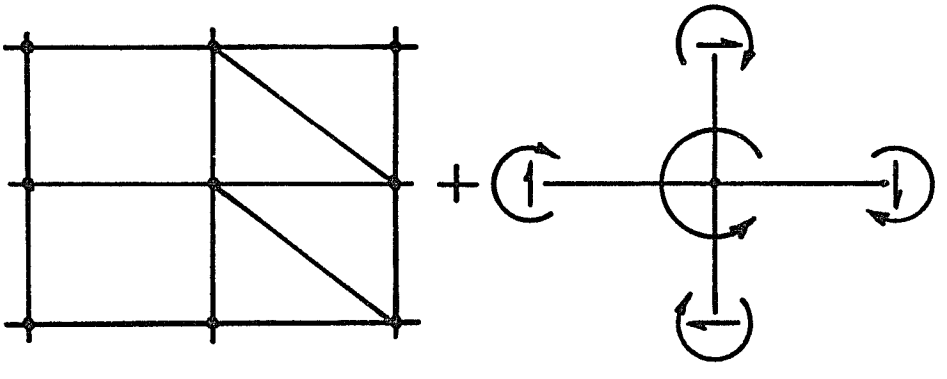

Figure 100. Design of Framing Members for Moment Caused by Connection Eccentricity.

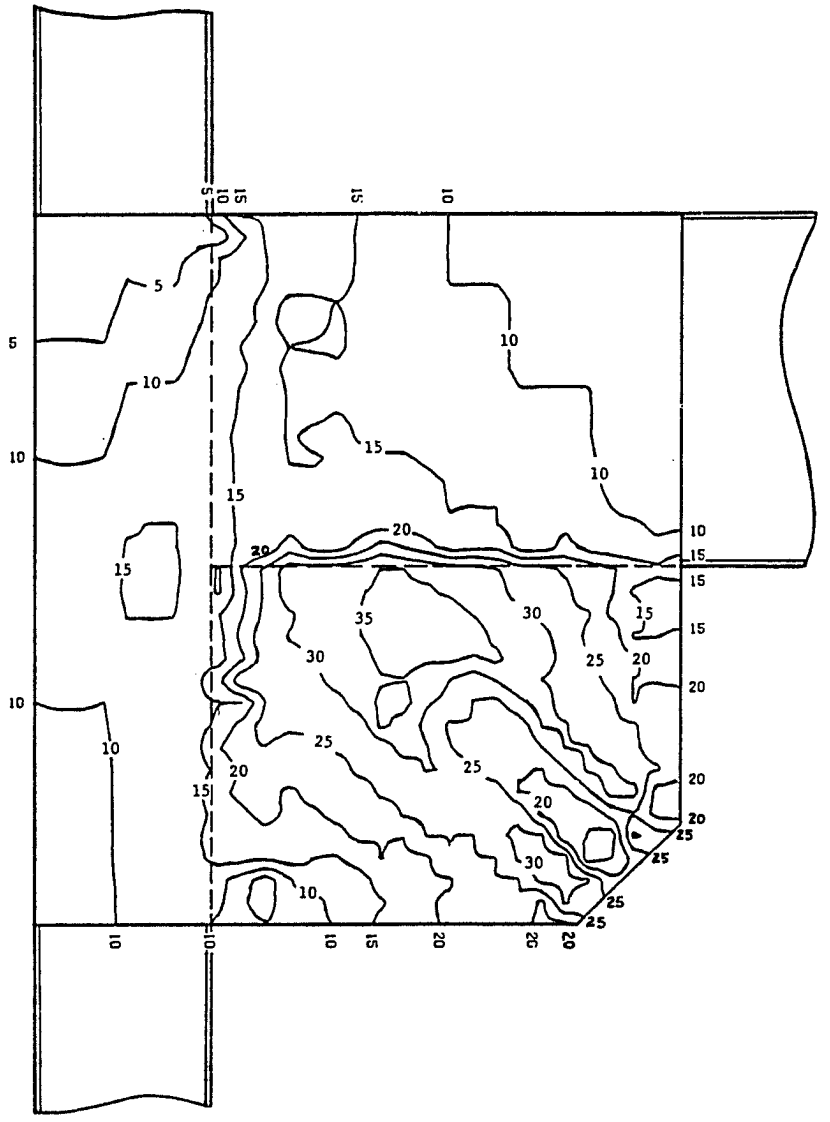

Figure 101. Typical Effective Stress Contours (ksi) in Gusset Plate, Beam Web, and Column Web.

Chapter 11

SUMMARY

The modeling techniques presented herein accurately and economically simulate the structural behavior of steel diagonal bracing connections. Preliminary studies indicated that the gusset plate causes the beam-to-column connection to act rigidly. The analytical results were compared to full-scale physical connection tests to verify the modeling techniques.

The finite element results support the Whitmore criterion for predicting the maximum normal stress in gusset plates. The block shear criterion was developed from the analyses to determine the tensile strength of gusset plates. The block shear procedure provides results identical to the Whitmore criterion.

Parametric studies of diagonal bracing connections were conducted to determine the force distributions in the gusset-to-frame connections. Results indicate that frame action plays an important role in the force distributions. Fastener forces do not act in pure shear as assumed by current design procedures; however, current methods were shown to be conservative. As the brace load approaches the ultimate load of the plate, connection forces become aligned with the brace. Furthermore, reducing the plate size for the same brace load increases the uniformity of the connector force distributions.

Design equations based on the analytical results were developed to estimate the fastener force distributions for design purposes. These equations are functions of the brace load magnitude and direction, and the plate aspect ratio. This procedure reduces the required number of bolts and weld sizes by 5% to 20% of those required by the current design procedure. Double angles with a single bolt in double shear can be used without considering prying action. Eccentric diagonal bracing connections can be designed without modifying the design equations.

In K-bracing connections the neutral axis of the connection deviates from a straight line. Smaller and more economical gusset plates are created when the working point is near a revised neutral axis that includes both the beam and gusset plate. Gusset-to-beam fastener force distributions were determined for K-bracing connections. Fastener forces are not in pure shear. Design recommendations were presented for K-bracing connections.

The buckling strength of gusset plates can be computed using the Whitmore section and criterion. Buckling modes in gusset plates have maximum distortion along the longest unsupported edge. The critical buckling load of a gusset plate can be increased by, (1) adding stiffeners to long edges, (2) by increasing plate thickness, and (3) by reducing plate dimensions.

Design procedures for diagonal bracing connections can be summarized as follows:

1. Obtain brace design load from frame analysis.
2. Design brace-to-gusset connection(s) using usual procedures for tension connections.
3. Choose sufficient plate dimensions to accommodate brace-to-gusset connection(s).
4. Calculate required plate thickness using the block shear criterion.
5. Check buckling strength of gusset plate; if required, add stiffners, reduce plate dimensions, or increase plate thickness.
6. Design plate-to-frame connections based on gusset force distribution design equations; connection should span entire plate edge.
7. Add stiffeners to webs of framing members having a thickness significantly less than gusset plate thickness.
8. For an eccentric connection, the frame should be checked for the resulting additional moment.

APPENDIX A

RICHARD CURVE PARAMETERS

Richard Curve Parameters for Welds

The curve parameters for a fillet weld can be computed as follows:

Elastic Stiffness = K = (20000)(a)(l) (kips/inch)

Plastic Stiffness = K_p = 0

Reference Load = R_o = 0.733 (a)(l)(s) (kips)

Curve Parameter = n = 1

where a = weld size (1/4", 5/16",...)

l = tributary length (1", 3", 5",...)

s = electric strength in ksi (E60, E70,...)

Table 10. Single Bolt-Single Shear Force Deformation Curve Parameter Summary.

Bolt	Plates	K	K_p	R_o	n
3/4" A325	1/4 - 1/4 A36	7250.	10.	20.	1.0
"	5/16 - 5/16 A36	9063.	-10.	50.	0.4
"	3/8 - 3/8 A36	10875.	0.	40.	0.5
"	7/16 - 7/16 A36	12700.	10.	40.	0.5
"	1/2 - 1/2 A36	14500.	20.	30.	0.7
"	1/4 - 3/8 A36	8700.	-30.	30.	0.6
"	1/4 - 1/2 A36	9667.	-30.	30.	0.6
"	3/8 - 1/2 A36	12400.	0.	40.	0.5
"	3/8 - 3/8 A572*	10875.	20.	30.	0.7
7/8" A325	5/16 - 5/6 A36	9063.	9.	30.	0.7
"	3/8 - 3/8 A36	10875.	20.	40.	0.5
"	7/16 - 7/16 A36	12700.	0.	50.	0.5
"	1/2 - 1/2 A36	14500.	10.	40.	0.7
"	1/4 - 3/8 A36	8700.	20.	30.	0.8
"	1/4 - 1/2 A36	9667.	20.	30.	1.1
"	3/8 - 1/2 A36	12400.	10.	40.	0.6
"	3/8 - 3/8 A572*	10875.	10.	40.	0.6
1" A325	1/2 - 1/2 A36	14500.	20.	50.	0.5
"	5/8 - 5/8 A36	18125.	0.	90.	0.4
3/4" A490	1/2 - 1/2 A36	14500.	-10.	70.	0.4
"	5/8 - 5/8 A36	18125.	10.	60.	0.4
7/8" A490	1/2 - 1/2 A36	14500.	40.	40.	0.7
"	5/8 - 5/8 A36	18125.	40.	50.	0.5
"	1/2 - 1/2 A572*	14500.	40.	50.	0.6
1" A490	1/2 - 1/2 A36	14500.	40.	50.	0.5
"	5/8 - 5/8 A36	18125.	20.	70.	0.5

* Gr 50

Table 11. Richard Curve Parameters for Bolted Double Angles Loaded in Tension

Gage Length (inches)	Angle Thickness (inches)	K (Kips/in.)	K_p (Kips/in.)	R_o (Kips)	n
3	1/2	850	22	20	1.1
3	3/8	350	12	10	2.0
2 - 1/4	1/2	2000	23	32	0.7
2 - 1/4	3/8	850	20	19	1.2
2 - 1/4	1/4	250	11	7	2.5
1 - 3/4	1/2	4200	31	42	1.0
1 - 3/4	3/8	1800	27	28	0.9
1 - 3/4	1/4	550	24	9	3.8

APPENDIX B

COMPUTER PROGRAMS UTILIZED

Program Name	Function	Author(s)
NODEM	2d Mesh Generation	Williams
INELAS	Nonlinear Finite Element Analysis	Richard
NASTRAN	General Purpose Finite Element Analysis	MSC*
NASPLOT	Mesh Plotting for NASTRAN	MSC*
VECPLT	Fastener Force and Displacement Plotting	Hormby, Williams
MODPLT	Mesh Plotting for INELAS	Williams
CONPLT	2d Contour Plotting	Williams
MOP	Surface Plotting	Hormby
DESEQN	Development of Design Equations	Williams
XYPLOT	General 2D Plotting of Figures and Graphs	Williams

* The MacNeal-Schwendler Corporation

REFERENCES

1. Beaufoy, L. A. and Moharram, "Derived Moment-Angle Curves for Web-Cleat Connections," Preliminary Publication, Third Congress, International Association for Bridge and Structural Engineering, 1948.

2. Birkemoe, P. C., R. A. Eubanks, and W. H. Munse, "Distribution of Stresses and Partition of Loads in Gusseted Connections," Structural Research Series Report No. 343, Department of Civil Engineering, University of Illinois, Urbana, Illinois, March, 1969.

3. Birkemoe, P. C. and M. I. Gilmor, "Behavior of Bearing Critical Double-Angle Beam Connections," Engineering Journal, AISC, Vol. 15, No. 4, 1978, pp. 109-115.

4. Bjorhovde, R. and S. K. Chakrabarti, "Tests of Full Size Gusset Plate Connections," Journal of the Structural Division, ASCE, Vol. 111, No. ST3, March 1985.

5. Blewitt, J. R. and R. M. Richard, "Experimental and Analytical Force Deformation Curves for Bolted Double Angle Connections," Research Report prepared for AISC, Department of Civil Engineering and Engineering Mechanics, University of Arizona, Tucson, Arizona, December, 1984.

6. Butler, L. J. and G. L. Kulak, "Strength of Fillet Welds as a Function of Load," Welding Journal Research Supplement, May, 1971.

7. Chesson, E., Jr. and W. H. Munse, "Behavior of Riveted Truss-Type Connections," Transactions, ASCE, Vol 123, 1958, pp. 1,087-1,129.

8. Chesson, E., Jr. and W. H. Munse, "Riveted and Bolted Joints: Truss-Type Tensile Connections," Journal of the Structural Division, ASCE, Vol. 89, No. ST1, February, 1963, pp. 67-106.

9. Cook, R. D., Concepts and Applications of Finite Element Analysis, 2nd Edition, Wiley, New York, 1981.

10. Crawford, S. F. and G. L. Kulak, "Eccentrically Loaded Bolted Connections," Journal of the Structural Division, ASCE, Vol. 97, No. ST3, March, 1971, pp. 765-783.

11. Davis, C. S., "Computer Analysis of Stresses in a Gusset Plate," M.S. Thesis, Department of Civil Engineering, University of Washington, Seattle, Washington, 1967.

12. Desai, S., "Applications of the Finite Element Method to the Problem of Gusseted Connections," Fritz Engineering Laboratory Report (Internal), January 1970.

13. Fisher, J. W. and J. H. A. Struik, Guide to Design Criteria for Bolted and Riveted Structural Joints, Wiley, New York, 1974.

14. Gaylord, E. H., Jr. and C. N. Gaylord, Design of Steel Structures, McGraw-Hill, New York, 1957.

15. Goldberg, J. E. and R. M. Richard, "Analysis of Nonlinear Structures," Journal of the Structural Division, ASCE, Vol. 89, No. ST4, August, 1963, pp. 333-351.

16. Hamm, K. R., "The Analysis and Behavior of Deep Bolted Angle Connections," M.S. Thesis, Department of Civil Engineering and Engineering Mechanics, University of Arizona, Tucson, Arizona, 1984.

17. Hardash, S. G. and R. Bjorhovde, "New Design Criteria for Gusset Plates in Tension," Engineering Journal, AISC, 2nd Quarter, 1985, Vol. 22, No. 2, pp. 77-94.

18. Hardin, B. O., "Experimental Investigation of the Primary Stress Distribution in the Gusset Plates of a Double-Plane Pratt Truss Joint with Chord Slice at the Joint," Bulletin No. 49, Engineering Experiment Station, University of Kentucky, Lexington, Kentucky, September, 1958.

19. Irvan, W. G., Jr., "Experimental Study of Primary Stresses in Gusset Plates of a Double-Plane Pratt Truss," Bulletin No. 46, Engineering Experiment Station, University of Kentucky, Lexington, Kentucky, December, 1957.

20. Lewitt, C. W., E. Chesson Jr., and W. H. Munse, "Restraint Characteristics of Flexible Riveted and Bolted Beam-to-Column Connections," Structural Research Series Report No. 296, Department of Civil Engineering, University of Illinois, Urbana, Illinois, March, 1966.

21. Manual of Steel Construction, 8th Edition, AISC, Chicago, Illinois, 1980.

22. Mendelson, A., Plasticity: Theory and Application, The MacMillian Co., New York, 1968.

23. Perna, F. J., "Photoelastic Stress Analysis with Special Reference to Stresses in Gusset Plates," M.S. Thesis, University of Tennessee, Knoxville, Tennessee, 1941.

24. Rabern, D. A., "Stress, Strain, and Force Distributions in Gusset Plate Connections," M.S. Thesis, Department of Civil Engineering and Engineering Mechanics, University of Arizona, Tucson, Arizona, 1983.

25. Rickles, J. M. and J. A. Yura, "Strength of Double-Row Bolted-Web Connections," Journal of the Structural Division, ASCE, Vol. 109, No. ST1, January, 1983, pp. 126-142.

26. Richard, R. M., "A Study of Structural Systems Having Conservative Nonlinear Elements," Doctoral Dissertation, Purdue University, Lafayette, Indiana, 1961.

27. Richard, R. M., Private Communication, Department of Civil Engineering and Engineering Mechanics, University of Arizona, Tucson, Arizona, November, 1985.

28. Richard, R. M., User's Manual for Nonlinear Finite Element Analysis Program INELAS, Department of Civil Engineering and Engineering Mechanics, University of Arizona, Tucson, Arizona, 1968 (updated 1985).

29. Richard, R. M. and B. J. Abbott, "A Versatile Elastic-Plastic Stress-Strain Formula," Journal of the Engineering Mechanics Division, ASCE, August, 1975.

30. Richard, R. M. and J. R. Blacklock, "Finite Element Analysis of Inelastic Structures," AIAA Journal, Vol. 7, No. 3, March, 1969.

31. Richard, R. M., P. E. Gillett, J. D. Kreigh, and B. A. Lewis, "The Analysis and Design of Single Plate Framing Connections," Engineering Journal, AISC, No. 2, 1980.

32. Richard, R. M., D. A. Rabern, D. E. Hormby, and G. C. Williams, "Analytical Models for Steel Connections," Behavior of Metal Structures, Proceedings of the W. H. Munse Symposium, ASCE, May, 1983, pp. 128-155.

33. Rust, T. H., "Steel Gusset Plates," Proceedings of the 13th Semi-Annual Eastern Photoelastic Conference, Department of Mechanical Engineering, Massachusets Institute of Technology, Cambridge, Massachusets, 1941, p. 55.

34. Rust, T. H., "Specification and Design of Steel Gusset Plates," Transactions, ASCE, Vol. 105, 1940, pp. 142-166.

35. Sandel, J. A., "Photoelastic Analysis of Gusset Plates," M.S. Thesis, University of Tennessee, Knoxville, Tennessee, 1950.

36. Struik, J. H. A., "Applications of Finite Element Analysis to Nonlinear Plane Stress Problems," Doctoral Dissertation, Department of Civil Engineering, Lehigh University, Bethlehem, Pennsylvania, November, 1972.

37. Thornton, W. A., "Bracing Connections for Heavy Construction," Engineering Journal, AISC, 3rd Quarter, 1984.

38. Timoshenko, S. P. and J. M. Gere, Theory of Elastic Stability, 2nd Edition, McGraw-Hill, New York, 1961.

39. Vasarhelyi, D. D., "Tests of Gusset Plate Models," Journal of the Structural Division, ASCE, Vol. 97, No. ST2, February, 1971, pp. 665-678.

40. Waddell, J. A. L., Bridge Engineering, Wiley, New York, 1916, pp. 521-524.

41. Whitmore, R. E., "Experimental Investigation of Stresses in Gusset Plates," M.S. Thesis, University of Tennessee, Knoxville, Tennessee, 1950.

42. Whitmore, R. E., "Experimental Investigation of Stresses in Gusset Plates," Bulletin No. 16, Engineering Experiment Station, University of Tennessee, Knowville, Tennessee, May, 1952.

43. Yura, J. A., P. C. Birkmoe, and J. M. Rickles, "Beam-Web Shear Connections - An Experimental Study," Journal of the Structural Division, ASCE, Vol. 108, No. ST2, February, 1982, pp. 311-326.